

University of Alberta

Molybdenum Cofactor Insertion in *Escherichia coli*
Dimethyl Sulfoxide Reductase

by

Huipo Tang

A thesis submitted to the Faculty of Graduate Studies and Research
in partial fulfillment of the requirements for the degree of

Master of Science

Department of Biochemistry

©Huipo Tang

Fall 2012

Edmonton, Alberta

Permission is hereby granted to the University of Alberta Libraries to reproduce single copies of this thesis and to lend or sell such copies for private, scholarly or scientific research purposes only. Where the thesis is converted to, or otherwise made available in digital form, the University of Alberta will advise potential users of the thesis of these terms.

The author reserves all other publication and other rights in association with the copyright in the thesis and, except as herein before provided, neither the thesis nor any substantial portion thereof may be printed or otherwise reproduced in any material form whatsoever without the author's prior written permission.

Abstract

Molybdenum is a metal present in all forms of life. Most commonly, it forms the molybdenum cofactor (Moco) in the active site of molybdoenzymes. In bacteria, dimethyl sulfoxide (DMSO) reductase is a molybdoenzyme that is part of the anaerobic respiratory chain. *E. coli* DMSO reductase (DmsABC) belongs to a family called the complex iron-sulfur molybdoenzymes, which contain iron-sulfur clusters to transfer electrons through the enzyme. In *E. coli* nitrate reductase A, another member of this family, there is a [4Fe-4S] cluster called FS0 that also plays a role in enzyme maturation. In this thesis, DmsABC is used as a model system to explore the interplay between the FS0 cluster assembly and Moco insertion. This is achieved by generating site-directed mutations in the FS0-coordinating sequence and evaluation of effects of these mutations on assemblies of FS0 and Moco *in vivo* complementation and *in vitro* biochemical, enzymology and spectroscopic assays.

Acknowledgements

I would like to thank foremost my supervisor, Dr. Joel H. Weiner, who has been an incredible mentor during my years in the lab for one undergrad Honors research project, one summer studentship and my Master research project. Not only his passion for science and wealth of knowledge have been inspiring; he has taught me the calm perseverance that is so valuable in pursuing our goals. I cannot be more grateful for his patience, understanding and encouragement.

I would also like to give a huge gift of gratitude to Dr. Richard A. Rothery, for his close guidance throughout the project and numerous meaningful discussions. Thank you for taking me into the wonderland of EPR. Although never met in person, I would like to give special thank to James Voss for his contributions to this project.

Many thanks must be given to Gillian McCuaig, who taught me many lab techniques, watched out for me when I just came into the lab and knew little about the real laboratory, and always kept the lab running smoothly in top conditions. To Nasim Boroumand, thank you for your help and expertise with the purification of DmsABC. I also thank you for all the laugh-filled, heart-warming or tearful “girl-talks” we shared over the years. I would also like to thank Quang Tran, Victor Cheng, Greg Workun, Glen Zhang, Zhongwei Zhao, Kamila Moquin, Francois Chartier, Maryam Zarepour, Justin Fedor, Matt Solomonson, Francesca Sebastian and Yanfei Zhang for being wonderful lab-mates and making my time in the lab joyful and memorable.

I would like to thank my supervisory committee, Dr. Joanne Lemieux and Dr. Bernard Lemire, for their guidance and thoughtful suggestions over the years. I would also like to thank Dr. Frank Nargang and Dr. Richard Fahlman for being my examiners.

I want to give my thank to the agencies providing financial support that made this project possible: the Canadian Institutes for Health Research, Natural Sciences and Engineering Research Council of Canada and Alberta Scholarship Programs.

Last but not least, I would like to thank those who are outside my academic life but have given me unconditional love and support to make past few years possible. Thank you to my parents who are always there for me no matter what. A big thank to my husband, Zhenyong, who's always by my side through the ups and downs, and who would willingly be my chauffeur and body-guard when I need to do a weekend harvest or an extra mid-night reading. And finally, my daughter, whose smiles always brighten the day and fill me with energy.

Table of Contents

Chapter 1 – General Introduction	1
1.1 Introduction	
1.2 Respiration and Regulations in <i>Escherichia coli</i>	
1.3 Biosynthesis of Prosthetic Groups	
1.3.1 Moco	
1.3.2 Iron-sulfur Clusters	
1.4 Targeting of Prefolded Complex Enzyme	
1.4.1 <i>tat</i> -transport	
1.4.2 System-specific Chaperon	
1.5 Dimethyl Sulfoxide Reductase (DmsABC)	
1.5.1 Overview	
1.5.2 The <i>dms</i> Operon	
1.5.3 DmsA	
1.5.4 DmsB	
1.5.5 DmsC	
1.5.6 DmsD	
1.5.7 Topology of DmsABC	
1.6 Thesis Objectives	
1.7 Figures	
1.8 References	

Chapter 2 – Correct Assembly of Iron Sulfur Cluster FS0 into *Escherichia coli* Dimethyl Sulfoxide Reductase (DmsABC) is a Pre-requisite for Molybdenum Cofactor Insertion.....58

- 2.1 Introduction
- 2.2 Experimental Procedures
- 2.3 Results and Discussion
- 2.4 Conclusion
- 2.5 Tables and Figures
- 2.6 References
- 2.7 Appendix: Supplementary Figures

Chapter 3 – A Mutant Conferring Cofactor-Dependent Assembly of *Escherichia coli* Dimethyl Sulfoxide Reductase91

- 3.1 Introduction
- 3.2 Materials and Methods
- 3.3 Results and Discussion
- 3.4 Conclusion
- 3.5 Tables and Figures
- 3.6 References
- 3.7 Appendix: Supplementary Figures

Chapter 4 – Conclusions and Future Directions..... 127

- 4.1 Conclusions and Summaries
- 4.2 Future Directions
- 4.3 References

List of Tables

Table 2.1	Bacterial strains and plasmids	77
Table 2.2	Enzyme and Mo-bisPGD cofactor quantifications and enzyme activities determined by <i>in vitro</i> reduction assays and <i>in vivo</i> . growth experiments	78
Table 3.1	Bacterial strains and plasmids	111
Table 3.2	Enzyme activities determined by TMAO-dependent oxidation of reduced benzyl viologen or lapachol.	111

List of Figures

Figure 1.1	The <i>E. coli</i> respiratory chain.	32
Figure 1.2	Molybdenum cofactors (Moco).	33
Figure 1.3	Biosynthesis of molybdenum cofactor (Moco).	34
Figure 1.4	Stereo views of iron-sulfur clusters.	35
Figure 1.5	Biosynthesis of [Fe-S] cluster via ISC system.	36
Figure 1.6	The <i>tat</i> translocation system.	37
Figure 1.7	<i>E. Coli</i> DMSO reductase.	38
Figure 1.8	Catalytic mechanism for the catalytic cycle of <i>Rhodobacter</i> DMSO reductase proposed by Johnson <i>et. al.</i> (55).	39
Figure 1.9	Surface representation of the structure of DMSO reductase from <i>Rhodobacter capsulatus</i> (PDB file 3DMR).	40
Figure 1.10	Coordination of the [Fe-S] clusters (FS1-4) in DmsB proposed by Rothery <i>et. al.</i> (194).	40
Figure 1.11	A topology model of <i>E. coli</i> DmsC (Swissprot accession number P187777).	41
Figure 1.12	The X-ray crystal structure of <i>E. coli</i> DmsD (PDB file 3EFP).	42
Figure 2.1	Electron transfer relay architecture and predicted DmsA structure around FS0.	79
Figure 2.2	Sequences of DmsA mutants in comparison with Cys group sequences of FdnG and NarG.	80
Figure 2.3	Low field EPR spectrum of purified DmsABC and NarGHI.	81
Figure 2.4	A. Sodium dodecyl sulfate-PAGE gel of DmsABC and its mutants.	82
	B. Effect of mutations of residues close to FS0 or the proximal pterin on the low field DmsABC EPR spectrum.	83

Figure 2.5	Mo-bisPGD cofactor occupancies and enzyme turn-over rates.	84
Figure 2.6	Purification of <i>E. coli</i> DmsABC.	88
Figure 2.7	High field EPR spectrum of reduced (A) and oxidized (B) DmsABC wild-type and mutants enzymes.	89
Figure 2.8	EPR characterization of Mo-bisPGD cofactor in DmsA ^{CS1+R61K} BC.	90
Figure 3.1	Electron-transfer relay architecture and predicted DmsA structure around FS0.	112
Figure 3.2	Tungstate decreases enzyme maturation in a DmsA-Cys59Ser mutant.	113
Figure 3.3	Effect of tungstate on respiratory growth on DMSO supported by DmsABC and DmsA ^{C59S} BC.	114
Figure 3.4	Loss of cofactor inhibits assembly of DmsA ^{C59S} BC.	115
Figure 3.5	Effect of tungstate on DmsA ^{C59S} BC assembly determined by EPR spectroscopy of the DmsABC [4Fe-4S] clusters.	116
Figure 3.6	EPR characterization of Mo-bisPGD in the DmsA-C59S mutant.	117
Figure 3.7	EPR spectra of the purified DmsA-Cys59Ser variant.	119
Figure 3.8	Model for DmsABC maturation.	120
Figure 3.9	Tungstate prevent assembly of DmsA-Cys59Ser mutant to the membrane when Moco is not available.	126
Figure 3.10	DmsABC and DmsA ^{C59S} BC do not support respiratory growth of <i>E. coli</i> DSS301 (Δ <i>dmsABC</i>) on DMSO when Moco is not available.	126

List of Abbreviations

ATP/AMP	adenosine triphosphate/monophosphate
BV/ BVH•	benzyl viologen/reduced benzyl viologen
CISM	complex iron-sulfur molybdoenzyme
CMP	cytidine monophosphate
cPMP	cyclic pyranopterin monophosphate
DmsABC	<i>Escherichia coli</i> dimethyl sulfoxide reductase
DMS	dimethyl sulfide
DMSO	dimethyl sulfoxide
<i>E. coli</i>	<i>Escherichia coli</i>
EcDms	<i>E. coli</i> DMSO reductase
E_m	midpoint potential
EPR	electron paramagnetic resonance
ETR	electron transfer relay
EXAFS	extended X-ray absorption resonance
FdnGHI	<i>E. coli</i> formate dehydrogenase-N
[Fe-S]/FS	iron-sulfur
GTP/GMP	guanosine triphosphate/monophosphate
HOQNO	2- <i>n</i> -heptyl-4-hydroxyquinoline- <i>N</i> -oxide
LPC/ LPCH ₂	lapachol/reduced lapachol
MPT	molybdopterin
Mo-bisPGD	molybdo-bis(pyranopterin guanine dinucleotide)
MQ/MQH ₂	menaquinone/menaquinol

NarGHI	<i>E. coli</i> nitrate reductase
PGD	pyranopterin guanine dinucleotide
PCD	pyranopterin cytosine dinucleotide
pmf	proton motive force
PMSF	phenylmethylsulfonyl fluoride
PPT	pyranopterin
Q-site	quinone-binding site
RhDms	<i>Rhodobacter</i> DMSO reductase
SDS-PAGE	sodium dodecyl sulfate polyacrylamide gel electrophoresis
<i>tat</i>	twin arginine translocation
TMAO	trimethylamine <i>N</i> -oxide
WT	wild-type

Chapter 1

General Introduction

1.1 Introduction

Escherichia coli is a facultative bacterium that can make use of a wide diversity of substrates in addition to oxygen for respiration. This is achieved by an array of respiratory oxidoreductases that are membrane bound multi-subunit complex enzymes. These complex enzymes catalyze oxidation/reduction of substrates at distinct active sites that are linked by an internal electron transfer relay. Metals and organic cofactors are incorporated and are required for the redox reactions and electron transfer. The family of metalloproteins our lab studies is the Complex Iron-sulfur Molybdoenzymes (CISM), which incorporate a molybdenum cofactor (Moco) in the active site and iron-sulfur clusters to transfer electrons. Maturation of these complex enzymes is a complicated pathway that involves folding of the protein, assembly of the subunits, incorporation of the cofactors, targeting to and/or translocation across the membrane, and attachment to the membrane. The dimethyl sulfoxide reductase (DmsABC) is used as a model system in this thesis to study the mechanism and role of Moco insertion in maturation of CISM family proteins.

1.2 Respiration and Regulations in *Escherichia coli*

The chemiosmotic mechanism discovered by Peter Mitchell hypothesized that electron transfer through the respiratory chain is coupled to proton translocation across the membrane (1). The resulting transmembrane electrochemical gradient or pmf (proton motive force) is

used to generate ATP. In *E. coli*, the respiratory chains are made of primary dehydrogenases and terminal reductases coupled by quinones (2) (Figure 1.1). Reductants such as NADH and succinate donate electrons to primary dehydrogenases, whereas oxidants such as O₂ and nitrate receive electrons from the terminal reductases. There have been 15 primary dehydrogenases and 10 terminal reductases identified (2). However, not all of them are present in the cell at the same time. Expression of a certain combination of the enzymes forming the respiratory chain is tightly regulated at multiple levels to maximize energy production and growth rate (2, 3).

Substrate availability is a major determinant of which terminal reductase is to be expressed. Oxygen is the preferred terminal electron acceptor as it generates the most energy. When oxygen is available, the cell favors aerobic respiration over anaerobic respiration through global regulations by the ArcA/B (Anoxic Redox Control) two-component system and FNR (Fumarate and Nitrate Reduction) protein. During anaerobic respiration, an additional level of control by the Nar two-component system is present to ensure that the respiratory chain using substrates producing the most energy is expressed. For example, nitrate is preferred over fumarate and DMSO, thus nitrate will induce the nitrate respiratory chain, and suppress expression of enzymes of other anaerobic respiratory chains.

The ArcB/A is a two-component system that consists of the membrane sensor kinase ArcB and the response regulator ArcA containing a helix-turn-helix DNA binding motif (4–7). Under anaerobic or reducing condition, ArcB

undergoes ATP-dependent autophosphorylation at His292 (8). The phosphoryl group is then transferred to Asp576 and then His717 of ArcB, which transphosphorylates ArcA at Asp54 (9, 10). The phosphorylated ArcA represses expression of enzymes for aerobic respiration and activates operons encoding proteins for fermentative metabolism (4, 11–13). Furthermore, the autophosphorylation of ArcB is enhanced by anaerobic metabolites (14, 15). Under aerobic conditions, ArcB acts as a phosphatase that is specific for dephosphorylation of ArcA-P, and therefore preventing ArcA from interacting with the DNAs (16, 17). It has been shown that oxidized quinone inhibits the kinase activity of ArcB by disrupting the dimerization via intermolecular disulfide bond (18, 19).

The FNR protein is an important gene regulator that orchestrates the aerobic to anaerobic transition. It regulates the expression of hundreds of genes, including the *dmsABC* operon, to adapt *E. coli* for anaerobic respiration when oxygen is not available (20, 21). The FNR protein functions as an iron-sulfur cluster containing oxygen sensor and exists in three states described here as 4Fe-FNR, 2Fe-FNR and apoFNR (22–26). The 4Fe-FNR protein is active and binds to DNA as dimers, where each monomer coordinates an oxygen labile [4Fe-4S] cluster with four cysteine residues (22, 27–30). It was found that binding of one FNR dimer upregulates gene expression whereas binding of tandem of dimers downregulates it (31, 32). Exposure to oxygen converts the [4Fe-4S] cluster to a [2Fe-4S] cluster, which destabilizes the dimer resulting in inactive 2Fe-FNR monomers that do not bind to DNA or

regulate gene expression (23, 33–35). Long exposure of oxygen results in formation of cluster-free apoFNR (33, 36, 37), which is the inactive and dominant form of FNR found in cells under aerobic growth (24). Both 2Fe-FNR and apoFNR can be degraded by the protease ClpXP at the expense of ATP (38). Tolla *et al.* proposed a model of FNR regulation on the shift between aerobic and anaerobic growth (26). In this model, oxygen deactivation and continual cell production of apoFNR and 4Fe-FNR maintains a constant cycling of FNR between its three states, which is tuned so that the apoFNR predominates under aerobic conditions. Absence of oxygen leads to rapid accumulation of 4Fe-FNR, which dimerizes to form the active transcription factor.

The two homologous Nar systems: the NarX/L and NarQ/P two-component systems, mediate nitrate- and nitrite-regulated gene expression in *E. coli*, respectively (39). Like the ArcB/A two component system, NarX and NarQ are membrane bound sensor kinases/phosphatases, while NarL and NarP are response regulators that binds to DNA (40). In response to nitrate and nitrite, NarX and NarQ will autophosphorylate and transphosphorylate NarL and NarP, respectively (41–43). The phosphorylated response regulators activate operons that encode enzymes for nitrate/nitrite respiration and repress operons for other respiratory chains. For example, phosphorylated NarL activates operons encoding nitrate reductase and related formate dehydrogenase (44, 45), but repress gene expression of DMSO reductase and fumarate reductase (46, 47).

1.3 Biosynthesis of prosthetic groups

1.3.1 Moco

The molybdenum cofactor (Moco) is the prosthetic group common to all molybdoenzymes except nitrogenase (48–50). The simplest form of the cofactor is composed of the metal molybdenum and a pterin group termed pyranopterin (PPT) (Figure 1.2) (commonly termed molybdopterin (MPT) (51, 52) since it was first identified in Moco; however, this type of pterin is also able to coordinate tungsten in tungsten cofactor (53). Therefore, pyranopterin, so named based on the composition of the pterin group, seems to be a more precise terminology (54).) The PPT is a tricyclic system consisting of a pterin group with a fused pyran ring, whose dithiolene provides two sulfur ligands for molybdenum binding (51, 52). In the majority of the *E. coli* molybdoenzymes, including DmsABC studied in this thesis, a single molybdenum is bound to two pterin moieties, each is a PPT variant called pyranopterin guanine dinucleotide (PGD), forming a cofactor termed Mo-bisPGD (50, 55). Each PGD has a guanosine monophosphate (GMP) covalently attached to the pyran ring phosphate of PPT via pyrophosphate linkage (Figure 1.2). The guanine is replaced by cytosine in another variant called pyranopterin cytosine dinucleotide (PCD). The Moco in enzymes belonging to xanthine oxidase family contains a single PCD (48–50). The biosynthesis of Mo-bisPGD cofactor is a sequential occurrence of biosynthesis of PPT followed by insertion of molybdenum, and eventually attachment of GMP (50, 56) (Figure 1.3).

The synthesis of PPT is a two-step process carried out by proteins encoded by operon *MoaABCDE*. First, 5'-GTP is converted to cPMP facilitated by MoaA and MoaC (57, 58). MoaA is a S-adenosylmethionine (SAM)-dependent enzyme that binds and activates GTP to form reactive radical intermediates (57, 58). MoaC is believed to be involved in the cleavage of the pyrophosphate from the intermediate and formation of the cyclic phosphate group of cPMP (59, 60). The next step is to insert two sulfur atoms at the C1' and C2' positions of cPMP by the MPT synthase, which is a heterotetramer consisting of two small (MoaD) and two large (MoaE) subunits (61–63). The MoaE protein contains the cPMP binding pocket, into which the C-terminus of adjacent MoaD is also inserted (64, 65). The thiocarboxylate group on the C-terminus of the activated MoaD (MoaD-SH) donates the sulfur atom to cPMP for the formation of dithiolene group in PPT (62, 63). It is very important to regenerate MoaD-SH for MPT synthase to act catalytically. MoeB has been identified as the MPT synthase sulfurase (66, 67). MoeB catalyzes the adenylation of MoaD and forms a complex with the activated MoaD (68). IscS (see section 1.3.2) with enzyme-bound persulfide interacts with the MoaD-MoeB complex and functions as the sulfur donor (69, 70).

After the synthesis of the PPT, molybdenum is inserted into the cofactor facilitated by MoeA and MogA in *E. coli*. Under physiological molybdenum concentration, MogA is essential to activate the PPT by adenylation to form PPT-AMP intermediate that is competent for molybdenum insertion mediated by MoeA (71–74). Molybdenum uptake is

carried out by ModABC, which function as an ATP-binding cassette (ABC) transporter (75, 76).

The final step in Mo-bisPGD biosynthesis is the attachment of GMP from GTP to the C4' phosphate of PPT facilitated by MobA (77, 78). MobA is essential and sufficient for this reaction (77, 79), while the function of the other *mob* gene product, MobB, is still unknown. It is still unclear whether the bis-PGD is assembled on MobA or at the cofactor binding sites of the molybdoenzymes (50). The crystal structure of the octameric form of MobA showed a central channel that is lined with hydrophilic residues and wide enough to accommodate bis-PGD (77). This makes MobA a possible candidate for bis-PGD binding and its storage prior to insertion into the apoprotein. Furthermore, TorD has been shown to be able to interact with Mo-PPT (precursor of Mo-bisPGD) and MobA in addition to apoTorA (80). It was suggested that this type of system-specific chaperone might have a role in the last step of Mo-bisPGD cofactor biosynthesis by bringing all the components close together.

Moco biosynthesis is closely regulated by the cell's requirement for Moco and molybdenum availability. The *moaABCDE* operon is the main target for transcriptional and translational regulation (50, 81). Expression of this operon is enhanced under anaerobic conditions governed by the FNR protein (81, 82). Molybdate-bound ModE binds to the *moa* promoter region and upregulates transcription of the operon (81). Additionally, the ModE-molybdate complex is a positive regulator for transcription of

molybdoenzymes such as DmsABC and NarGHI (83), and a transcription repressor of the *modABCD* operon to prevent excess molybdate uptake (84). In addition to controls by ModE and FNR, there is also a RNA motif upstream of the *moa* operon that functions as a riboswitch, which senses Moco and controls gene expression (85).

1.3.2 Iron-sulfur clusters

Iron-sulfur, [Fe-S], clusters are functionally versatile prosthetic groups ubiquitously found in all living organisms (86–88). In addition to their primary role in electron transfer, they also carry out functions including substrate binding and activation, sensing of reactive species, regulation of gene expression and enzyme activity, controlling protein structure in vicinity, coupling electron and proton transfers, disulfide reduction and sulfur donation (87, 89). The most common forms of simple iron-sulfur clusters are [2Fe-2S] and [4Fe-4S] (Figure 1.4), in which the Fe ions are linked by sulfide bonds and coordinated by sulfhydryl groups of four Cys residues of the protein. The [3Fe-4S] cluster is a variant of the [4Fe-4S] cluster and one of the Cys ligands is replaced by an Asp, His, Trp or Ser (89).

The biosynthesis of iron-sulfur clusters is carried out by three distinct machineries: NIF (nitrogen fixation), ISC (iron-sulfur cluster formation) and SUF (sulfur mobilization). In *E coli*, the ISC system is the primary housekeeping machinery for assembly of simple [Fe-S] clusters (90), while the SUF system functions under stress conditions such as oxidative stress

and iron starvation (91, 92). All these systems share a common mechanism, which involves a cysteine desulfurase (NifS, IscS and SufS) that uses cysteine as the sulfur donor and a scaffold protein (U-type: NifU, IscU and SufU; A-type: IscA and SufA) that provide the site for cluster assembly and transfer of the formed cluster to the target apoprotein (87, 88, 93, 94) (Figure 1.5). The cysteine desulfurase is a pyridoxal phosphate-dependent enzyme that catalyzes decomposition of L-cysteine and forms an enzyme-bound cysteine persulfide with the liberated sulfur (95–97). The proteins and molecules that donate iron to the scaffold proteins remain unclear. The delivered iron and sulfur form a [Fe-S] cluster at the scaffold proteins, which have three conserved cysteine residues for cluster ligation (88, 94, 98). While it is clear that the U-type proteins function primarily as scaffold proteins, A-type proteins may have additional roles in [Fe-S] cluster biosynthesis. IscA was suggested to be an alternative scaffold that also mediates cluster transfer from IscU to the target apoprotein (99). IscA has also been suggested to be the iron donor for IscU (100, 101). To transfer the preformed cluster to its target, the holo-scaffold protein first forms a complex with the apoprotein and then performs transfer through cysteine thiol exchange with the free cysteine thiols of the target protein (88). The apo-scaffold eventually dissociates from the holoprotein (88).

There are also other components that are important for [Fe-S] cluster assembly. HscA that interacts with IscU (102) and SufC of the SufBCD complex exhibit ATPase activities, which are enhanced by interactions with

HscB (103, 104) and SufB (105), respectively. In the Isc system, bacterial ferredoxin was demonstrated to donate electrons to reductively fuse two [2Fe-2S] cluster to form one [4Fe-4S] cluster at IscU (106). *E. coli* CyaY was shown to function as an iron donor for iron-sulfur cluster assembly on IscU (107).

1.4 Translocation and targeting of folded complex enzyme

1.4.1 *tat*-transport

The twin-arginine translocation (*tat*) pathway transports fully-folded proteins across biological membranes. It is widespread in bacteria, archaeobacteria and plants but absent in the majority of eukaryotic organisms including humans. In bacteria, the *tat* machinery exports a huge variety of proteins from the cytoplasm across the cytoplasmic membrane. The *tat* system is crucial for many functions such as anaerobic respiration, quorum sensing and motility, cell envelope remodeling and virulence (108–110).

The proteins to be exported by the *tat* pathway are characterized by a “SRRXFLK” twin arginine motif in their signal peptide at the N-terminus (111). In *E. coli*, the Tat translocase is a complex of the Tat A, B and C proteins (Figure 1.6 left panel). *E. coli* also contains TatE which is a paralogue of TatA; they have overlapping function and can partially substitute for each other (112). The TatBC complex recognizes the twin arginine motif and binds the signal sequence deep in its binding-pocket (110, 113). The substrate protein is then laterally transported to the protein-conducting pore formed by TatA

next to the TatBC complex. A recent study by Fröbel *et al.* demonstrated that the interaction with the Tat translocase, which involves initial contact with TatA, is driven by the proton motive force (110, 114). The pmf-dependent recruitment of TatA proteins and progressive oligomerization form the transmembrane path to export folded proteins. Gohlke *et al.* constructed a 3D image of the TatA homo-oligomer using single-particle electron microscopy. This oligomer forms a protein-conducting channel of various diameters to accommodate proteins of different sizes (115). However, the model of TatA homo-oligomer forming a protein-conducting channel in the vicinity of TatBC complex has been challenged by several findings. TatBC complex has usually been found to contain TatA, which functions to stabilize the complex (116). There has been observation of a homo-oligomer of TatB that encapsulates the folded mature domain of the substrate (117). Translocation of the protein by Tat translocase can occur even when its signal sequence is covalently bound to TatC (118). These findings suggest that TatB and TatC are present in the pore structure. An alternative model against the pore structure also remains possible. This model suggests that the proteins directly pass through the membrane destabilized by accumulation of TatA monomers in the vicinity of the TatBC complex (119) (Figure 1.6 Right Panel).

In contrast to the Sec pathway, which transports the nascent peptide across the membrane, the *tat* pathway needs a quality control system to prevent export of proteins that have not been folded or assembled properly.

A large group of *tat*-translocated proteins are redox enzymes that require insertion of cofactors whose biosynthesis and insertion machinery are in the cytoplasm. The protein of interest in this thesis, *E. coli* DmsABC, is one of these proteins. For DmsABC to function, both DmsA and DmsB have to be translocated to anchor on the periplasmic side of the membrane. However only DmsA contains the *tat* signal sequence at its N-terminus. This is an example of a situation where proper assembly of the subunits has to occur before translocation. A family of system-specific chaperones has been shown to act as proofreading chaperones that coordinate maturation and targeting of these redox enzymes. Well-characterized examples such as TorD for TMAO reductase (TorA) and DmsD for DmsABC will be discussed in sections 1.4.2 and 1.5.4, respectively. In addition to the proofreading chaperones, an intrinsic quality control function has been suggested for Tat translocase. Studies using model *tat* substrates have clearly demonstrated that the folded state, rather than recognition of the *tat* signal sequence, dictates whether a protein is translocated via the *tat* pathway. For example, alkaline phosphatase (PhoA) fused to a *tat* leader peptide is only exported when correctly folded by disulfide bond formation under oxidizing conditions (120–122). Cytochrome c is normally exported via the Sec pathway in its unfolded state, however a variant with a fused *tat* signal sequence is transferred by the *tat* machinery after heme insertion and folding (123). How the Tat translocase can reject incompatible substrate remains a question needing further investigation. Site-specific cross-linking by Panahandeh *et al.*

(122) showed that the signal sequence of unfolded TorA-PhoA could not insert into the TatBC-binding pocket although it physically interacts with the Tat complex. Matos *et al.* demonstrated the *tat*-dependent degradation of an improperly assembled *tat* substrate. Mutations that interfere with proper assembly of FeS proteins completely block *tat*-dependent export. The mutants are rapidly degraded only when the FeS proteins can interact with the Tat translocase (124). The total surface area of a *tat* precursor also seems to play a role. Unstructured *tat* signal-containing peptides not exceeding a length of 100-120 amino acids can be translocated by the Tat translocase if they do not contain any hydrophobic residues (125).

1.4.2 System-specific Chaperones

Protein-specific chaperones are essential for maturation of enzymes in the DMSO reductase family in multiple ways including assisting cofactor insertion, protection of apoproteins and coordinating maturation and targeting (126). Important examples of this family of chaperones include TorD for TorA (periplasmic TMAO reductase), NarJ for NarG (nitrate reductase (NarGHI)) and DmsD for DmsA (DMSO reductase (DmsABC)) from *Escherichia coli*.

The presence of NarJ, encoded by the *narGHJI* operon, is directly required for insertion of the FSO cluster and Mo-bisPGD cofactor into NarG in the cytoplasm and indirectly required for the maturation of NarI in a time-dependent fashion (127, 128). NarJ interacts at two distinct sites of

apponitrate reductase (129). The interaction between the chaperone and an unknown site is believed to be crucial for the protein interactions between the apoNarG and the molybdenum cofactor biosynthetic proteins (130). The interaction of NarJ with the N-terminal tail, especially the hydrophobic interactions with the helical N-terminal NarG peptide (1-15), prevents premature membrane anchoring of the apoenzyme (131). This maintains the apoenzyme in its soluble form, which is competent for cofactor insertion, and allows time for NarI to be fully matured (128, 129). It is notable that NarJ interacts with the N-terminal tail of NarG in a *tat* system dependent fashion although NarGH is not translocated across the membrane (132).

Another example is TorD, which has two roles. It facilitates the maturation of TorA by binding to apoTorA and altering its conformation to make it competent for molybdenum cofactor insertion (133–135). TorD also promotes TorA activation as the binding of TorD protects the apoTorA from proteolytic degradation when molybdenum cofactor is limiting or at elevated temperatures (42°C) (135, 136). It has also been shown that TorD can bind the molybdenum cofactor and may interact with the cofactor biosynthesis protein MobA (80). Another function of TorD is to mediate “proofreading” to prevent export of immature apoTorA through the *tat* system (137, 138) by binding to the TorA signal sequence independent of the twin-arginine motif (126, 139–141). It is important to note that deletion of the signal sequence of TorA has no effect on TorD’s ability to facilitate molybdenum cofactor insertion and TorD has another binding site on the mature domain of TorA

(139, 142). Therefore, TorD, like NarJ, binds apoTorA at two distinct sites and its two roles are independent. It was shown that TorD is a GTP binding protein (140) and the intrinsic GTPase activity of TorD has also been studied (143). Considering the involvements of TorD in multiple steps of TorA maturation, it was proposed that the interactions between TorD and its substrates are regulated by GTP hydrolysis. DmsD from *E. coli* will be discussed in section 1.5.4.

1.5 DMSO reductase

1.5.1 Overview

Dimethyl sulfide (DMS) is a volatile natural sulfur compound that is a major intermediate in the global sulfur cycle and plays an important role in global climate control (144). DMS is generated by degradation of dimethylsulfoniopropionate or reduction of DMSO.

In the absence of oxygen and nitrate, DMSO reductase (DmsABC) is the sole terminal reductase responsible for anaerobic growth of *E. coli* on DMSO. It is a heterotrimeric protein comprised of a catalytic subunit (DmsA) with Mo-bisPGD cofactor in the active site, a four iron-sulfur cluster containing electron transfer subunit (DmsB), and a membrane anchoring subunit (DmsC) with a quinol-binding site (Q-site) (Figure 1.7). The non-structural protein, DmsD, functions as a system-specific chaperone that aids the maturation of DmsABC. Oxidation of menaquinol to menaquinone at the Q-site is coupled to reduction of DMSO to DMS at the DmsA active site via an

electron transfer relay (ETR) formed by the [4Fe-4S] clusters. Enzymatic turn-over by DmsABC is electroneutral and does not generate a proton gradient across the membrane (145).

1.5.2 The *dms* Operon

The *dms* operon is located at 20 minutes on the *E. coli* chromosome. It has three open reading frames encoding polypeptides of DmsA, B and C, sequentially from 5' to 3'. DmsD is encoded by the *ynfI* (*dmsD*) open reading frame of the *ynfEFGHI* operon which is a paralogue of the *dms* operon (146, 147).

Gene expression of *dmsABC* is governed by the availability of oxygen, nitrate and molybdenum through regulation by the FNR protein, the NarX/L two-component system and the ModE protein (47, 83, 148). The availability of the enzyme's substrates, such as DMSO or TMAO, has no effect on its transcription (47). There are two promoters: P1 and P2, for the transcriptional start site (83). Both FNR and phosphorylated NarL bind to the upstream of P1 (148). Binding of FNR initiates transcription under anaerobic condition, whereas binding of NarL in response to nitrate prevents binding of FNR and RNA polymerase and thus represses transcription of *dmsABC* (39, 47, 148). The predominant repression by phosphorylated NarL over FNR activation maintains the respiratory hierarchy where nitrate is preferred over DMSO for maximum energy production and growth. The ModE protein binds upstream of the P2 promoter and is essential for FNR and NarL

regulation of *dmsABC* expression (47, 83). It also regulates the *modABCD* and *moaABCDE* operons, which functions in molybdate uptake and Moco biosynthesis (see Section 1.3.1).

1.5.3 DmsA

E. coli. DmsA (EcDmsA) is the catalytic subunit (90.4 kDa precursor; 85.8 kDa mature) with a Mo-bisPGD cofactor in its active site, where dimethyl sulfoxide (DMSO) is reduced to dimethyl sulfide (DMS) (149, 150)(Figure 1.7 Bottom). The oxo group is transferred in exchange of two electrons from the electron transfer relay (ETR), and is released from the enzyme complex in form of water. Figure 1.8 is the catalytic mechanism of *Rhodobacter* DMSO reductase proposed by Johnson *et al.*, which should be very similar to the mechanism of *E. coli* DMSO reductase (55). DmsA also contains a [4Fe-4S] cluster called FS0 (Chapter 2) that is coordinated by four highly conserved Cys residues (Cys18, 22, 26 and 59) in the N-terminus of mature DmsA. The premature form of DmsA has a N-terminal leader sequence, also called the *tat* leader since it contains a twin-arginine motif with consensus sequence of SRRXFLK (111, 151). It has been demonstrated that the *tat* leader of DmsA has multiple roles in the enzyme maturation pathway: it is the binding site for the system-specific chaperone (DmsD); it is the signal peptide for translocation via the *tat* machinery; and it is essential for assembly and protein stability of precursor DmsA in the cytoplasm (111, 151, 152).

Molybdenum-containing enzymes have been divided into three families based on the structures of the molybdenum cofactors in their active sites: the xanthine oxidase (XO) family, the sulfite oxidase (SO) family and the DMSO reductase (DMSOR) family (48, 50) (Figure 1.2). DmsA belongs to the DMSOR family in which the pterin cofactor forming the Moco is a tricyclic system consisting of a pterin group with a fused pyran ring whose phosphate group is attached to a guanosine monophosphate via a pyrophosphate bond. This pterin cofactor is called pyranopterin guanine dinucleotide (PGD). The pyran ring also has two sulfur atoms attached in a dithiolene linkage that coordinate the Mo atom. The pyran ring is attached to an H (monophosphate form) in the SO family or a cytosine nucleotide in the XO family (50). A stable and fluorescent oxidized derivative of the pterin cofactor, Form A, can be formed by acidification in the presence of iodine and boiling (153). This is experimentally important in assaying the molybdenum cofactor content in this study. In DmsA, the Mo atom is coordinated by two pterin cofactors, namely the P-PGD (proximal to the active site) and the Q-PGD (distal to the active site); there is only one pterin cofactor in the other two families (48, 50, 55, 154). The Mo atom is hexacoordinated by the two cis-dithiolenes (a total of four sulfurs) and two other ligands from the amino acid (DmsA-Ser160) and substrates. Some proteins such as TMAO reductase can function with either tungsten (W) or molybdenum (Mo) coordinated by the pterin cofactors in the active site (155). Supplementation of the minimal growth medium with high levels of W to compete with endogenous Mo however

results in the assembly of an inactive apo-DMSO reductase lacking the metal cofactor (150).

Potentiometric titration and Electron Paramagnetic Resonance (EPR) spectroscopy have determined the midpoint potentials for the Mo (VI/V) and Mo (V/IV) transitions to be -15mV and -175mV, respectively (156). Protein film voltammetry studies were used to show that the enzyme activity is maximal within a narrow window of electrode potential that coincides with the appearance of the Mo (V) species (157). Heffron *et al.* further determined that the one-electron transfer processes at the Mo cofactor function as “switches” that turn the enzyme off beyond the critical potentials and separate the three distinct states of the enzyme. This is called “tunnel diode” behavior. It was also proposed that the most influential step during catalysis is the reduction of Mo(V) to Mo(IV)-H⁺ (157).

The only DmsA structures determined are crystal structures of the periplasmic DmsA of *Rhodobacter sphaeroides* and *Rh. capsulatus* (RhDmsA) (158–161). Since RhDmsA and EcDmsA share significant sequence similarity (46% similar, 30% identical), RhDmsA may serve as a model for understanding the structure of EcDmsA. The RhDmsA is composed of four domains and contains a Mo-bisPGD cofactor in its active site but no FSO (Figure 1.9). Domains I, II and III encircle a deep funnel/cleft leading to the molybdenum-binding site (159, 160). DMSO is bound in a channel, with dimensions of approximately 10Å wide and 8 Å deep, connecting the base of the active cleft and the Mo atom (161). Residues 384 to 390 are seen in the

cleft leading to the active site and Trp388 forms a lid trapping the substrate (161). Domain II and III are the dinucleotide-binding domains. Domain IV is on the other side of the protein opposite to the active cleft, and interacts with the pterin moieties (158, 160). Domain IV is also where the FS0 cluster in EcDmsA is predicted to be located and it includes the contact point with DmsB.

E. coli DMSO reductase has been shown to have a broad substrate specificity and it can reduce a variety of S- and N-oxides in addition to DMSO (162). Extensive kinetic analyses have shown that substrate affinity has a primary role in determining enzyme specificity as K_m values vary 470-fold while K_{cat} values vary only 20-fold for the 22 substrates tested. Sulfoxides and pyridine N-oxide exhibited the lowest K_m values, followed by aliphatic N-oxides (162). It was also shown that the substrate specificity relies on how well the substrate can be accommodated by the tunnel leading to the active site (158, 162). Mutagenesis analysis by Simala-Grant and Weiner further identified amino acids that are part of the active site funnel and important in substrate binding and catalysis (163). These are Thr132, Gly151, Ala162, Gln163 and Arg201. Variants Ala162Gln and Arg201Gln caused at least a 35-fold change in the K_m values, while the Thr132Ser variant caused a more moderate change in both K_m and K_{cat} values (163).

1.5.4 DmsB

DmsB is the 22.7 kDa electron transfer subunit of *E. coli* DMSO reductase. It interacts with DmsA to form the catalytic dimer, and its C-terminal region interacts with DmsC to attach DmsAB to the cytoplasmic membrane (149). The ETR in DmsB connects the Mo-bisPGD active site and the Q-site. DmsB contains 16 highly conserved Cys residues that are arranged in 4 groups and serve as ligands for four [4Fe-4S] clusters (20, 164). In each group, the four Cys residues are arranged in a consensus sequence of $C_A-X_2-C_B-X_n-C_C-X_n-C_D$, which resembles the typical Cys motif found in bacterial ferredoxins. Models for ferredoxins-like Cys groups indicate that the [4Fe-4S] cluster is coordinated by the first three Cys residues ($C_{A,B,C}$) from one group and the terminal Cys (C_D) from another group (165, 166) (Figure 1.10). DmsB is highly homologous to FdnH and NarH, which are the electron transfer subunits of formate dehydrogenase-N (FdnGHI) and nitrate reductase (NarGHI), respectively. While FdnH also contain four [4Fe-4S] clusters (167), NarH contains three [4Fe-4S] clusters and one [3Fe-4S] cluster, which is coordinated by three Cys residues and a Trp at the position of C_B (168, 169). The four [4Fe-4S] clusters of DmsB form the ETR facilitating rapid electron transfer. They are named FS1-4, with FS1 being closest to the Mo-bisPGD cofactor and FS4 being closest to the Q-site. The midpoint potentials (E_m) of the [Fe-S] clusters in DmsB were determined to be -50mV (FS4), -120mV (FS3), -330mV (FS2), and -240mV (FS1) (164).

Sequence comparison shows that the Cys residue in DmsB that is equivalent to the Trp residue coordinating the [3Fe-4S] cluster in NarH, is DmsB-Cys102 of the Group III cysteine motif (164). Mutations of Cys102 to Trp, Ser, Tyr and Phe resulted in the assembly of a [3Fe-4S] cluster in place of the [4Fe-4S] cluster in the wild-type enzyme (170, 171). This cluster had an E_m value of ~ 275 mV (172). All the Cys102 variants were unable to support anaerobic growth on DMSO (170). Analysis of the EcDmsB EPR spectra allowed assignment of the E_m -50 mV signal to the [4Fe-4S] cluster with Cys102 as a coordinating ligand (170). This cluster receives electrons directly from menaquinol oxidation and corresponds to FS4 of the ETR in DmsB. Rothery and Weiner pointed out that the FS4 cluster is conformationally and functionally linked to the MQH₂ binding site in DmsC (171). A mutagenesis study on the residues surrounding the FS4 cluster showed that positively charged residues are responsible for fine-tuning the E_m of the [Fe-S] cluster by approximately 15-25 mV per charge (172). Furthermore, Pro80, Ser81 and Tyr104 of DmsB have been shown to be important for MQH₂ binding and oxidation; in particular the Tyr residue plays a major role in controlling the redox properties of FS4 and communication with the Q-site (172).

1.5.5 DmsC

DmsC is the 30.7 kDa, membrane intrinsic subunit that is necessary for DmsAB anchoring, stability and functional electron transport (149).

Expression of DmsAB in the absence of DmsC leads to accumulation of catalytic dimers in the cytoplasm, that are thermolabile and only catalytically active with artificial electron donors (149, 173). DmsC contains a quinol-binding site, where menaquinol (MQH₂) is oxidized to menaquinone (MQ) and two electrons are donated to the electron transfer relay of the enzyme (149, 171, 174). Despite the low sequence homology, the DmsC subunit resembles the membrane anchoring FrdCD subunits of fumarate reductase, which carry out similar functions. The most important similarity is the presence of a His residue at the membrane interface that is important for quinol binding and oxidation in both enzymes (171, 175, 176).

A model of DmsC has been constructed using *phoA* (alkaline phosphatase) and *blaM* (β -lactamase) gene fusions and hydrophobicity analysis (174) (Figure 1.11). The model indicated that DmsC is comprised of eight transmembrane α -helices connected by three relatively large periplasmic loops (P1-P3) and four small cytoplasmic loops (C1-C4), with both amino and carboxyl termini exposed to the periplasm (20, 174). The overall distribution of Arg + Lys residues is three on the periplasmic side and eight on the cytoplasmic side, which agrees with the positive inside rules of von Heijne (174, 177). It was further emphasized that the entire DmsC polypeptide is required for membrane anchoring of DmsAB, as truncation of DmsC results in accumulation of DmsAB in the cytoplasm (174).

Three menaquinol analogues have been found to bind the Q-site, and their optical, solubility and redox properties make them suitable for studies

of the enzymology of *E. coli* anaerobic reductases. Two hydroxylated naphthoquinols: reduced plumbagin (PBH₂, 5-hydroxy-2-methyl-1, 4-naphthoquinol) and reduced lapachol [LPCH₂, 2-hydroxy-3-(3-methyl-2-butenyl)-1, 4-naphthoquinol], act as substrates; but only LPCH₂ is a good substrate for DMSO reductase (178). 2-n-heptyl-4-hydroxyquinoline N-oxide (HOQNO), the other menaquinol analogue, binds to the DmsC Q-site with 1:1 stoichiometry and a dissociation constant of 6nM (179). It acts as an inhibitor for MQH₂ oxidation. A single mutation of DmsC-His65 to Arg blocks HOQNO binding and indicates that there is a single Q-site in DmsC (179). The membrane anchor of nitrate reductase, NarI, has two hemes whereas DmsC lacks cytochromes or any other redox active cofactor. This means that electrons from MQH₂ oxidation have to be directly transferred to the [Fe-S] cluster in DmsB concomitantly with MQH₂ oxidation. This has been supported by the demonstrated conformational and functional link between the Q-site and the FS4 cluster and the important role of several DmsB residues in MQH₂ binding and oxidation (see section 1.5.4) (171, 172).

Mutagenesis studies have identified two residues: His65 and Glu87, to be important for the function of DmsC. His65 is placed near the periplasmic surface of the membrane by the topology model of DmsC (174). Mutation of His65 to Arg abolished MQH₂ oxidation and disrupted the conformational link between the Q-site and FS4 cluster (171). It was suggested that DmsB-Cys102 and DmsC-His65 are in close proximity in the holoenzyme, both facilitating the interactions between the Q-site and FS4 cluster (171).

Mutations of Glu87 to Lys and Gln rendered the enzyme inactive and significantly reduced/abolished HOQNO inhibitor binding. Variant DmsC-Glu87Asp on the other hand behaved as a wild-type enzyme. This suggests that Glu87 acts as a proton acceptor in the Q-site (180).

1.5.6 DmsD

DmsD was first purified as one of proteins that binds to the twin-arginine leader of DmsA (181). It is encoded by the *ynfI* reading frame of the *ynfEFGHI* operon. DmsD has been found to be a chaperone necessary for DmsABC maturation (147, 152). DmsD has also been found to bind to the precursor form of TorA (152). However, the TorA and DmsA leader sequences are not completely functionally interchangeable. TorA leader can rescue membrane targeting but not proper assembly of the protein when fused to DmsA (151).

Purified DmsD can be found mainly in three forms: monomer, dimer, and a heterogeneously folded monomer with multi-conformations, which displayed a ladder of bands on native-PAGE (ladder form) (182). All three folding forms of DmsD bind to the leader sequence equally in 1:1 molar ratio with a dissociation constant of 0.22 μM (183). This is strong binding comparable to the interactions of TorA-TorD and NarG-NarJ with dissociation constants of 1.7 μM (140) and 0.16 μM (184), respectively.

Two crystal structures of the *E. coli* DmsD, one with resolution of 2.0 Å (Figure 1.12A, PDB 3EFP) and the other with resolution of 2.4Å (PDB 3CW0)

were published in 2009 (185, 186). The two structures are essentially identical. Both structures show evidence for the existence of a hydrophobic groove on the surface of DmsD that function as a putative binding pocket for the DmsA leader peptide. Mutagenesis studies by Chan *et al.* predicted several residues that are crucial for binding of the DmsA leader peptide to DmsD. They predicted the position of a “hot pocket” of residues for leader binding on the surface of the model DmsD structure from *Salmonella typhimurium* (187, 188) (Figure 1.12B). Using docking and molecular dynamics simulation experiments, Stevens *et al.* proposed a model for the mechanism of recognition of DmsA leader by DmsD, suggesting intimate interactions between the conserved twin-arginine motif and DmsD (186).

Although DmsD binds to the *tat* leader of DmsA, DmsD is not required for *tat*-dependent translocation of proteins with DmsA leader sequence. A chimera of DmsA-GFP can be transported into the periplasm as effectively in $\Delta dmsD$ mutant as in the wild-type (147). It was shown that DmsD is retained in the cytoplasm in a $\Delta TatABCDE$ strain, while it is localized to the inner membrane of wild-type *E. coli* (189). Papish *et al.* further showed that this interaction with the membrane-associated Tat translocase requires interaction with the TatB and TatC subunits. This interaction however does not depend on the presence of DMSO reductase (189). The membrane localization of DmsD is also affected by the growth conditions such that it is found membrane-associated under anaerobic conditions but primarily in the cytoplasm under aerobic conditions (189).

DmsD has been classified as a member of a family of TorD-like system-specific chaperones or redox-enzyme maturation proteins (REMP). It was suggested that DmsD acts as a chaperone assisting DmsA maturation (147) in a similar manner as TorD assists the assembly of TorA (133, 134). A recent study suggested that DmsD can have interactions with both general molecular chaperones (including DnaK and GroEL) and proteins in Moco biosynthesis pathway (including MoeB, MobB and MoeA) (190). Unlike NarJ and TorD, which have been found to interact with proteins involved in late stages of Moco biosynthesis and insertion, DmsD might also have a role in the early stage of Moco biosynthesis through interaction with MoeB. However, there is an important difference between DmsD and other members of the REMF family. Both TorD and NarJ bind to a second site on the mature portion of their cognate partner, assisting cofactor insertion. However, there has not been any direct evidence that DmsD interacts with the mature part of DmsA.

1.5.7 Topology of DmsABC

Although there has been a long time debate about the subcellular orientation of DmsABC, it is now generally accepted that the catalytic dimer (DmsAB) is translocated across the membrane via the *tat* pathway and anchors to DmsC in the membrane at the periplasmic side. Computational and biochemical evidence have become available to support the periplasmic location of DmsAB. The highly conserved residues, which should be important for subunit-subunit interactions, are concentrated in the

periplasmically-oriented loops in the predicted model of DmsC (174, 191). The mutagenesis studies on residues around FS4 of DmsB and Q-site defining residues in DmsC provided further support of the idea (171, 172, 180). His65 and Glu87 of DmsC are important Q-site residues (171, 180) and are predicted to be on the periplasmic side of the membrane in the model (174). This means that the Q-site is probably close to the periplasm/membrane interface. It was also shown that there is a conformational and functional link between the FS4 cluster and the Q-site (171, 172), suggesting that FS4 is in vicinity of the Q-site, therefore likely on the periplasmic side of the membrane. Furthermore, the enzymatic turn-over process of DmsABC does not generate a pmf. (145). This means the active site of the enzyme should be in the periplasm so that it can make use of the protons equivalent to those released from menaquinol oxidation. The lack of evidence for the presence of any heme groups that could function to transfer electrons or proton across the membrane also supports the idea that the DmsB and the Q-site are on the same side of the membrane (191). All the above implications of periplasmic location of DmsAB were however made based on the assumption that the topology model of DmsC predicting the location of the Q-site was correct.

Direct biochemical evidence for the periplasmic location of DmsAB has also been obtained. In a $\Delta dmsC$ mutant with in-frame deletion of chromosomal *dmsC* and expressing DmsAB at physiological level, DmsA's reductase activity and hexahistidine-tagged DmsB are mainly found in the periplasm, suggesting that DmsAB is attached to DmsC on the periplasmic

side of the membrane (192). This prediction was further supported with activity assays using membrane impermeant TMAO as substrate (192). The BVH-dependent TMAO reductase activities measured for intact whole cell was not increased by membrane disruption, indicating the TMAO reduction was carried out in periplasm.

1.6 Thesis Objectives

It is believed that Moco insertion is the last step before targeting of the mature protein to its site of function in the maturation pathway of complex molybdoenzymes. The insertion of cofactor into the apoprotein often induces a conformational change that signals the formation of the mature protein. This is important for making the mature protein suitable for interaction with the transport mechanism if the enzyme is exported. *E. coli* DmsABC, along with another closely related enzyme EcNarGHI, is an interesting exception such that the apoprotein can be stably assembled and targeted to the cytoplasmic membrane. This thesis will investigate the effects of DmsA mutants on cofactor insertion to better understand the mechanisms and role of Mo-bisPGD assembly in maturation pathway of molybdoenzymes.

The objectives of this thesis were:

1. Demonstrating direct evidence for the presence of FS0 close to Mo-bisPGD cofactor in DmsA.

2. Elucidation of the interplay between FSO assembly and Mo-bisPGD cofactor insertion.
3. Characterization of a mutant whose protein folding, translocation and membrane targeting is cofactor dependent.
4. Construction of a model for the maturation pathway of DmsABC.

1.7 Figures

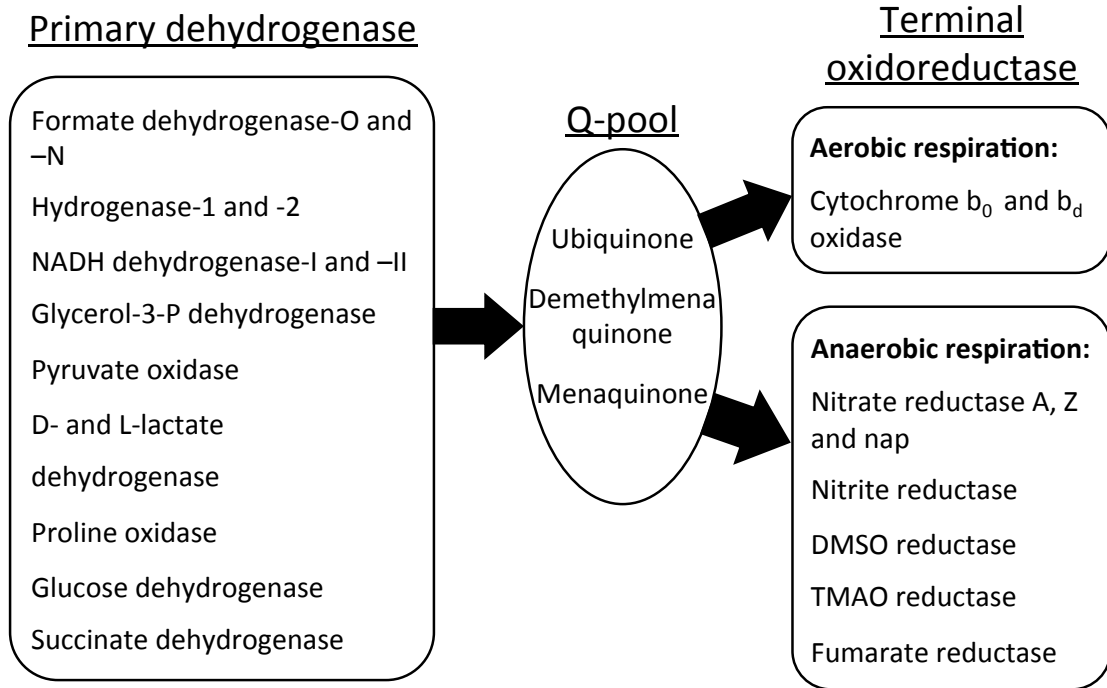


Figure 1.1 The *E. coli* respiratory chain. Primary dehydrogenase and terminal reductase are connected by the membrane soluble quinone pool to form the respiratory chain. The expression of the enzymes is regulated by environmental conditions and substrate availability to maximize energy generation and growth rate. The arrows in the diagram indicate the direction of the electron flow in the respiratory chain.

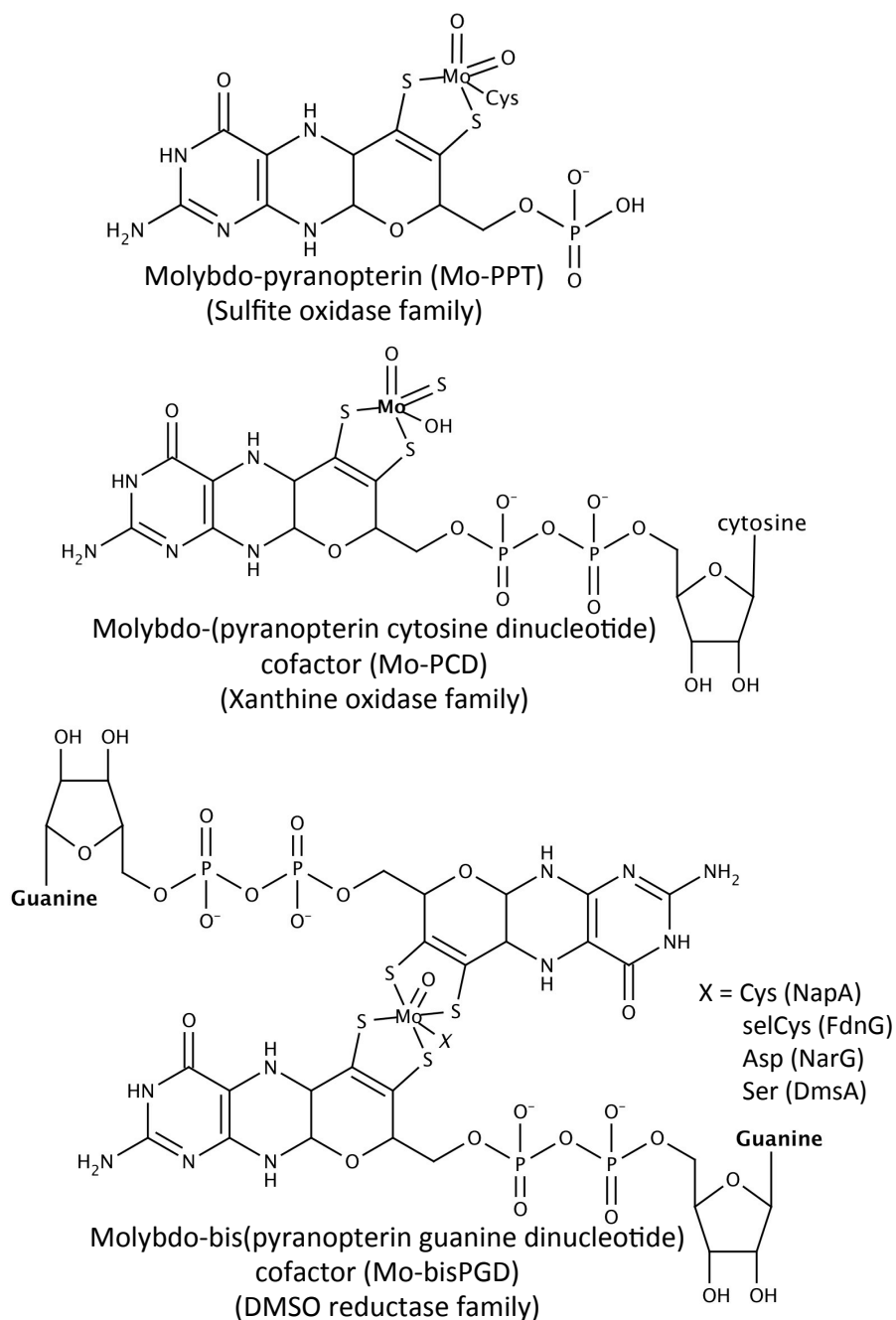


Figure 1.2 Molybdenum cofactors (Moco). The pterin cofactor of the Moco is a tricyclic system consisting of a pterin group fused to a pyrano ring, which ligates the Mo atom with its dithiolene sulfurs. The phosphate group of the pyrano ring is also attached to different R groups: H for Mo-PPT, CMP for Mo-PCD, and GMP for bisMo-PGD. These three forms of Moco are found in molybdoenzymes classified into three families, sulfite oxidase (SO) family, xanthine oxidase (XO) family, and DMSO reductase family, respectively. Chemical structures were drawn using MarvinSketch 5.9.4 (Marvin, 2012, ChemAxon, <http://www.chemaxon.com>).

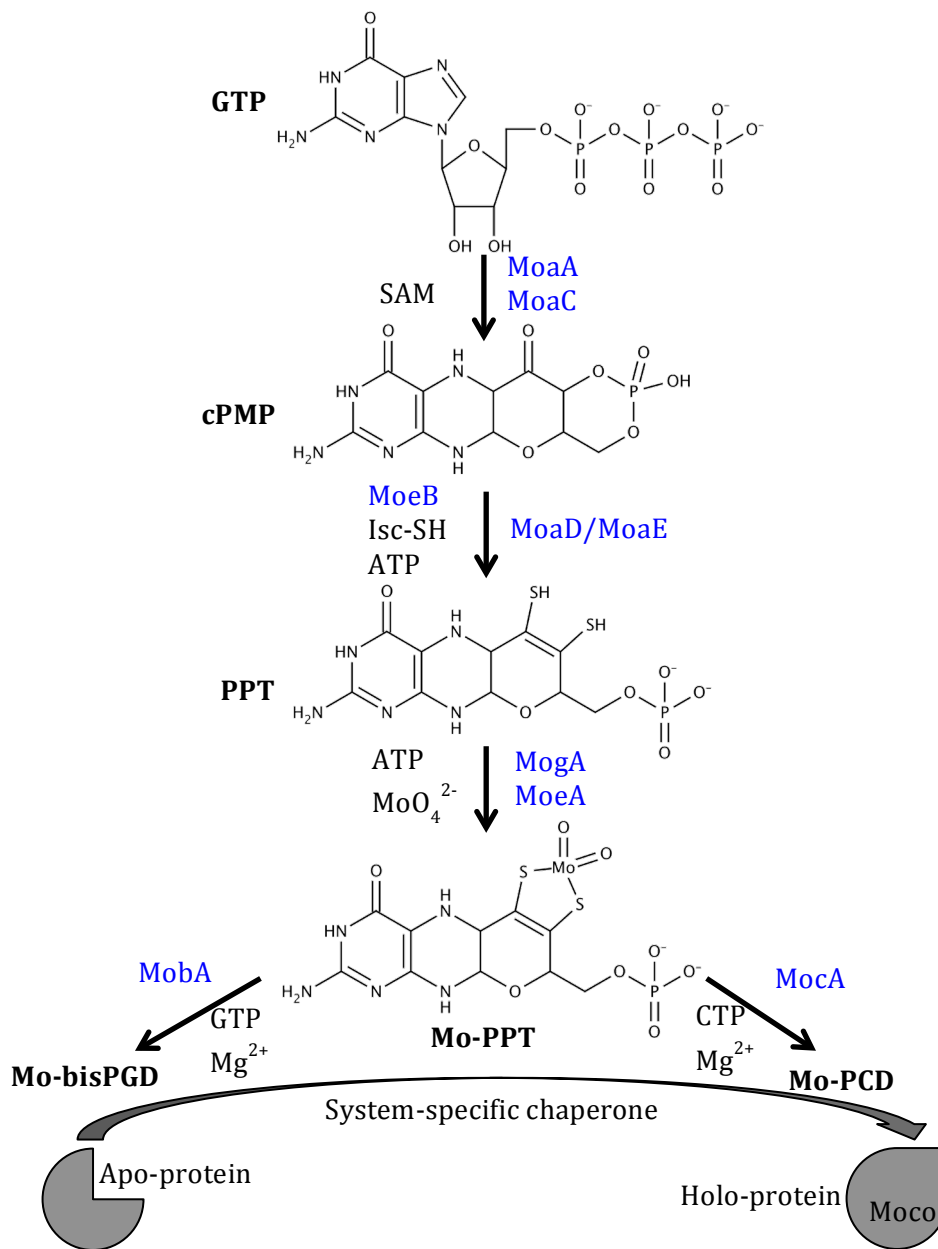


Figure 1.3 Biosynthesis of molybdenum cofactor (Moco). The assembly of Moco is a complex multi-step pathway that involves enzymes shown in blue. MoaA initiates the reaction by converting GTP to a reactive intermediate, which is converted to cPMP by MoaC. MoaD/MoaE functions together as the PPT synthase to generate PPT, while MoaB is a sulfurase regenerating functional form of MoaD. MogA and MoeA catalyze Mo insertion. Other variants of the Moco are formed through attachment of a GMP or CMP to the pyran ring facilitated by MobA or MocA, respectively. The final insertion of Moco into the apo-protein is assisted by system-specific chaperones such as TorD for TorA. Chemical structures were drawn using MarvinSketch 5.9.4 (Marvin, 2012, ChemAxon, <http://www.chemaxon.com>).

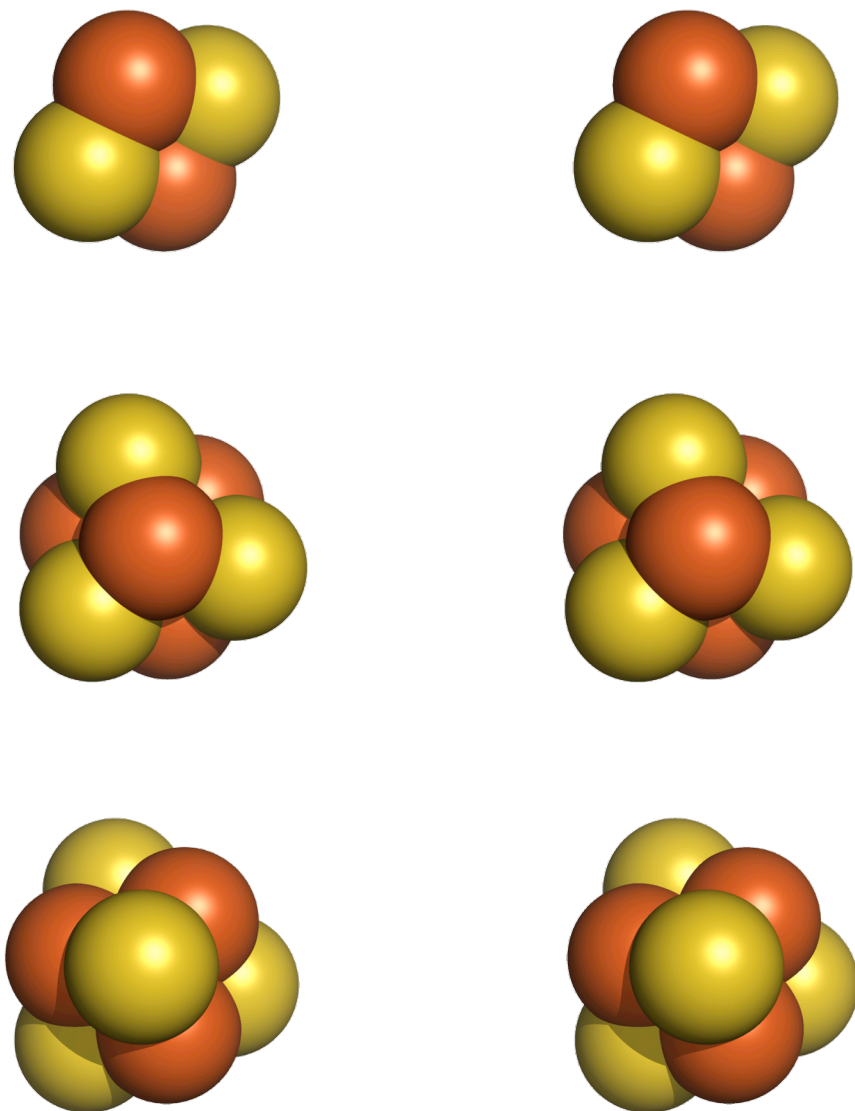


Figure 1.4 Stereo views of iron-sulfur clusters. Top to bottom: [2Fe-2S] cluster, [4Fe-4S] cluster, and [3Fe-4S] cluster. Iron is coloured orange and sulfur is coloured yellow. The image is generated by PyMol v1.5 (DeLano Scientific LLC.).

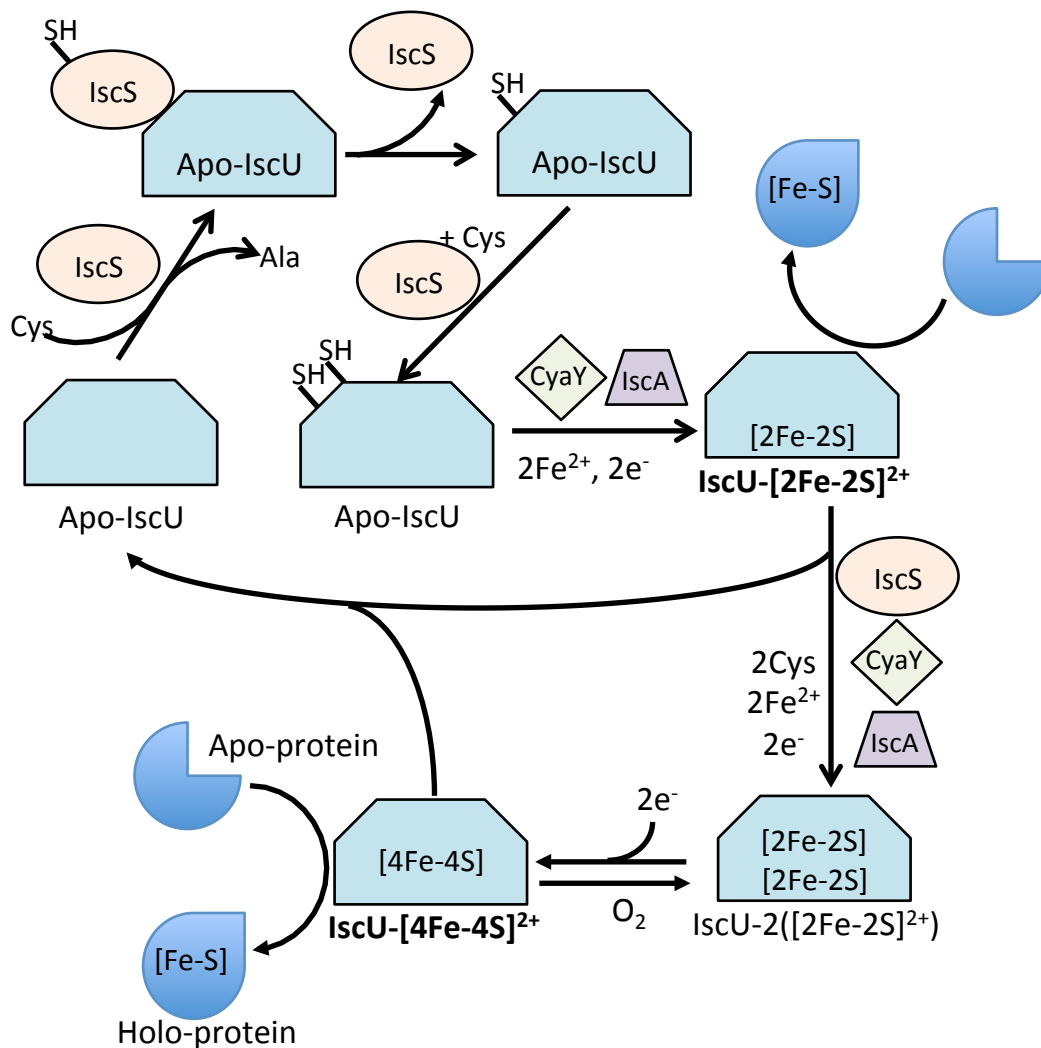


Figure 1.5 Biosynthesis of [Fe-S] cluster via the ISC system. The assembly of [Fe-S] clusters is carried out on the scaffold protein (IscU) which functions both as the receptor for deposition of iron and sulfur atoms and as the machinery for forming the structured cluster from the metals. IscS functions as a desulfurase of the L-cysteine and donates sulfur to IscU. IscA and CyaY have been proposed to act as iron donors to IscU.

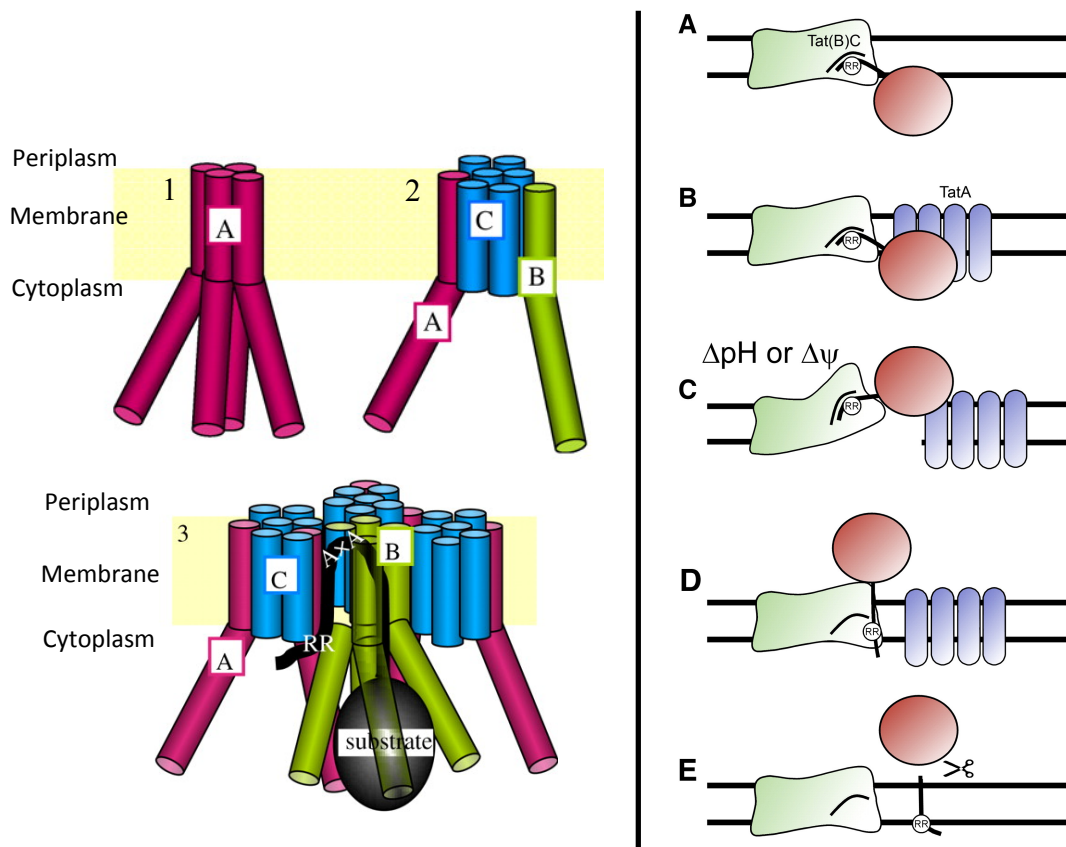


Figure 1.6 The *tat* translocation system. **Left panel** shows models of major Tat complexes observed and their interaction with the *tat* substrate (110). (1) TatA complex, which is shown as a tetramer. TatA can form homo-oligomeric complexes with a pore-like structure of varying diameters. (2) The Tat(A)BC complex. The TatBC complexes from Gram-negative bacteria often contain TatA, which functions to stabilize the TatBC complex. (3) The TatABC complex. The *tat* signal sequence forms a hairpin-like insertion deep into the binding pocket of TatBC complex. TatB homo-oligomerizes and encapsulates the folded mature protein part of the substrate. TatA has been recruited to the complex. **Right panel** shows an alternative model for the translocation mechanism of the *tat* pathway created by Natale *et al* in their review in 2008 (193). (A) *tat* substrates interact with the TatBC complex and deeply binds its leader sequence into the binding site. (B) Monomers or tetramers of TatA are recruited in a pmf-dependent manner. (C) Conformational change of TatBC complex pulls the substrate through the membrane destabilized by accumulation of TatA. (D) After translocation of the substrate, the membrane is sealed and the substrate is laterally released. (E) The substrate is processed by signal sequence peptidases to generate the mature protein.

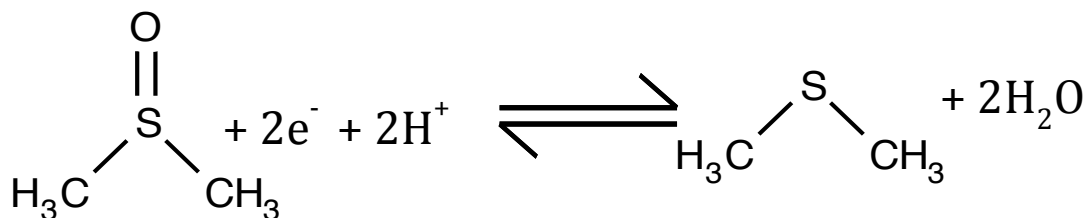
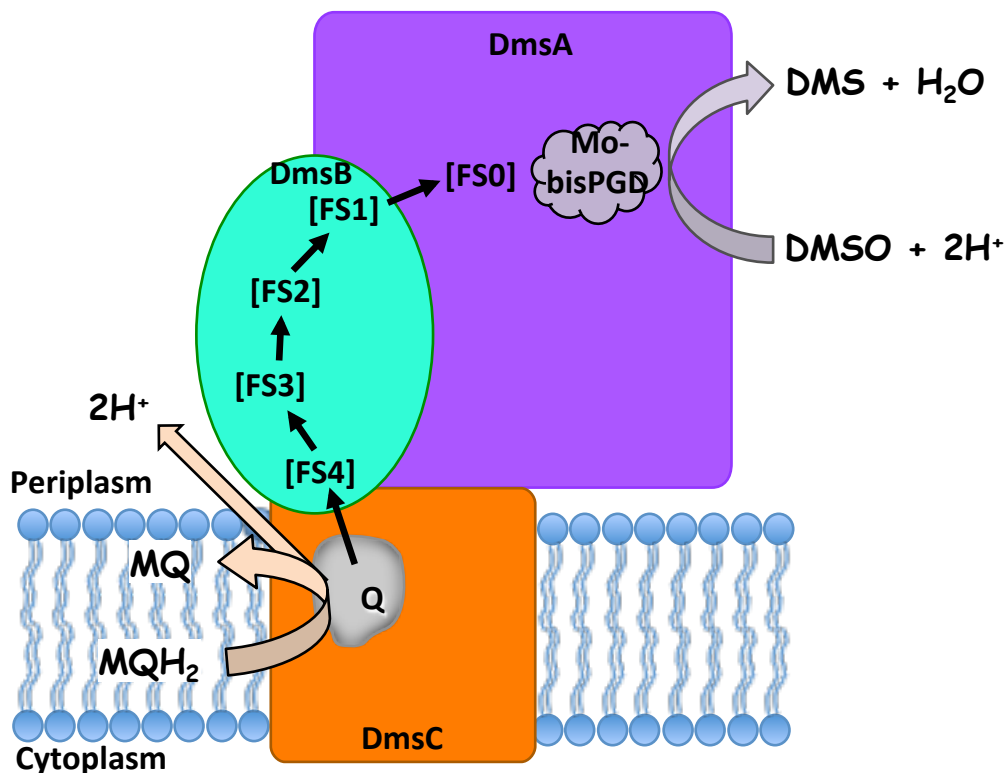


Figure 1.7 *E. Coli* DMSO reductase. **Top:** A schematic representation of DMSO reductase. Menaquinol (MQH₂) binds to the Q-site where it is oxidized to menaquinone (MQ). Two protons are released into the periplasm and two electrons are transferred through the electron transfer relay formed by four [4Fe-4S] clusters (FS1-FS4) in DmsB. DMSO is reduced to DMS at the active site releasing a water. **Bottom:** The reaction catalyzed by DMSO reductase. Chemical structures were drawn using MarvinSketch 5.9.4 (Marvin, 2012, ChemAxon, <http://www.chemaxon.com>).

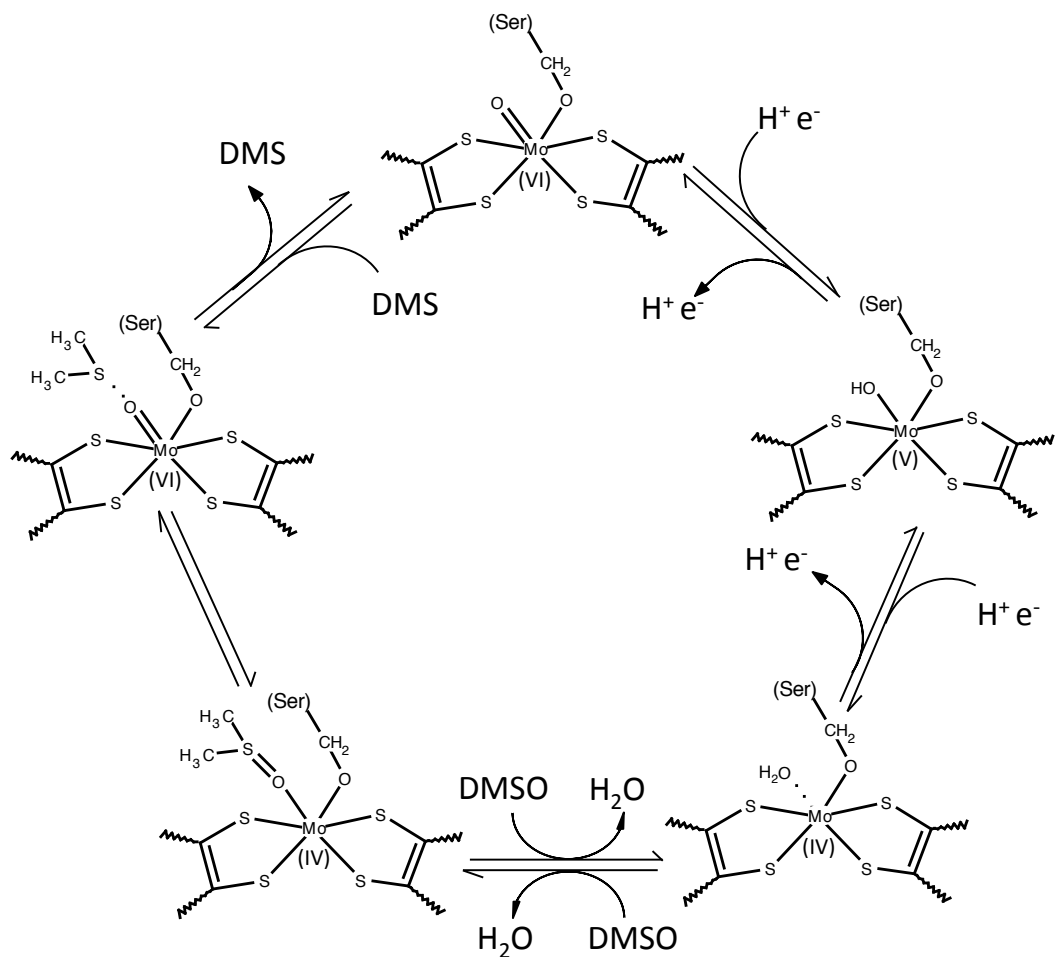


Figure 1.8 Catalytic mechanism for the catalytic cycle of *Rhodobacter* DMSO reductase proposed by Johnson *et al* (55). Chemical structures were drawn using MarvinSketch 5.9.4 (Marvin, 2012, ChemAxon, <http://www.chemaxon.com>).

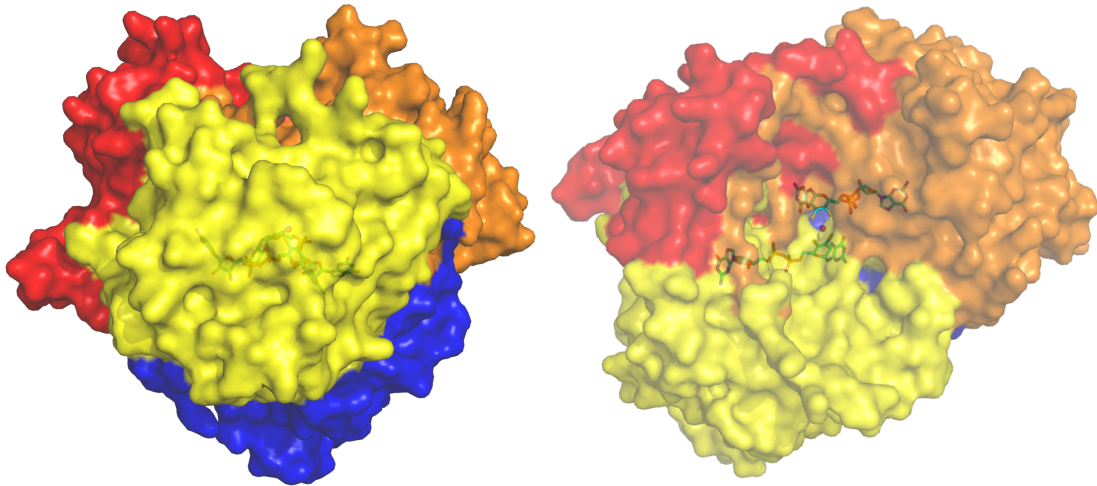


Figure 1.9 Surface representation of the structure of DMSO reductase from *Rhodobacter capsulatus* (PDB file 3DMR). Shown on the left is the side view, while shown on the right is the top view looking into the active site funnel. The four domains I-IV are colored red, yellow, orange and blue, respectively. The Mo atom is shown as a sphere colored magenta. The PGD cofactors are shown as sticks. Images were generated using PyMol v1.5 (DeLano Scientific LLC.).

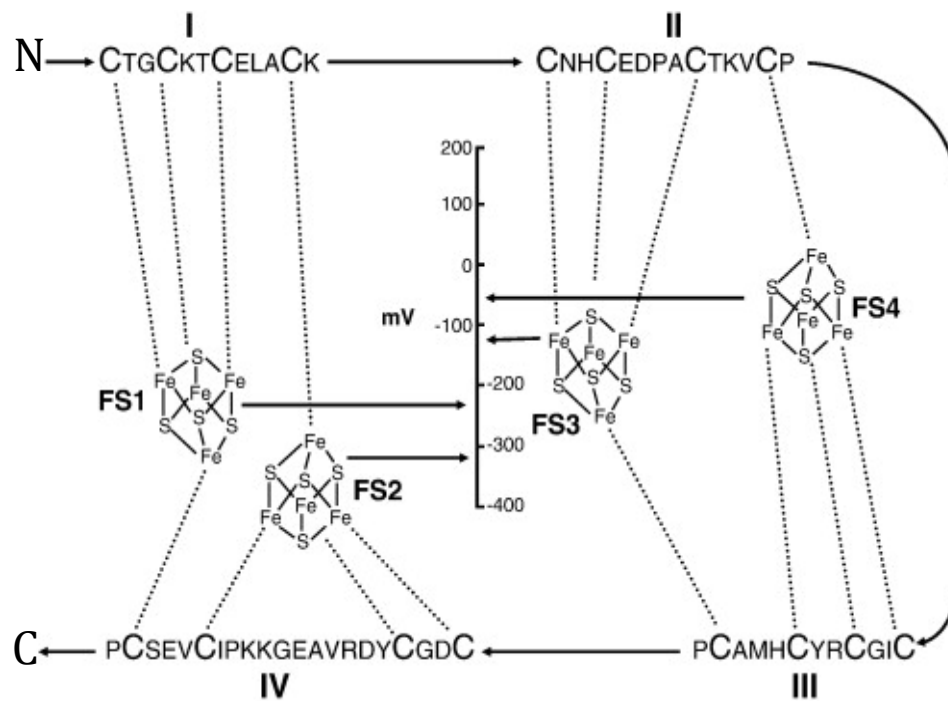


Figure 1.10 Coordination of the [Fe-S] clusters (FS1-4) in DmsB proposed by Rothery *et al.* (194). The iron-sulfur clusters FS1-FS4 are listed from left to right on the diagram. However, the electron flow is from right to left through the electron transfer relay.

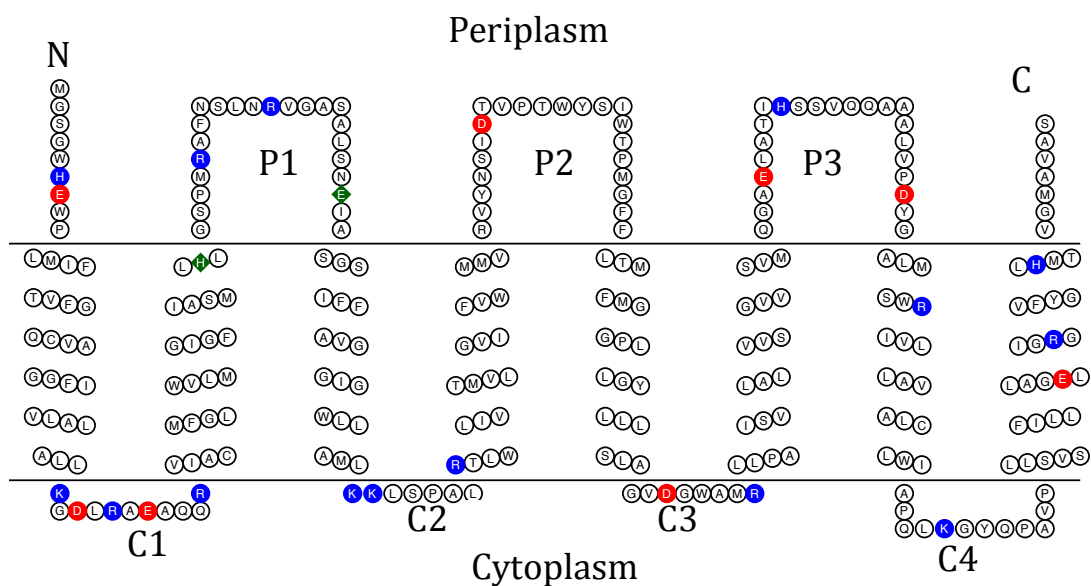


Figure 1.11 A topology model of *E. coli* DmsC (Swissprot accession number P187777). The acidic residues are highlighted red and basic residues highlighted blue. His65 and Glu87 are represented in diamonds and colored deep green. This display of the topology model is generated by TOPO2 (Johns S.J., TOPO2, Transmembrane protein display software, <http://www.sacs.ucsf.edu/TOPO2/>).

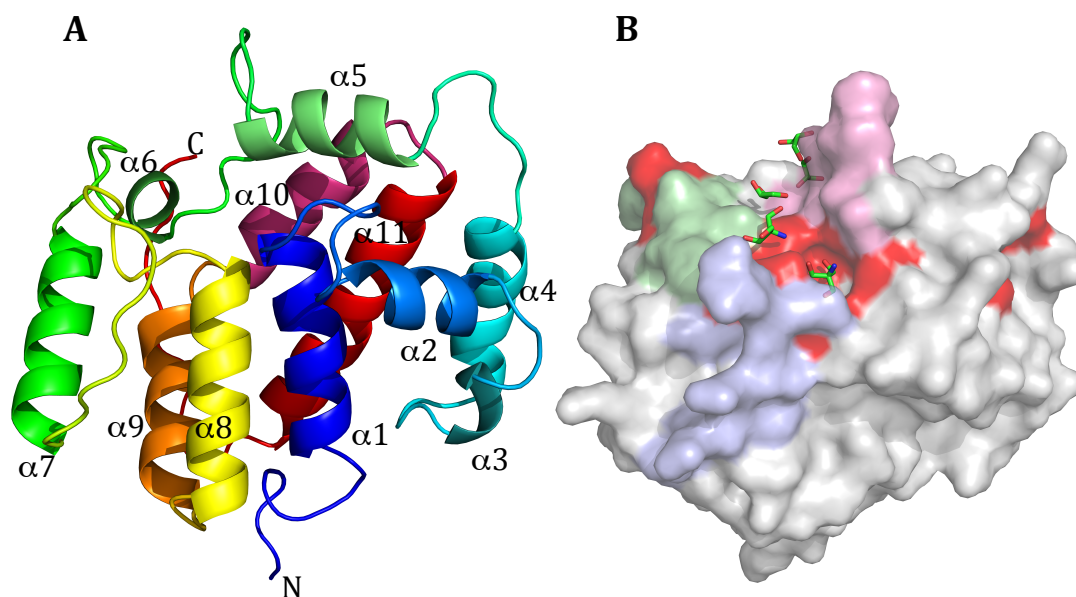


Figure 1.12 The X-ray crystal structure of *E. coli* DmsD (PDB file 3EFP). **A.** The cartoon representation of the crystal structure of DmsD with resolution of 2.01 Å. The helices α 1- α 11 are colour coded as following: blue, marine, deep teal, cyan, lime, forest, green, yellow, orange, warm pink and red from N terminal to C terminal. **B.** Surface representation of the crystal structure of DmsD. Three loops forming the DmsA leader binding pocket are colored pink (loop1, between α 5- α 6), pale green (loop2, between α 6- α 7) and light blue (loop3, between α 7- α 8). Residues determined to be in the leader-binding pocket by Chan *et al.* are colored red. Strong electron density for small molecules (two tris(hydroxymethyl)aminomethane and three glycerol) are found in the proposed leader binding pocket, and they are represented in sticks. Images were generated using PyMol v1.5 (DeLano Scientific LLC).

1.8 Reference

1. Mitchell, P. (1967) Proton-translocation phosphorylation in mitochondria, chloroplasts and bacteria: natural fuel cells and solar cells. *Fed. Proc.* **26**, 1370–1379
2. Udden, G., and Bongaerts, J. (1997) Alternative respiratory pathways of *Escherichia coli*: energetics and transcriptional regulation in response to electron acceptors. *Biochim. Biophys. Acta - Bioenergetics* **1320**, 217–234
3. Gennis, R. B., and Stewart, V. (1996) in *FC Neidhardt, F. C. (ed). Escherichia coli and Salmonella: cellular and molecular biology* 2nd Ed., pp. 217–261, ASM Press, Washington, D.C.
4. Iuchi, S., and Lin, E. C. (1988) *arcA* (*dye*), a global regulatory gene in *Escherichia coli* mediating repression of enzymes in aerobic pathways. *Proc. Natl. Acad. Sci. U.S.A.* **85**, 1888–1892
5. Iuchi, S., Cameron, D. C., and Lin, E. C. (1989) A second global regulator gene (*arcB*) mediating repression of enzymes in aerobic pathways of *Escherichia coli*. *J. Bacteriol.* **171**, 868–873
6. Iuchi, S., Matsuda, Z., Fujiwara, T., and Lin, E. C. C. (1990) The *arcB* gene of *Escherichia coli* encodes a sensor-regulator protein for anaerobic repression of the *arc* modulon. *Mol. Microbiol.* **4**, 715–727
7. Alvarez, A. F., and Georgellis, D. (2010) in *Methods in Enzymology: Two-Component Signaling Systems, Part C* pp. 205–228, Academic Press [online]<http://www.sciencedirect.com/science/article/pii/S0076687910710120> (Accessed May 21, 2012).
8. Iuchi, S. (1993) Phosphorylation/Dephosphorylation of the receiver module at the conserved aspartate residue controls transphosphorylation activity of histidine kinase in sensor protein ArcB of *Escherichia coli*. *J. Biol. Chem.* **268**, 23972–23980
9. Georgellis, D., Lynch, A. S., and Lin, E. C. (1997) In vitro phosphorylation study of the Arc two-component signal transduction system of *Escherichia coli*. *J. Bacteriol.* **179**, 5429–5435
10. Kwon, O., Georgellis, D., and Lin, E. C. C. (2000) Phosphorelay as the sole physiological route of signal transmission by the Arc two-component system of *Escherichia coli*. *J. Bacteriol.* **182**, 3858–3862
11. Gunsalus, R. P., and Park, S.-J. (1994) Aerobic-anaerobic gene regulation in *Escherichia coli*: control by the ArcAB and Fnr regulons. *Res. Microbiol.* **145**, 437–450
12. Lynch, A. S., and Lin, E. C. (1996) Transcriptional control mediated by the ArcA two-component response regulator protein of *Escherichia coli*: characterization of dna binding at target promoters. *J. Bacteriol.* **178**, 6238–6249
13. Liu, X., and De Wulf, P. (2004) Probing the ArcA-P modulon of *Escherichia coli* by whole genome transcriptional analysis and sequence recognition profiling. *J. Biol. Chem.* **279**, 12588–12597

14. Georgellis, D., Kwon, O., and Lin, E. C. C. (1999) Amplification of signaling activity of the Arc two-component system of *Escherichia coli* by anaerobic metabolites. *J. Biol. Chem.* **274**, 35950–35954
15. Rodriguez, C., Kwon, O., and Georgellis, D. (2004) Effect of D-lactate on the physiological activity of the ArcB sensor kinase in *Escherichia coli*. *J. Bacteriol.* **186**, 2085–2090
16. Georgellis, D., Kwon, O., De Wulf, P., and Lin, E. C. C. (1998) Signal decay through a reverse phosphorelay in the Arc two-component signal transduction system. *J. Biol. Chem.* **273**, 32864–32869
17. Peña-Sandoval, G. R., Kwon, O., and Georgellis, D. (2005) Requirement of the receiver and phosphotransfer domains of ArcB for efficient dephosphorylation of phosphorylated ArcA in vivo. *J. Bacteriol.* **187**, 3267–3272
18. Georgellis, D., Kwon, O., and Lin, E. C. (2001) Quinones as the redox signal for the arc two-component system of bacteria. *Science* **292**, 2314–2316
19. Malpica, R., Franco, B., Rodriguez, C., Kwon, O., and Georgellis, D. (2004) Identification of a quinone-sensitive redox switch in the ArcB sensor kinase. *PNAS* **101**, 13318–13323
20. Bilous, P. T., and Weiner, J. H. (1988) Molecular cloning and expression of the *Escherichia coli* dimethyl sulfoxide reductase operon. *J. Bacteriol.* **170**, 1511–1518
21. Kang, Y., Weber, K. D., Qiu, Y., Kiley, P. J., and Blattner, F. R. (2005) Genome-wide expression analysis indicates that FNR of *Escherichia coli* K-12 regulates a large number of genes of unknown function. *J. Bacteriol.* **187**, 1135–1160
22. Kiley, P. J., and Beinert, H. (1998) Oxygen sensing by the global regulator, FNR: the role of the iron-sulfur cluster. *FEMS Microbiol. Rev.* **22**, 341–352
23. Crack, J., Green, J., and Thomson, A. J. (2004) Mechanism of oxygen sensing by the bacterial transcription factor fumarate-nitrate reduction (FNR). *J. Biol. Chem.* **279**, 9278–9286
24. Reinhart, F., Achebach, S., Koch, T., and Uden, G. (2008) Reduced apo-fumarate nitrate reductase regulator (ApoFNR) as the major form of FNR in aerobically growing *Escherichia coli*. *J. Bacteriol.* **190**, 879–886
25. Green, J., Crack, J. C., Thomson, A. J., and LeBrun, N. E. (2009) Bacterial sensors of oxygen. *Curr. Opin. Microbiol.* **12**, 145–151
26. Tolla, D. A., and Savageau, M. A. (2010) Regulation of aerobic-to-anaerobic transitions by the FNR cycle in *Escherichia coli*. *J. Mol. Biol.* **397**, 893–905
27. Melville, S. B., and Gunsalus, R. P. (1990) Mutations in FNR that alter anaerobic regulation of electron transport-associated genes in *Escherichia coli*. *J. Biol. Chem.* **265**, 18733–18736
28. Green, J., Sharrocks, A. D., Green, B., Geisow, M., and Guest, J. R. (1993) Properties of FNR proteins substituted at each of the five cysteine residues. *Mol. Microbiol.* **8**, 61–68

29. Lazazzera, B. A., Beinert, H., Khoroshilova, N., Kennedy, M. C., and Kiley, P. J. (1996) DNA binding and dimerization of the Fe-S-containing FNR protein from *Escherichia coli* are regulated by oxygen. *J. Biol. Chem.* **271**, 2762–2768
30. Moore, L. J., and Kiley, P. J. (2001) Characterization of the dimerization domain in the FNR transcription factor. *J. Biol. Chem.* **276**, 45744–45750
31. Marshall, F. A., Messenger, S. L., Wyborn, N. R., Guest, J. R., Wing, H., Busby, S. J., and Green, J. (2001) A novel promoter architecture for microaerobic activation by the anaerobic transcription factor FNR. *Mol. Microbiol.* **39**, 747–753
32. Barnard, A. M. L., Green, J., and Busby, S. J. W. (2003) Transcription regulation by tandem-bound FNR at *Escherichia coli* promoters. *J. Bacteriol.* **185**, 5993–6004
33. Khoroshilova, N., Popescu, C., Münck, E., Beinert, H., and Kiley, P. J. (1997) Iron-sulfur cluster disassembly in the FNR protein of *Escherichia coli* by O₂: [4Fe-4S] to [2Fe-2S] conversion with loss of biological activity. *Proc. Natl. Acad. Sci. U.S.A.* **94**, 6087–6092
34. Crack, J. C., Gaskell, A. A., Green, J., Cheesman, M. R., Le Brun, N. E., and Thomson, A. J. (2008) Influence of the environment on the [4Fe-4S]²⁺ to [2Fe-2S]²⁺ cluster switch in the transcriptional regulator FNR. *J. Am. Chem. Soc.* **130**, 1749–1758
35. Sutton, V. R., Mettert, E. L., Beinert, H., and Kiley, P. J. (2004) Kinetic analysis of the oxidative conversion of the [4Fe-4S]²⁺ cluster of FNR to a [2Fe-2S]²⁺ Cluster. *J. Bacteriol.* **186**, 8018–8025
36. Sutton, V. R., Stubna, A., Patschkowski, T., Münck, E., Beinert, H., and Kiley, P. J. (2003) Superoxide destroys the [2Fe-2S]²⁺ cluster of FNR from *Escherichia coli*. *Biochemistry* **43**, 791–798
37. Achebach, S., Selmer, T., and Udden, G. (2005) Properties and significance of apoFNR as a second form of air-inactivated [4Fe-4S]•FNR of *Escherichia coli*. *FEBS J.* **272**, 4260–4269
38. Mettert, E. L., and Kiley, P. J. (2005) ClpXP-dependent proteolysis of FNR upon loss of its O₂-sensing [4Fe-4S] cluster. *J. Mol. Biol.* **354**, 220–232
39. Stewart, V. (1994) Dual interacting two-component regulatory systems mediate nitrate- and nitrite-regulated gene expression in *Escherichia coli*. *Res. Microbiol.* **145**, 450–454
40. Wang, H., and Gunsalus, R. P. (2003) Coordinate regulation of the *Escherichia coli* formate dehydrogenase FdnGHI and FdhF genes in response to nitrate, nitrite, and formate: roles for NarL and NarP. *J. Bacteriol.* **185**, 5076–5085
41. Rabin, R. S., and Stewart, V. (1993) Dual response regulators (NarL and NarP) interact with dual sensors (NarX and NarQ) to control nitrate- and nitrite-regulated gene expression in *Escherichia coli* K-12. *J. Bacteriol.* **175**, 3259–3268
42. Cavicchioli, R., Chiang, R. C., Kalman, L. V., and Gunsalus, R. P. (1996) Role of the periplasmic domain of the *Escherichia coli* NarX sensor-

- transmitter protein in nitrate-dependent signal transduction and gene regulation. *Mol. Microbiol.* **21**, 901–911
43. Lee, A. I., Delgado, A., and Gunsalus, R. P. (1999) Signal-dependent phosphorylation of the membrane-bound NarX two-component sensor-transmitter protein of *Escherichia coli*: nitrate elicits a superior anion ligand response compared to nitrite. *J. Bacteriol.* **181**, 5309–5316
 44. Stewart, V. (1982) Requirement of Fnr and NarL functions for nitrate reductase expression in *Escherichia coli* K-12. *J. Bacteriol.* **151**, 1320–1325
 45. Berg, B. L., and Stewart, V. (1990) Structural genes for nitrate-inducible formate dehydrogenase in *Escherichia coli* K-12. *Genetics* **125**, 691–702
 46. Iuchi, S., and Lin, E. C. (1987) The *narL* gene product activates the nitrate reductase operon and represses the fumarate reductase and trimethylamine N-oxide reductase operons in *Escherichia coli*. *Proc. Natl. Acad. Sci. U.S.A.* **84**, 3901–3905
 47. Cotter, P. A., and Gunsalus, R. P. (1989) Oxygen, nitrate, and molybdenum regulation of *dmsABC* gene expression in *Escherichia coli*. *J. Bacteriol.* **171**, 3817–3823
 48. Hille, R. (1996) The mononuclear molybdenum enzymes. *Chem. Rev.* **96**, 2757–2816
 49. Schwarz, G., Mendel, R. R., and Ribbe, M. W. (2009) Molybdenum cofactors, enzymes and pathways. *Nature* **460**, 839
 50. Leimkühler, S., Wuebbens, M. M., and Rajagopalan, K. V. (2011) The history of the discovery of the molybdenum cofactor and novel aspects of its biosynthesis in bacteria. *Coord. Chem. Rev.* **255**, 1129–1144
 51. Rajagopalan, K. V. (1991) Novel aspects of the biochemistry of the molybdenum cofactor. *Adv. Enzymol. Relat. Areas Mol. Biol.* **64**, 215–290
 52. Rajagopalan, K. V., and Johnson, J. L. (1992) The pterin molybdenum cofactors. *J. Biol. Chem.* **267**, 10199–10202
 53. Johnson, M. K., Rees, D. C., and Adams, M. W. W. (1996) Tungstoenzymes. *Chem. Rev.* **96**, 2817–2840
 54. Romão, M. J. (2009) Molybdenum and tungsten enzymes: a crystallographic and mechanistic overview. *Dalton Transactions*, 4053
 55. Johnson, J. L., Bastian, N. R., and Rajagopalan, K. V. (1990) Molybdopterin guanine dinucleotide: a modified form of molybdopterin identified in the molybdenum cofactor of dimethyl sulfoxide reductase from *Rhodobacter sphaeroides* form a specialis denitrificans. *Proc. Natl. Acad. Sci. U.S.A.* **87**, 3190–3194
 56. Schwarz, G. (2005) Molybdenum cofactor biosynthesis and deficiency. *Cell. Mol. Life Sci.* **62**, 2792–2810
 57. Hänzelmann, P., and Schindelin, H. (2004) Crystal structure of the S-adenosylmethionine-dependent enzyme MoaA and its implications for molybdenum cofactor deficiency in humans. *Proc. Natl. Acad. Sci. U.S.A.* **101**, 12870–12875
 58. Hänzelmann, P., and Schindelin, H. (2006) Binding of 5'-GTP to the C-terminal FeS cluster of the radical S-adenosylmethionine enzyme MoaA

- provides insights into its mechanism. *Proc. Natl. Acad. Sci. U.S.A.* **103**, 6829–6834
59. Hänzelmann, P., Hernández, H. L., Menzel, C., García-Serres, R., Huynh, B. H., Johnson, M. K., Mendel, R. R., and Schindelin, H. (2004) Characterization of MOCS1A, an oxygen-sensitive iron-sulfur protein involved in human molybdenum cofactor biosynthesis. *J. Biol. Chem.* **279**, 34721–34732
 60. Kanaujia, S. P., Jeyakanthan, J., Nakagawa, N., Balasubramaniam, S., Shinkai, A., Kuramitsu, S., Yokoyama, S., and Sekar, K. (2010) Structures of apo and GTP-bound molybdenum cofactor biosynthesis protein MoaC from *Thermus thermophilus* HB8. *Acta Crystallogr. D Biol. Crystallogr.* **66**, 821–833
 61. Pitterle, D. M., and Rajagopalan, K. V. (1989) Two proteins encoded at the chlA locus constitute the converting factor of *Escherichia coli* chlA1. *J. Bacteriol.* **171**, 3373–3378
 62. Pitterle, D. M., Johnson, J. L., and Rajagopalan, K. V. (1993) In vitro synthesis of molybdopterin from precursor Z using purified converting factor. Role of protein-bound sulfur in formation of the dithiolene. *J. Biol. Chem.* **268**, 13506–13509
 63. Gutzke, G., Fischer, B., Mendel, R. R., and Schwarz, G. (2001) Thiocarboxylation of molybdopterin synthase provides evidence for the mechanism of dithiolene formation in metal-binding pterins. *J. Biol. Chem.* **276**, 36268–36274
 64. Rudolph, M. J., Wuebbens, M. M., Rajagopalan, K. v., and Schindelin, H. (2001) Crystal structure of molybdopterin synthase and its evolutionary relationship to ubiquitin activation. *Nat. Struct. Mol. Biol.* **8**, 42
 65. Rudolph, M. J., Wuebbens, M. M., Turque, O., Rajagopalan, K. V., and Schindelin, H. (2003) Structural studies of molybdopterin synthase provide insights into its catalytic mechanism. *J. Biol. Chem.* **278**, 14514–14522
 66. Pitterle, D. M., and Rajagopalan, K. V. (1993) The biosynthesis of molybdopterin in *Escherichia coli*. Purification and characterization of the converting factor. *J. Biol. Chem.* **268**, 13499–13505
 67. Rajagopalan, K. V. (1997) Biosynthesis and processing of the molybdenum cofactors. *Biochem. Soc. Trans.* **25**, 757–761
 68. Leimkühler, S., Wuebbens, M. M., and Rajagopalan, K. V. (2001) Characterization of *Escherichia coli* MoeB and its involvement in the activation of molybdopterin synthase for the biosynthesis of the molybdenum cofactor. *J. Biol. Chem.* **276**, 34695–34701
 69. Leimkühler, S., and Rajagopalan, K. V. (2001) A sulfurtransferase is required in the transfer of cysteine sulfur in the in vitro synthesis of molybdopterin from precursor Z in *Escherichia coli*. *J. Biol. Chem.* **276**, 22024–22031
 70. Zhang, W., Urban, A., Mihara, H., Leimkühler, S., Kurihara, T., and Esaki, N. (2010) IscS functions as a primary sulfur-donating enzyme by

- interacting specifically with MoeB and MoeA in the biosynthesis of molybdopterin in *Escherichia coli*. *J. Biol. Chem.* **285**, 2302–2308
71. Kuper, J., Llamas, A., Hecht, H.-J., Mendel, R. R., and Schwarz, G. (2004) Structure of the molybdopterin-bound Cnx1G domain links molybdenum and copper metabolism. *Nature* **430**, 803–806
 72. Llamas, A., Mendel, R. R., and Schwarz, G. (2004) Synthesis of adenylated molybdopterin: an essential step for molybdenum insertion. *J. Biol. Chem.* **279**, 55241–55246
 73. Llamas, A., Otte, T., Multhaupt, G., Mendel, R. R., and Schwarz, G. (2006) The mechanism of nucleotide-assisted molybdenum insertion into molybdopterin: a novel route toward metal cofactor assembly. *J. Biol. Chem.* **281**, 18343–18350
 74. Nichols, J. D., and Rajagopalan, K. V. (2005) In vitro molybdenum ligation to molybdopterin using purified components. *J. Biol. Chem.* **280**, 7817–7822
 75. Self, W. T., Grunden, A. M., Hasona, A., and Shanmugam, K. T. (2001) Molybdate transport. *Res. Microbiol.* **152**, 311–321
 76. Aguilar-Barajas, E., Díaz-Pérez, C., Ramírez-Díaz, M. I., Riveros-Rosas, H., and Cervantes, C. (2011) Bacterial transport of sulfate, molybdate, and related oxyanions. *Biometals* **24**, 687–707
 77. Lake, M. W., Temple, C. A., Rajagopalan, K. V., and Schindelin, H. (2000) The crystal structure of the *Escherichia coli* MobA protein provides insight into molybdopterin guanine dinucleotide biosynthesis. *J. Biol. Chem.* **275**, 40211–40217
 78. Neumann, M., Stöcklein, W., and Leimkühler, S. (2007) Transfer of the molybdenum cofactor synthesized by *Rhodobacter capsulatus* MoeA to XdhC and MobA. *J. Biol. Chem.* **282**, 28493–28500
 79. Temple, C. A., and Rajagopalan, K. V. (2000) Mechanism of assembly of the bis(molybdopterin guanine dinucleotide)molybdenum cofactor in *Rhodobacter sphaeroides* dimethyl sulfoxide reductase. *J. Biol. Chem.* **275**, 40202–40210
 80. Genest, O., Neumann, M., Seduk, F., Stöcklein, W., Méjean, V., Leimkühler, S., and Iobbi-Nivol, C. (2008) Dedicated metallochaperone connects apoenzyme and molybdenum cofactor biosynthesis components. *J. Biol. Chem.* **283**, 21433–21440
 81. Anderson, L. A., McNairn, E., Leubke, T., Pau, R. N., and Boxer, D. H. (2000) ModE-dependent molybdate regulation of the molybdenum cofactor operon moa in *Escherichia coli*. *J. Bacteriol.* **182**, 7035–7043
 82. Uden, G., Achebach, S., Holighaus, G., Tran, H. G., Wackwitz, B., and Zeuner, Y. (2002) Control of FNR function of *Escherichia coli* by O₂ and reducing conditions. *J. Mol. Microbiol. Biotechnol.* **4**, 263–268
 83. McNicholas, P. M., Chiang, R. C., and Gunsalus, R. P. (1998) Anaerobic regulation of the *Escherichia coli* dmsABC operon requires the molybdate-responsive regulator ModE. *Mol. Microbiol.* **27**, 197–208
 84. Grunden, A. M., and Shanmugam, K. T. (1997) Molybdate transport and regulation in bacteria. *Arch. Microbiol.* **168**, 345–354

85. Regulski, E. E., Moy, R. H., Weinberg, Z., Barrick, J. E., Yao, Z., Ruzzo, W. L., and Breaker, R. R. (2008) A widespread riboswitch candidate that controls bacterial genes involved in molybdenum cofactor and tungsten cofactor metabolism. *Mol. Microbiol.* **68**, 918–932
86. Beinert, H. (1997) Iron-sulfur clusters: nature's modular, multipurpose structures. *Science* **277**, 653–659
87. Johnson, D. C., Dean, D. R., Smith, A. D., and Johnson, M. K. (2005) Structure, function, and formation of biological iron-sulfur clusters. *Annual Review of Biochemistry* **74**, 247–281
88. Fontecave, M., and Ollagnier-de-Choudens, S. (2008) Iron–sulfur cluster biosynthesis in bacteria: mechanisms of cluster assembly and transfer. *Arch. Biochem. Biophys.* **474**, 226–237
89. Beinert, H. (2000) Iron-sulfur proteins: ancient structures, still full of surprises. *J. Biol. Inorg. Chem.* **5**, 2–15
90. Takahashi, Y., and Nakamura, M. (1999) Functional assignment of the ORF2-iscS-iscU-iscA-hscB-hscA-fdx-ORF3 gene cluster involved in the assembly of Fe-S clusters in *Escherichia coli*. *J. Biochem.* **126**, 917–926
91. Takahashi, Y., and Tokumoto, U. (2002) A third bacterial system for the assembly of iron-sulfur clusters with homologs in archaea and plastids. *J. Biol. Chem.* **277**, 28380–28383
92. Fontecave, M., Choudens, S., Py, B., and Barras, F. (2005) Mechanisms of iron–sulfur cluster assembly: the SUF machinery. *J. Biol. Inorg. Chem.* **10**, 713–721
93. Bandyopadhyay, S., Chandramouli, K., and Johnson, M. K. (2008) Iron-sulphur cluster biosynthesis. *Biochem. Soc. Trans.* **36**, 1112–1119
94. Peters, J. W., and Broderick, J. B. (2012) Emerging paradigms for complex iron-sulfur cofactor assembly and insertion. *Annual Review of Biochemistry* **81**, null
95. Zheng, L., White, R. H., Cash, V. L., and Dean, D. R. (1994) Mechanism for the desulfurization of L-cysteine catalyzed by the nifS gene product. *Biochemistry* **33**, 4714–4720
96. Mihara, H., Kurihara, T., Yoshimura, T., and Esaki, N. (2000) Kinetic and mutational studies of three NifS homologs from *Escherichia coli*: mechanistic difference between L-cysteine desulfurase and L-selenocysteine lyase reactions. *J. Biochem.* **127**, 559–567
97. Mihara, H., and Esaki, N. (2002) Bacterial cysteine desulfurases: their function and mechanisms. *Appl. Microbiol. Biotechnol.* **60**, 12–23
98. Ayala-Castro, C., Saini, A., and Outten, F. W. (2008) Fe-S cluster assembly pathways in bacteria. *Microbiol. Mol. Biol. Rev.* **72**, 110–125
99. Ollagnier-de-Choudens, S., Sanakis, Y., and Fontecave, M. (2004) SufA/IscA: reactivity studies of a class of scaffold proteins involved in [Fe-S] cluster assembly. *J. Biol. Inorg. Chem.* **9**, 828–838
100. Ding, H., and Clark, R. J. (2004) Characterization of iron binding in IscA, an ancient iron-sulphur cluster assembly protein. *Biochem. J.* **379**, 433–440

101. Ding, B., Smith, E. S., and Ding, H. (2005) Mobilization of the iron centre in IscA for the iron-sulphur cluster assembly in IscU. *Biochem. J.* **389**, 797–802
102. Hoff, K. G., Cupp-Vickery, J. R., and Vickery, L. E. (2003) Contributions of the LPPVK motif of the iron-sulfur template protein IscU to interactions with the Hsc66-Hsc20 chaperone system. *J. Biol. Chem.* **278**, 37582–37589
103. Hoff, K. G., Silberg, J. J., and Vickery, L. E. (2000) Interaction of the iron-sulfur cluster assembly protein IscU with the Hsc66/Hsc20 molecular chaperone system of *Escherichia coli*. *Proc. Natl. Acad. Sci. U.S.A.* **97**, 7790–7795
104. Silberg, J. J., Tapley, T. L., Hoff, K. G., and Vickery, L. E. (2004) Regulation of the HscA ATPase reaction cycle by the co-chaperone HscB and the iron-sulfur cluster assembly protein IscU. *J. Biol. Chem.* **279**, 53924–53931
105. Eccleston, J. F., Petrovic, A., Davis, C. T., Rangachari, K., and Wilson, R. J. M. I. (2006) The kinetic mechanism of the SufC ATPase: the cleavage step is accelerated by SufB. *J. Biol. Chem.* **281**, 8371–8378
106. Chandramouli, K., Unciuleac, M.-C., Naik, S., Dean, D. R., Huynh, B. H., and Johnson, M. K. (2007) Formation and properties of [4Fe-4S] clusters on the IscU scaffold protein. *Biochemistry* **46**, 6804–6811
107. Layer, G., Ollagnier-de Choudens, S., Sanakis, Y., and Fontecave, M. (2006) Iron-sulfur cluster biosynthesis: characterization of *Escherichia coli* CYaY as an iron donor for the assembly of [2Fe-2S] clusters in the scaffold IscU. *J. Biol. Chem.* **281**, 16256–16263
108. Berks, B. C., Palmer, T., and Sargent, F. (2005) Protein targeting by the bacterial twin-arginine translocation (Tat) pathway. *Curr. Opin. Microbiol.* **8**, 174–181
109. Stevenson, L. G., Strisovsky, K., Clemmer, K. M., Bhatt, S., Freeman, M., and Rather, P. N. (2007) Rhomboid protease AarA mediates quorum-sensing in *Providencia stuartii* by activating TatA of the twin-arginine translocase. *Proc. Natl. Acad. Sci.* **104**, 1003–1008
110. Fröbel, J., Rose, P., and Müller, M. (2012) Twin-arginine-dependent translocation of folded proteins. *Phil. Trans. R. Soc. B* **367**, 1029–1046
111. Berks, B. C. (1996) A common export pathway for proteins binding complex redox cofactors? *Mol. Microbiol.* **22**, 393–404
112. Sargent, F., Bogsch, E. G., Stanley, N. R., Wexler, M., Robinson, C., Berks, B. C., and Palmer, T. (1998) Overlapping functions of components of a bacterial Sec-independent protein export pathway. *EMBO J.* **17**, 3640–3650
113. Alami, M., Lüke, I., Deitermann, S., Eisner, G., Koch, H.-G., Brunner, J., and Müller, M. (2003) Differential interactions between a twin-arginine signal peptide and its translocase in *Escherichia coli*. *Molecular Cell* **12**, 937–946

114. Fröbel, J., Rose, P., and Müller, M. (2011) Early contacts between substrate proteins and TatA translocase component in twin-arginine translocation. *J. Biol. Chem.* **286**, 43679–43689
115. Gohlke, U. (2005) The TatA component of the twin-arginine protein transport system forms channel complexes of variable diameter. *Proc. Natl. Acad. Sci.* **102**, 10482–10486
116. Mangels, D., Mathers, J., Bolhuis, A., and Robinson, C. (2005) The core TatABC complex of the twin-arginine translocase in *Escherichia coli*: TatC drives assembly whereas TatA is essential for stability. *J. Mol. Biol.* **345**, 415–423
117. Maurer, C., Panahandeh, S., Jungkamp, A.-C., Moser, M., and Müller, M. (2010) TatB functions as an oligomeric binding site for folded Tat precursor proteins. *Mol. Biol. Cell* **21**, 4151–4161
118. Gérard, F., and Cline, K. (2006) Efficient twin arginine translocation (tat) pathway transport of a precursor protein covalently anchored to its initial cpTatC binding site. *J. Biol. Chem.* **281**, 6130–6135
119. Brüser, T., and Sanders, C. (2003) An alternative model of the twin arginine translocation system. *Microbiol. Res.* **158**, 7–17
120. DeLisa, M. P., Tullman, D., and Georgiou, G. (2003) Folding quality control in the export of proteins by the bacterial twin-arginine translocation pathway. *Proc. Natl. Acad. Sci. U.S.A.* **100**, 6115–6120
121. Richter, S., and Brüser, T. (2005) Targeting of unfolded PhoA to the Tat translocon of *Escherichia coli*. *J. Biol. Chem.* **280**, 42723–42730
122. Panahandeh, S., Maurer, C., Moser, M., DeLisa, M. P., and Müller, M. (2008) Following the path of a twin-arginine precursor along the TatABC translocase of *Escherichia coli*. *J. Biol. Chem.* **283**, 33267–33275
123. Sanders, C., Wethkamp, N., and Lill, H. (2001) Transport of cytochrome c derivatives by the bacterial Tat protein translocation system. *Mol. Microbiol.* **41**, 241–246
124. Matos, C. F. R. O., Robinson, C., and Di Cola, A. (2008) The Tat system proofreads FeS protein substrates and directly initiates the disposal of rejected molecules. *EMBO J.* **27**, 2055–2063
125. Cline, K., and McCaffery, M. (2007) Evidence for a dynamic and transient pathway through the TAT protein transport machinery. *EMBO J.* **26**, 3039–3049
126. Genest, O., Méjean, V., and Iobbi-Nivol, C. (2009) Multiple roles of TorD-like chaperones in the biogenesis of molybdoenzymes. *FEMS Microbiol. Lett.* **297**, 1–9
127. Blasco, F., Dos Santos, J., Magalon, A., Frixon, C., Guigliarelli, B., Santini, C., and Giordano, G. (1998) NarJ is a specific chaperone required for molybdenum cofactor assembly in nitrate reductase A of *Escherichia coli*. *Mol. Microbiol.* **28**, 435–447
128. Lanciano, P., Vergnes, A., Grimaldi, S., Guigliarelli, B., and Magalon, A. (2007) Biogenesis of a respiratory complex is orchestrated by a single accessory protein. *J. Biol. Chem.* **282**, 17468–17474

129. Vergnes, A., Pommier, J., Toci, R., Blasco, F., Giordano, G., and Magalon, A. (2006) NarJ chaperone binds on two distinct sites of the aponitrate reductase of *Escherichia coli* to coordinate molybdenum cofactor insertion and assembly. *J. Biol. Chem.* **281**, 2170–2176
130. Vergnes, A., Gouffi-Belhabich, K., Blasco, F., Giordano, G., and Magalon, A. (2004) Involvement of the molybdenum cofactor biosynthetic machinery in the maturation of the *Escherichia coli* nitrate reductase A. *J. Biol. Chem.* **279**, 41398–41403
131. Zakian, S., Lafitte, D., Vergnes, A., Pimentel, C., Sebban-Kreuzer, C., Toci, R., Claude, J., Guerlesquin, F., and Magalon, A. (2010) Basis of recognition between the NarJ chaperone and the N-terminus of the NarG subunit from *Escherichia coli* nitrate reductase. *FEBS J.* **277**, 1886–1895
132. Li, H., and Turner, R. J. (2009) In vivo associations of *Escherichia coli* NarJ with a peptide of the first 50 residues of nitrate reductase catalytic subunit NarG. *Can. J. Microbiol.* **55**, 179–188
133. Pommier, J., Méjean, V., Giordano, G., and Iobbi-Nivol, C. (1998) TorD, a cytoplasmic chaperone that interacts with the unfolded trimethylamine N-oxide reductase enzyme (TorA) in *Escherichia coli*. *J. Biol. Chem.* **273**, 16615–16620
134. Ilbert, M., Méjean, V., Giudici-Orticoni, M.-T., Samama, J.-P., and Iobbi-Nivol, C. (2003) Involvement of a mate chaperone (TorD) in the maturation pathway of molybdoenzyme TorA. *J. Biol. Chem.* **278**, 28787–28792
135. Genest, O., Ilbert, M., Méjean, V., and Iobbi-Nivol, C. (2005) TorD, an essential chaperone for TorA molybdoenzyme maturation at high temperature. *J. Biol. Chem.* **280**, 15644–15648
136. Genest, O., Seduk, F., Théraulaz, L., Méjean, V., and Iobbi-Nivol, C. (2006) Chaperone protection of immature molybdoenzyme during molybdenum cofactor limitation. *FEMS Microbiol. Lett.* **265**, 51–55
137. Weiner, J. H., Bilous, P. T., Shaw, G. M., Lubitz, S. P., Frost, L., Thomas, G. H., Cole, J. A., and Turner, R. J. (1998) A novel and ubiquitous system for membrane targeting and secretion of cofactor-containing proteins. *Cell* **93**, 93–101
138. Berks, B. C., Sargent, F., and Palmer, T. (2000) The Tat protein export pathway. *Mol. Microbiol.* **35**, 260–274
139. Jack, R. L., Buchanan, G., Dubini, A., Hatzixanthis, K., Palmer, T., and Sargent, F. (2004) Coordinating assembly and export of complex bacterial proteins. *EMBO J.* **23**, 3962–3972
140. Hatzixanthis, K., Clarke, T. A., Oubrie, A., Richardson, D. J., Turner, R. J., and Sargent, F. (2005) Signal peptide–chaperone interactions on the twin-arginine protein transport pathway. *PNAS* **102**, 8460–8465
141. Chan, C. S., Chang, L., Rommens, K. L., and Turner, R. J. (2009) Differential interactions between Tat-specific redox enzyme peptides and their chaperones. *J. Bacteriol.* **191**, 2091–2101

142. Ilbert, M., Méjean, V., and Iobbi-Nivol, C. (2004) Functional and structural analysis of members of the TorD family, a large chaperone family dedicated to molybdoproteins. *Microbiology* **150**, 935–943
143. Guymer, D., Maillard, J., Agacan, M. F., Brearley, C. A., and Sargent, F. (2010) Intrinsic GTPase activity of a bacterial twin-arginine translocation proofreading chaperone induced by domain swapping. *FEBS J.* **277**, 511–525
144. Lovelock, J. E., Maggs, R. J., and Rasmussen, R. A. (1972) Atmospheric dimethyl sulphide and the natural sulphur cycle. *Nature* **237**, 452
145. Bogachev, A. V., Murtazina, R. A., and Skulachev, V. P. (1996) H⁺/e⁻ stoichiometry for NADH dehydrogenase I and dimethyl sulfoxide reductase in anaerobically grown *Escherichia coli* cells. *J. Bacteriol.* **178**, 6233–6237
146. Lubitz, S. P., and Weiner, J. H. (2003) The *Escherichia coli* ynfEFGHI operon encodes polypeptides which are paralogues of dimethyl sulfoxide reductase (DmsABC). *Arch. Biochem. Biophys.* **418**, 205–216
147. Ray, N., Oates, J., Turner, R. J., and Robinson, C. (2003) DmsD is required for the biogenesis of DMSO reductase in *Escherichia coli* but not for the interaction of the DmsA signal peptide with the Tat apparatus. *FEBS Lett.* **534**, 156–160
148. Bearson, S. M. D., Albrecht, J. A., and Gunsalus, R. P. (2002) Oxygen and nitrate-dependent regulation of *dmsABC* operon expression in *Escherichia coli*: sites for Fnr and NarL protein interactions. *BMC Microbiol.* **2**, 13
149. Sambasivarao, D., and Weiner, J. H. (1991) Dimethyl sulfoxide reductase of *Escherichia coli*: an investigation of function and assembly by use of in vivo complementation. *J. Bacteriol.* **173**, 5935–5943
150. Rothery, R. A., Grant, J. L., Johnson, J. L., Rajagopalan, K. V., and Weiner, J. H. (1995) Association of molybdopterin guanine dinucleotide with *Escherichia coli* dimethyl sulfoxide reductase: effect of tungstate and a mob mutation. *J. Bacteriol.* **177**, 2057–2063
151. Sambasivarao, D., Turner, R. J., Simala-Grant, J. L., Shaw, G., Hu, J., and Weiner, J. H. (2000) Multiple roles for the twin arginine leader sequence of dimethyl sulfoxide reductase of *Escherichia coli*. *J. Biol. Chem.* **275**, 22526–22531
152. Oresnik, I. J., Ladner, C. L., and Turner, R. J. (2001) Identification of a twin-arginine leader-binding protein. *Mol. Microbiol.* **40**, 323–331
153. Johnson, J. L., Hainline, B. E., Rajagopalan, K. V., and Arison, B. H. (1984) The pterin component of the molybdenum cofactor. Structural characterization of two fluorescent derivatives. *J. Biol. Chem.* **259**, 5414–5422
154. Hille, R. (1999) Molybdenum enzymes. *Essays Biochem.* **34**, 125–137
155. McMaster, J., and Enemark, J. H. (1998) The active sites of molybdenum- and tungsten-containing enzymes. *Curr. Opin. Chem. Biol.* **2**, 201–207

156. Trieber, C. A., Rothery, R. A., and Weiner, J. H. (1996) Consequences of removal of a molybdenum ligand (DmsA-Ser-176) of *Escherichia coli* dimethyl sulfoxide reductase. *J. Biol. Chem.* **271**, 27339–27345
157. Heffron, K., Léger, C., Rothery, R. A., Weiner, J. H., and Armstrong, F. A. (2001) Determination of an optimal potential window for catalysis by *E. coli* dimethyl sulfoxide reductase and hypothesis on the role of Mo(V) in the reaction pathway. *Biochemistry* **40**, 3117–3126
158. Schindelin, H., Kisker, C., Hilton, J., Rajagopalan, K. V., and Rees, D. C. (1996) Crystal structure of DMSO reductase: redox-linked changes in molybdopterin coordination. *Science* **272**, 1615–1621
159. Schneider, F., Löwe, J., Huber, R., Schindelin, H., Kisker, C., and Knäblein, J. (1996) Crystal structure of dimethyl sulfoxide reductase from *Rhodobacter capsulatus* at 1.88 Å resolution. *J. Mol. Biol.* **263**, 53–69
160. McAlpine, A. S., McEwan, A. G., Shaw, A. L., and Bailey, S. (1997) Molybdenum active centre of DMSO reductase from *Rhodobacter capsulatus*: crystal structure of the oxidised enzyme at 1.82-Å resolution and the dithionite-reduced enzyme at 2.8-Å resolution. *J. Biol. Inorg. Chem.* **2**, 690–701
161. McAlpine, A. S., McEwan, A. G., and Bailey, S. (1998) The high resolution crystal structure of DMSO reductase in complex with DMSO. *J. Mol. Biol.* **275**, 613–623
162. Simala-Grant, J. L., and Weiner, J. H. (1996) Kinetic analysis and substrate specificity of *Escherichia coli* dimethyl sulfoxide reductase. *Microbiology (Reading, Engl.)* **142 (Pt 11)**, 3231–3239
163. Simala-Grant, J. L., and Weiner, J. H. (1998) Modulation of the substrate specificity of *Escherichia coli* dimethylsulfoxide reductase. *Eur. J. Biochem.* **251**, 510–515
164. Cammack, R., and Weiner, J. H. (1990) Electron paramagnetic resonance spectroscopic characterization of dimethyl sulfoxide reductase of *Escherichia coli*. *Biochemistry* **29**, 8410–8416
165. Bruschi, M., and Guerlesquin, F. (1988) Structure, function and evolution of bacterial ferredoxins. *FEMS Microbiol. Rev.* **4**, 155–175
166. Moura, J. J., Macedo, A. L., and Palma, P. N. (1994) Ferredoxins. *Meth. Enzymol.* **243**, 165–188
167. Jormakka, M., Törnroth, S., Byrne, B., and Iwata, S. (2002) Molecular basis of proton motive force generation: structure of formate dehydrogenase-N. *Science* **295**, 1863–1868
168. Blasco, F., Iobbi, C., Giordano, G., Chippaux, M., and Bonnefoy, V. (1989) Nitrate reductase of *Escherichia coli*: completion of the nucleotide sequence of the *nar* operon and reassessment of the role of the alpha and beta subunits in iron binding and electron transfer. *Mol. Gen. Genet.* **218**, 249–256
169. Guigliarelli, B., Asso, M., More, C., Augier, V., Blasco, F., Pommier, J., Giordano, G., and Bertrand, P. (1992) EPR and redox characterization of iron-sulfur centers in nitrate reductases A and Z from *Escherichia coli*. Evidence for a high-potential and a low-potential class and their

- relevance in the electron-transfer mechanism. *Eur. J. Biochem.* **207**, 61–68
170. Rothery, R. A., and Weiner, J. H. (1991) Alteration of the iron-sulfur cluster composition of *Escherichia coli* dimethyl sulfoxide reductase by site-directed mutagenesis. *Biochemistry* **30**, 8296–8305
 171. Rothery, R. A., and Weiner, J. H. (1996) Interaction of an engineered [3Fe-4S] cluster with a menaquinol binding site of *Escherichia coli* DMSO reductase. *Biochemistry* **35**, 3247–3257
 172. Cheng, V. W. T., Rothery, R. A., Bertero, M. G., Strynadka, N. C. J., and Weiner, J. H. (2005) Investigation of the environment surrounding iron-sulfur cluster 4 of *Escherichia coli* dimethylsulfoxide reductase. *Biochemistry* **44**, 8068–8077
 173. Sambasivarao, D., Dawson, H. A., Zhang, G., Shaw, G., Hu, J., and Weiner, J. H. (2001) Investigation of *Escherichia coli* dimethyl sulfoxide reductase assembly and processing in strains defective for the sec-independent protein translocation system membrane targeting and translocation. *J. Biol. Chem.* **276**, 20167–20174
 174. Weiner, J. H., Shaw, G., Turner, R. J., and Trieber, C. A. (1993) The topology of the anchor subunit of dimethyl sulfoxide reductase of *Escherichia coli*. *J. Biol. Chem.* **268**, 3238–3244
 175. Cole, S. T., Condon, C., Lemire, B. D., and Weiner, J. H. (1985) Molecular biology, biochemistry and bioenergetics of fumarate reductase, a complex membrane-bound iron-sulfur flavoenzyme of *Escherichia coli*. *Biochim. Biophys. Acta* **811**, 381–403
 176. Weiner, J. H., Cammack, R., Cole, S. T., Condon, C., Honoré, N., Lemire, B. D., and Shaw, G. (1986) A mutant of *Escherichia coli* fumarate reductase decoupled from electron transport. *Proc. Natl. Acad. Sci. U.S.A.* **83**, 2056–2060
 177. von Heijne, G. (1992) Membrane protein structure prediction. Hydrophobicity analysis and the positive-inside rule. *J. Mol. Biol.* **225**, 487–494
 178. Rothery, R. A., Chatterjee, I., Kiema, G., McDermott, M. T., and Weiner, J. H. (1998) Hydroxylated naphthoquinones as substrates for *Escherichia coli* anaerobic reductases. *Biochem. J.* **332**, 35–41
 179. Zhao, Z., and Weiner, J. H. (1998) Interaction of 2-N-heptyl-4-hydroxyquinoline-N-oxide with dimethyl sulfoxide reductase of *Escherichia coli*. *J. Biol. Chem.* **273**, 20758–20763
 180. Geijer, P., and Weiner, J. (2004) Glutamate 87 is important for menaquinol binding in DmsC of the DMSO reductase (DmsABC) from *Escherichia coli*. *Biochim. Biophys. Acta - Biomembranes* **1660**, 66–74
 181. Oresnik, I. J., Ladner, C. L., and Turner, R. J. (2001) Identification of a twin-arginine leader-binding protein. *Molecular Microbiology* **40**, 323–331
 182. Sarfo, K. J., Winstone, T. L., Papish, A. L., Howell, J. M., Kadir, H., Vogel, H. J., and Turner, R. J. (2004) Folding forms of *Escherichia coli* DmsD, a

- twin-arginine leader binding protein. *Biochem. Biophys. Res. Commun.* **315**, 397–403
183. Winstone, T. L., Workentine, M. L., Sarfo, K. J., Binding, A. J., Haslam, B. D., and Turner, R. J. (2006) Physical nature of signal peptide binding to DmsD. *Arch. Biochem. Biophys.* **455**, 89–97
184. Chan, C. S., Howell, J. M., Workentine, M. L., and Turner, R. J. (2006) Twin-arginine translocase may have a role in the chaperone function of NarJ from *Escherichia coli*. *Biochem. Biophys. Res. Commun.* **343**, 244–251
185. Ramasamy, S. K., and Clemons, W. M. (2009) Structure of the twin-arginine signal-binding protein DmsD from *Escherichia coli*. *Acta Crystallogr. F Struct. Biol. Crystal. Commun.* **65**, 746–750
186. Stevens, C. M., Winstone, T. M. L., Turner, R. J., and Paetzel, M. (2009) Structural analysis of a monomeric form of the twin-arginine leader peptide binding chaperone *Escherichia coli* DmsD. *J. Mol. Biol.* **389**, 124–133
187. Chan, C. S., Winstone, T. M. L., Chang, L., Stevens, C. M., Workentine, M. L., Li, H., Wei, Y., Ondrechen, M. J., Paetzel, M., and Turner, R. J. (2008) Identification of residues in DmsD for twin-arginine leader peptide binding, defined through random and bioinformatics-directed mutagenesis. *Biochemistry* **47**, 2749–2759
188. Qiu, Y., Zhang, R., Binkowski, T. A., Tereshko, V., Joachimiak, A., and Kossiakoff, A. (2008) The 1.38 Å crystal structure of DmsD protein from *Salmonella typhimurium*, a proofreading chaperone on the Tat pathway. *Proteins: Structure, Function, and Bioinformatics* **71**, 525–533
189. Papish, A. L., Ladner, C. L., and Turner, R. J. (2003) The twin-arginine leader-binding protein, DmsD, interacts with the TatB and TatC subunits of the *Escherichia coli* twin-arginine translocase. *J. Biol. Chem.* **278**, 32501–32506
190. Li, H., Chang, L., Howell, J. M., and Turner, R. J. (2010) DmsD, a Tat system specific chaperone, interacts with other general chaperones and proteins involved in the molybdenum cofactor biosynthesis. *Biochim. Biophys. Acta - Protein & Proteomics* **1804**, 1301–1309
191. Rothery, R. A., Kalra, N., Turner, R. J., and Weiner, J. H. (2002) Sequence similarity as a predictor of the transmembrane topology of membrane-intrinsic subunits of bacterial respiratory chain enzymes. *J. Mol. Microbiol. Biotechnol.* **4**, 133–150
192. Stanley, N. R., Sargent, F., Buchanan, G., Shi, J., Stewart, V., Palmer, T., and Berks, B. C. (2002) Behaviour of topological marker proteins targeted to the Tat protein transport pathway. *Mol. Microbiol.* **43**, 1005–1021
193. Natale, P., Brüser, T., and Driessen, A. J. M. (2008) Sec- and Tat-mediated protein secretion across the bacterial cytoplasmic membrane—distinct translocases and mechanisms. *Biochim. Biophys. Acta - Biomembranes* **1778**, 1735–1756

194. Rothery, R. A., Workun, G. J., and Weiner, J. H. (2008) The prokaryotic complex iron-sulfur molybdoenzyme family. *Biochim. Biophys. Acta* **1778**, 1897–1929

Chapter 2

Correct Assembly of Iron Sulfur Cluster FS0 into *Escherichia coli* Dimethyl Sulfoxide Reductase (DmsABC) is a Pre-requisite for Molybdenum Cofactor Insertion

*A version of this chapter was published:
Tang H., Rothery R. A., Voss J. E. and Weiner J.H. (2011) *The Journal of Biological Chemistry* **286**: 15147-15154.

2.1 Introduction

Escherichia coli is a facultative anaerobe able to respire with oxygen or alternative respiratory oxidants such as nitrate, nitrite, fumarate, and dimethyl sulfoxide (1, 2). Dimethyl sulfoxide reductase (DmsABC) is a terminal reductase that reduces dimethyl sulfoxide to dimethyl sulfide (3). It is a member of the bacterial CISM (complex iron-sulfur molybdoenzyme) family that includes *E. coli* formate dehydrogenases (FdnGHI and FdoGHI) (2, 4, 5), *E. coli* nitrate reductases (NarGHI and NarZYV) (6, 7), *Salmonella typhimurium* thiosulfate reductase (PhsABC) (8), and the *Wolinella succinogenes* and *Thermus thermophilus* (PsrABC) polysulfide reductases (9, 10). This family of enzymes contributes to the broad metabolic diversity that permits bacterial growth utilizing a wide range of respiratory substrates. Each structurally characterized enzyme of this family consists of a catalytic subunit with a molybdo-bis(pyranopterin guanine dinucleotide) (Mo-bisPGD) cofactor and an FS0 [4Fe-4S] cluster, an electron transfer subunit containing four [Fe-S] clusters, and a membrane anchor subunit containing a quinol/quinone-binding site (Q-site). Each enzyme catalyzes an overall reaction that involves transferring two electrons, through an electron transfer relay connecting the Q-site and the Mo-bisPGD cofactor, and reduction (or oxidation) of substrate at the catalytic molybdenum active site of the enzyme (see Fig. 2.1A). Although DmsABC does not contribute to the transmembrane proton electrochemical potential, it can support anaerobic growth with dimethyl sulfoxide as respiratory oxidant when coupled with an

appropriate proton-translocating dehydrogenase (11). DmsABC couples the oxidation of menaquinol within the hydrophobic membrane milieu to the reduction of water-soluble dimethyl sulfoxide in the membrane- extrinsic periplasmic domain of the enzyme (1, 12).

In *E. coli* DmsABC, it is the DmsA catalytic subunit that contains the Mo-bisPGD cofactor and an FS0 [4Fe-4S] cluster. The FS0 cluster is the last stepping stone of the electron transfer relay and transfers electrons from FS1 in DmsB to the cofactor in the active site of DmsA (see Fig. 2.1A). The N-terminal sequence of DmsA contains four highly conserved Cys residues, which form a ferredoxin-like Cys motif that, as we show below, coordinates FS0. In the CISM enzymes, the Cys group has the following consensus sequence: $(C_A/H_A)X_{2-3}C_BX_3C_CX_{27-34}C_DX(K/R)$ (1, 2). Sequences with two residues between C_A and C_B are classified as Type I sequences and typically have a Lys residue located after C_D (13, 14). DmsA is classified as a Type II sequence because it has three residues between C_A and C_B and an Arg residue after C_D . The third residue after C_A in DmsA is an Asn, which is highly conserved in DmsABC-type dimethyl sulfoxide reductases and NarGHI-type nitrate reductases across bacterial species (2). The interplay between the Type I and II sequences and molybdoenzyme assembly and function remains poorly understood.

Previous studies on the FS0-binding motif of DmsA indicated that mutating the second Cys residue to Ser or Ala results in assembly of a [3Fe-4S] cluster into DmsA (13) at the FS0 position. Careful analysis of the Mo(V)

EPR properties of the Mo-bisPGD cofactor indicated that there is a spin-spin interaction between the molybdenum center and a paramagnetic center with a midpoint potential of around -140 mV (15), but in none of these studies was the EPR spectrum of wild-type FS0 observed. In the case of another Type II enzyme, *E. coli* NarGHI, the FS0 spectrum was observed at low temperature at $g \sim 5.0$ (16, 17). Further studies revealed that FS0 insertion was closely linked to that of the Mo-bisPGD cofactor (18). An important distinction between the Type II Cys group sequence of DmsA and that of NarG is that there is a His in the C_A position of the latter and a Cys at this position in the former. It was not known whether the observation of a high spin FS0 EPR spectrum is related to the presence of His at the C_A position.

Maturation of the catalytically competent DmsABC requires efficient cofactor insertion into DmsA (19), association of DmsA and DmsB to form the DmsAB “catalytic dimer” (20), translocation of DmsAB across the cytoplasmic membrane via the *tat* translocon (3, 21, 22), and anchoring of DmsAB to the membrane through association with DmsC (20). However, assembly and targeting of the apoenzyme are not cofactor insertion-dependent (19, 23). In the case of NarGHI, NarJ functions as a system-specific chaperone participating in cofactor insertion (24, 25). In the case of DmsABC, the system-specific chaperone DmsD plays a role in targeting DmsAB to the *tat* translocon and may have additional roles in maturation (26). We have recently demonstrated by protein crystallography that, in NarGHI, FS0 assembly is a prerequisite for Mo-bisPGD insertion (18). It is therefore of

great interest to see if a similar sequence of cluster assembly and cofactor insertion occurs in the maturation of DmsABC.

In this study, we establish that DmsA contains a novel [4Fe-4S] FS0 cluster that has a high spin ground state ($S=3/2$) in its reduced form. By generating mutants of the DmsA N-terminal Cys group, we show that there is critical interplay between correct assembly of FS0 and molybdenum cofactor insertion. These results point toward a new paradigm for Mo-bisPGD cofactor-containing subunit maturation in which FS0 must be assembled prior to cofactor insertion.

2.2 Experimental Procedures

Bacterial Strains and Plasmids—*E. coli* strains DSS301 (20) and TOPP2 were used in this study (Table 2.1). DSS301 was used for the growth experiments. TOPP2 was used for enzyme expression and spectroscopic studies, as we found that it was optimal for DmsABC overexpression and assembly (27). The plasmids (Table 2.1) used for cloning and expression included pBR322, pDMS160 (28), and pATZ (EcoRI-EcoRV fragment of pDMS160 (28) cloned into pTZ18R (Amp^RlacZ' (Pharmacia)) (laboratory collection)). The sequence alignment for the residues mutated in this study is shown in Fig. 2.2.

Design of Mutants—A model for the structure of DmsA was generated using the ESyPred3D server (29) and the *E. coli* NarGHI structure as template (Protein Data Bank code 1Q16) (18). The PyMOL molecular graphics

program (Version 1.2.r1, DeLano Scientific LLC) was used to generate the images presented in Fig. 2.1.

Cloning and Site-directed Mutagenesis—Construction of the site-directed mutants was carried out following the QuikChange method (Stratagene) (27) using pATZ as the template for mutagenesis. Mutants were verified by DNA sequencing carried out by the Department of Biochemistry DNA Core Facility at the University of Alberta. The EcoRI-EcoRV fragments of DmsA containing the mutations were cloned back into the pDMS160 expression vector (30). The mutant plasmids were then transformed into *E. coli* DSS301 and TOPP2.

Growth of Bacteria in Glycerol/Dimethyl Sulfoxide Minimum Medium—The ability of the mutant DmsABC enzymes described herein to support respiratory growth on dimethyl sulfoxide was evaluated as follows. Appropriate plasmids were transformed into *E. coli* DSS301, and anaerobic growth was evaluated in sealed Klett flasks at 37 °C using glycerol/dimethyl sulfoxide minimum medium (27, 31). Culture turbidity was monitored using a Klett Summerson spectrophotometer equipped with a No. 66 filter (31).

Growth of Bacteria and Membrane Preparation—Wild-type and mutant plasmids were transformed into TOPP2 cells. The cells were then allowed to grow anaerobically for 24 h in 10 or 19 liters of glycerol/fumarate medium (28). Cells were harvested by centrifugation, washed, and resuspended in buffer containing 100mM MOPS and 5mM EDTA (pH 7). Membranes were prepared by cell lysis using an Avestin microfluidizer and

differential centrifugation. PMSF (2 mM final concentration) was added to the cell suspension prior to cell lysis. Membranes were washed, pelleted by ultracentrifugation, resuspended in 100 mM MOPS and 5 mM EDTA (pH 7), and flash-frozen with liquid N₂ before being stored at -70 °C prior to use (27).

Lowry Protein Assay—Protein concentrations of the membrane preparations were determined with the Lowry assay (32) modified by including 1% (w/v) SDS (33).

SDS-PAGE—45 µg of each protein were analyzed on a 12% SDS-polyacrylamide slab gel (34). 30 µg of purified DmsABC were loaded as a standard. Gel electrophoresis was run at 200 V for 45 min, and the gel was stained with Coomassie Brilliant Blue.

Measurement of DmsABC Enzyme Concentration by 2-n-Heptyl-4-hydroxyquinoline N-Oxide (HOQNO) Fluorescence Quench Titration—HOQNO is a menaquinol analog that binds to the DmsC quinol-binding site of DmsABC with 1:1 stoichiometry (35). The assay is based on the method of van Ark and Berden (36) and can be used to estimate the concentration of overexpressed DmsABC in membrane samples (27). Fluorescence was monitored at an excitation wavelength of 341nm and an emission wavelength of 479 nm as aliquots (2 µL) of 0.1 mM HOQNO were added to a membrane sample with final protein concentrations of 0.25, 0.5, 0.75, and 1.0 mg/mL in a total volume of 3.5 mL. Fluorescence readings were taken using a PerkinElmer LS 50B luminescence spectrophotometer. The concentration of enzyme was estimated as the concentration at which HOQNO fluorescence became

detectable in the sample cuvette (27).

Purification of DmsABC—Proteins were extracted from the membrane with 1% *n*-dodecyl- β -D-maltoside and 0.5 mM DTT in 100mM MOPS, 5mM EDTA, 10% glycerol, and 160 μ M PMSF (pH 7.0) for 1.5 h with gentle shaking on ice. The extraction mixture was then centrifuged at 40,000 rpm for 1.5 h to remove insoluble material, and DmsABC was separated from other proteins in the supernatant by FPLC using a Mono Q HR 10/10 anion exchange column and a GE Healthcare ÄKTA FPLC system. DmsABC was eluted from the column with a linear salt gradient (0–400mM KCl) in 50mM MOPS, 0.5mM EDTA, 10% glycerol, 0.05% *n*-dodecyl β -D-maltoside, and 0.5 mM DTT. Protein samples were concentrated by ultrafiltration.

Benzyl Viologen (BV)/Trimethylamine N-Oxide Oxidoreductase Activity Assay—The specific activities of the wild-type and mutant enzymes were measured as the rate of trimethylamine *N*-oxide-dependent oxidation of dithionite reduced BV by following the decrease in BV absorption at 570 nm (37). Enzyme activity is expressed as micromoles of BV oxidized per min/mg of total protein. The final concentration of trimethylamine *N*-oxide was 72 mM in 50 mM MOPS and 5 mM EDTA. The extinction coefficient for BV is 7.4 mM⁻¹ cm⁻¹.

Lapachol/Trimethylamine N-Oxide Oxidoreductase Activity Assay—Quinol-dependent enzyme activity was determined as the rate of trimethylamine *N*-oxide-dependent anaerobic oxidation of reduced lapachol (LPCH₂) (38). Lapachol was reduced by zinc in hydrochloric acid to form

LPCH₂, which was added to degassed 100 mM MOPS buffer containing 5 mM EDTA and 70 mM trimethylamine *N*-oxide in a closed cuvette. The reaction was initiated by the addition of enzyme. Lapachol absorbance at 481nm was monitored and used to calculate the activity as micromoles of LPCH₂ oxidized per min/mg of total protein. The extinction coefficient of lapachol is 2.66 mM⁻¹ cm⁻¹ (38).

Form A Fluorescence—The Form A fluorescence assay was used to estimate the relative amount of Mo-bisPGD in each DmsA enzyme preparation (23, 39). Form A molybdopterin derivatives were prepared by acidification of membrane preparations (10 mg/sample) with HCl and oxidation by boiling with 2% potassium iodide and 4% iodine (w/v). 200 μL of the acid denatured iodine-oxidized extracts was added to 3.5 ml of 1 M NH₄OH to measure the fluorescence (23). Excitation spectra were recorded at 240–420 nm (emission at 448 nm), and the emission spectra were recorded at 410–520 nm (excitation at 397 nm) using a PerkinElmer LS 50 luminescence spectrometer. Fluorescence spectra were corrected by subtraction of the spectrum of 1 M ammonium hydroxide as well as the spectrum of a membrane preparation of *E. coli* harboring only the pBR322 vector.

EPR Spectroscopy—Reduced samples were prepared by anaerobic incubation of purified DmsABC or membrane samples enriched in DmsABC with 6 mM sodium dithionite for 5 min at room temperature. All samples were prepared in 3-mm internal diameter quartz EPR tubes, rapidly frozen in

liquid nitrogen-chilled ethanol, and stored in liquid nitrogen until used. For analysis of [Fe-S] clusters, EPR spectra were recorded using a Bruker ELEXSYS E500 spectrometer equipped with a Bruker SHQE cavity and an Oxford Instruments ESR900 flowing helium cryostat.

2.3 Results And Discussion

Structural Relationship between FS0 and the Mo-bisPGD Cofactor—The catalytic subunit (NarG) of *E. coli* NarGHI is currently the best characterized Type II molybdoenzyme subunit (2, 16, 18, 40, 41). We used its structure (Protein Data Bank code 1Q16) to generate a model of DmsA in the FS0 region (Fig. 2.1, *B* and *C*). The segment comprising three residues between C_A and C_B, ¹⁹TVN²¹, is predicted to place the side chain of Asn-21 in close proximity to one dithiolene sulfur from each pyranopterin (Fig. 2.1*B*). The Arg residue that follows C_D in the FS0-coordinating motif (Arg-61) is predicted to be located between the proximal pterin and FS0 (Fig. 2.1*C*). Site-directed mutagenesis has demonstrated that this residue plays a critical role in electron transfer and intercenter interactions in *E. coli* DmsA (14, 15), and similar results have been obtained for the structurally characterized *E. coli* NarGHI (18) and *Ralstonia eutropha* NapA (42). We exploited our structural model to investigate the interplay between the FS0 [4Fe-4S] cluster and the Mo-bisPGD cofactor during the final stages of DmsABC maturation.

We generated mutants of residues predicted to surround the FS0 cluster of DmsA (*i*) to identify the EPR signature of FS0, (*ii*) to investigate the

effect of converting the DmsA Cys group from a Type II to a Type I sequence, and (iii) to investigate the interplay between FS0 assembly and Mo-bisPGD insertion. Fig. 2.2 shows the sequences of the mutant Cys groups generated herein. Arg-61 was mutated to Lys to emulate this feature of the Type I sequences. Asn-21 was deleted to investigate the effect of decreasing the C_A-C_B gap from three to two residues. Mutant enzyme CS1 contains multiple changes (V20Y, ΔAsn21, S25V, and R25G) to render the DmsA Cys group similar to that of *E. coli* formate dehydrogenase N (FdnGHI) (43, 44). R61K and CS1 complete the conversion of the DmsA Cys group from a Type II to a Type I sequence.

Direct Spectroscopic Evidence for the Presence of a High Spin [4Fe-4S] Cluster in DmsABC—EPR spectra recorded at $g \sim 2.0$ have provided no direct evidence for the existence of FS0 in DmsA (13, 15, 28, 37, 45). The emergence of a range of protein structures of molybdoenzyme subunits with N-terminal Cys groups allows us to predict that such a cluster must also exist in DmsA. In the case of the Type I enzymes, EPR spectra for FS0 have been reported and demonstrate that, in its reduced form, it has an $S = \frac{1}{2}$ ground state with well resolved EPR features at $g \sim 2.0$ (46, 47). EPR evidence for an FS0 cluster in DmsA is limited to the discovery that the Mo(V) form of the Mo-bisPGD cofactor is able to participate in a spin-spin interaction with an adjacent paramagnetic center during enzyme reduction (15). NarGHI, which is also a Type II enzyme, has been demonstrated to contain an FS0 cluster, which in its reduced form has a high spin ground state ($S = \frac{3}{2}$) (16–18). With the

availability of highly purified DmsABC coupled with improved EPR instrumentation, we reinvestigated the EPR spectrum of reduced DmsABC with the aim of identifying additional spectral features in the $g \sim 5.0$ region. Fig. 2.3 shows the spectrum at $g \sim 5.0$ of dithionite-reduced purified DmsABC. The spectrum of the reduced enzyme has a distinct peak at $g = 5.06$, consistent with it arising from a $[4\text{Fe-4S}]^+$ cluster with an $S = \frac{3}{2}$ ground state. Spectra of other $[4\text{Fe-4S}]^+$ systems with $S = \frac{3}{2}$ ground states typically exhibit two visible peaks, one at $g \sim 5.0$ corresponding to a $\Delta S = \pm \frac{1}{2}$ transition and another at a slightly higher g value corresponding to a $\Delta S = \pm \frac{3}{2}$ transition (16, 17, 48, 49). The existence of a single peak in EPR spectra of systems with an $S = \frac{3}{2}$ ground state is not unusual, as the optimum temperature for the observation of the $\Delta S = \pm \frac{3}{2}$ transition can be below those reachable with commonly used cryostats. Examples of $[4\text{Fe-4S}]^+$ clusters with an $S = \frac{3}{2}$ ground state that exhibit a single peak in the $g = 5.0$ region include those of *E. coli* fumarase A (50), component 1 from the iron-only nitrogenase of *Rhodobacter capsulatus* (51), and the 8Fe form of ferredoxin III from *Desulfovibrio africanus* (52). The intensity of the $g = 5.06$ feature of the DmsABC spectrum has a peak intensity at < 4.5 K and is almost undetectable at temperatures above ~ 20 K (data not shown). Overall, the observation of a low temperature peak at $g = 5$ in EPR spectra of reduced DmsABC is consistent with the presence of a high spin form ($S = \frac{3}{2}$ ground state) of

FS0. To confirm this, we studied the EPR properties of the range of mutants described in Fig. 2.2.

Assignment of the $g = 5.06$ Signal to FS0—Fig. 2.4A shows the effects of the mutations generated herein on DmsABC expression and assembly into the *E. coli* inner membrane. Each of the mutant enzymes was expressed to a level comparable with that of the wild-type enzyme (*cf. lane 4 with lanes 5–8*). Fig. 2.4B also shows EPR spectra of the mutant enzymes in the $g = 5$ region, providing evidence for assignment of the $g = 5.06$ peak to the FS0 cluster of DmsA. The R61K mutant retained a high spin signal centered at $g = 5.11$, indicating that, as is the case in NarGHI (18), mutation of the conserved basic residue C-terminal to the FS0-coordinating Cys group perturbs the FS0 EPR signal. Deletion of Asn-21 resulted in elimination of the signal, as did both the CS1 multimutant and the CS1 plus R61K mutant (Fig. 2.4B). Clearly, mutations of residues within the N-terminal Cys group of DmsA have significant effects on the EPR spectrum of reduced enzyme at $g \sim 5.0$. The spectrum of DmsABC in the $g = 2$ region is complicated by spectral overlap and spin-spin interactions between the four [4Fe-4S] clusters of DmsB (28, 37, 45), and for this reason, our analyses of the mutant spectra did not reveal evidence for additional features corresponding to a modified form of FS0 with an $S=1/2$ ground state in its reduced form (data not shown). One of the mutants, Δ Asn21, assembled a [3Fe-4S] cluster at the FS0 position (data not shown), which exhibited a spectrum in its oxidized state similar to those of the [3Fe-4S] clusters in mutants of DmsA previously reported by Trieber *et*

al. (13, 15). Overall, the EPR properties of the mutant enzymes allowed us to assign the $g = 5.06$ signal of reduced wild-type DmsABC to the FS0 cluster, which has an $S = \frac{3}{2}$ ground state in its reduced form.

Interplay between FS0 and Mo-bisPGD Insertion during DmsABC Maturation—A principal aim of this work was to examine the interplay between assembly of FS0 and insertion of Mo-bisPGD during DmsABC maturation. In the case of NarGHI, it is clear that Mo-bisPGD is not inserted in enzymes that lack FS0 (18, 25), and it is therefore important to determine whether this is an emerging paradigm for bacterial molybdoenzymes assembly. To address this question, we compared the relative amounts of Mo-bisPGD assayed using the Form A method (23, 39, 53) with estimates of DmsABC concentration measured by fluorescence quench titration (35, 45, 54, 55). The fluorophore used in this second assay is HOQNO, the fluorescence of which in free solution is completely quenched when bound to the Q-site of DmsABC (35) and of other enzymes such as *E. coli* fumarate reductase and NarGHI (54–56).

Fig. 2.5A shows fluorescence spectra of Form A preparations derived from membrane samples containing overexpressed wild-type and mutant DmsABC. The conservative mutation R61K had little effect on Mo-bisPGD assembly as judged by Form A preparation fluorescence levels. Membranes containing the multimitation CS1 enzyme yielded Form A preparations with only ~13% of the fluorescence levels of those from membranes containing overexpressed wild-type enzyme. Interestingly, when the CS1 multimitant

was combined with the R61K mutation, the Form A preparation fluorescence level returned to ~44% of that of the wild-type enzyme. Finally, removal of Asn-21 eliminated detectable Form A fluorescence (Fig. 2.5A) but did not prevent enzyme assembly into the *E. coli* inner membrane (Fig. 2.4A). This latter observation is notable for two reasons: (i) the CS1+R61K multimutant also has only two residues between the C_A and C_B positions yet is able to assemble cofactor, and (ii) the Δ Asn21 mutant assembles a [3Fe-4S] cluster at the FS0 position. Taken together, these observations indicate that the side chain of Asn-21 plays a critical role in facilitating Mo-bisPGD insertion into DmsA. These results complement those recently reported by us for cofactor insertion into NarG (18).

Table 2.2 summarizes the effects of the mutants studied herein on enzyme assembly and Mo-bisPGD insertion. Of the mutants studied, the Δ Asn21 mutant had the most dramatic effect on cofactor content, effectively eliminating detectable Form A derivative while retaining ~50% of wild-type levels of assembly into the cytoplasmic membrane (*cf.* Figs. 2.4A and 2.5A). Asn-21 is part of the loop connecting C_A and C_B of the N-terminal Cys group, and its side chain carboxamide nitrogen is predicted to be within H-bonding distance of dithiolene sulfurs from the two pterins of the Mo-bisPGD cofactor (Fig. 2.1B). It is therefore likely that Asn-21 side chain positioning is critical for Mo-bisPGD insertion.

Table 2.2 also summarizes the effects of the DmsA mutants on enzyme activity. Two assays were used, the BV/trimethylamine *N*-oxide

oxidoreductase assay and the LPCH₂/trimethylamine *N*-oxide oxidoreductase assay. The BV assay addresses the ability of the enzyme to catalyze substrate reduction with a nonspecific electron donor (BV), whereas the LPCH₂ assay addresses the ability of the enzyme to catalyze electron transfer through its electron transfer relay to the Mo-bisPGD cofactor. With the exception of the R61K mutant, enzyme activity was essentially eliminated in all of the mutants studied herein. In the case of CS1 plus R61K, a small amount of activity was rescued, but this did not correlate well with the amount of cofactor insertion detected in Form A fluorescence assays. A likely explanation for this is that the H-bonding contacts between the Asn-21 carboxamide nitrogen and the Mo-bisPGD dithiolene sulfurs are also critical in defining a catalytically competent molybdenum coordination environment.

Role of FS0 in DmsABC Maturation—As is the case for *E. coli* NarGHI (18), it is clear that the N-terminal Cys group of DmsA plays a critical role in controlling enzyme maturation by coordinating FS0 and Mo-bisPGD assembly. The results presented herein point to an emerging paradigm for Type II molybdoenzymes maturation: FS0 insertion is a prerequisite for enzyme maturation but is not a prerequisite for final assembly of the enzyme into the cytoplasmic membrane.

The mechanism of FS0 and Mo-bisPGD assembly likely involves [4Fe-4S] cluster insertion, generating a cofactor binding- competent conformation of DmsA. In the context of the work presented herein, correctly assembled FS0 dictates a correct conformation for the ¹⁸CTVNC²² sequence, which

allows subsequent Mo-bisPGD binding.

An important distinction between the two most characterized Type II enzymes is that whereas NarGH is anchored to the inner surface of the cytoplasmic membrane by NarI, DmsAB is translocated to the periplasm by the *tat* translocon and is anchored to the outer surface of the cytoplasmic membrane by DmsC (2, 22). In both cases, system-specific chaperones are involved, NarJ for NarGHI (24, 25) and DmsD for DmsABC (26, 57). It has been proposed in the case of NarGHI that NarJ is essential for Mo-bisPGD and FS0 insertion and binds to two sites on NarG, the first being the 50-amino acid pseudo *tat* leader at its N-terminus (58, 59) and the second being elsewhere in the protein. In the case of DmsABC, DmsD has been shown to bind to the *tat* leader, directing the fully folded cofactor containing DmsAB dimer to the periplasm via the *tat* translocon without an obligatory role in cofactor insertion (21). The apparently different roles of NarJ and DmsD have to be reconciled with their similar structures. When NarJ from *Archaeoglobus fulgidus* (60) is compared with DmsD from *E. coli* (61) using the secondary structure matching server (62), 132 amino acid residues align, corresponding to an overlap of 89% of NarJ residues and 65% of DmsD residues. It is therefore notable that NarJ appears to coordinate insertion of both FS0 and MobisPGD (25), whereas DmsD has a more specific role in directing DmsAB to the periplasm (21). Chan *et al.* (63) recently demonstrated a possible role of the *tat* translocon in enhancing the targeting of NarGH to the cytoplasmic membrane. The maturation of DmsABC is an example of one in which the

apoenzyme can be translocated by the *tat* translocon across the cytoplasmic membrane and assembled into its correct location in the absence of its Mo-bisPGD cofactor and/or its FS0 [4Fe-4S] cluster (19, 21, 23, 64). Further studies will be required to clarify the role of DmsD in DmsABC maturation.

We investigated the N-terminal Cys group of NarG using a combination of site-directed mutagenesis and protein crystallography (18, 41). The C_A residue of the NarG Cys group is in fact a His residue (His-49), and when mutated to a Cys, FS0 is still assembled into the enzyme along with the Mo-bisPGD cofactor without a detectable EPR signal in the $g = 5$ region. However, the observed high spin form of FS0 in DmsABC makes it clear that the presence of His at the C_A position in NarG is not the source of the EPR signal with an $S = 3/2$ ground state. When His-49 is mutated to Ser, neither FS0 nor Mo-bisPGD is assembled. In the crystal structure of this mutant, sequence ⁴⁹SGVNCTG⁵⁵ (equivalent to ¹⁸CTVNCGS²⁴ in DmsA) is unresolved, suggesting that the correct positioning of this sequence is critical for Mo-bisPGD cofactor insertion (18). In this study, disruption of the DmsA Cys group by generating the CS1 multimutant eliminated most of the Mo-bisPGD cofactor and prevented detection of FS0 by EPR. Combining this multimutant with an R61K mutant to generate a Type I Cys group sequence rescued Mo-bisPGD insertion (44% of the wild-type level) and a small amount of enzyme activity (Fig. 2.5B and Table 2.2). The most dramatic effect on cofactor insertion was elicited by the Δ Asn21 mutant. In this case, Mo-bisPGD insertion was completely eliminated, suggesting that the Asn-21 side chain

plays a critical role in facilitating Mo-bisPGD insertion.

2.4 Conclusions

Overall, we have used a combination of site-directed mutagenesis and a range of assays to identify the FS0 EPR signature of DmsABC. We have clearly demonstrated that sequence $^{18}\underline{\text{C}}_{\text{A}}\text{TVN}\underline{\text{C}}_{\text{B}}\text{G}^{23}$ plays a critical role in facilitating Mo-bisPGD binding, with deletion of Asn-21 having the most catastrophic effects. When the wild-type sequence $^{18}\underline{\text{C}}_{\text{A}}\text{TVN}\underline{\text{C}}_{\text{B}}\text{GSRC}\underline{\text{C}}_{\text{P}}^{27}$ is converted to a sequence similar to that of the FdnG subunit of *E. coli* formate dehydrogenase N ($^{18}\underline{\text{C}}_{\text{A}}\text{TYC}\underline{\text{C}}_{\text{B}}\text{GVGC}\underline{\text{C}}_{\text{C}}\text{G}^{26}$), cofactor binding is almost completely eliminated, but when the $^{18}\underline{\text{C}}_{\text{A}}\text{TYC}\underline{\text{C}}_{\text{B}}\text{GVGC}\underline{\text{C}}_{\text{C}}\text{G}^{26}$ multmutant is combined with an R61K mutant, generating a true Type I sequence, cofactor insertion is rescued. These results shed additional light on the maturation of members of the CISM family of bacterial molybdoenzymes.

2.5 Tables and Figures

Table 2.1: Bacterial Strains and Plasmids

	Description	Source
Strains		
DSS301	TG1, <i>kan</i> ^R Δ <i>dmsABC</i>	Lab Collection (210)
TOPP2	<i>rif</i> ^R [<i>F'</i> , <i>proAB</i> , <i>lacI</i> ^q Δ <i>M15</i> , <i>Tn10</i> , (<i>tet</i> ^R)]	Stratagene
Plasmids		
pBR322	Tet ^R Amp ^R	Pharmacia
pDMS160	<i>dmsABC</i> cloned into the EcoRI-Sall fragment of pBR322, Amp ^R	Lab Collection (191)
R61K	pDMS160 - <i>dmsA</i> ^{R61K} BC	This study
Δ N21	pDMS160 - <i>dmsA</i> ^{N21} BC	This study
CS1 ^a	pDMS160 - <i>dmsA</i> ^{CS1} BC	This study
CS1+R61K	pDMS160 - <i>dmsA</i> ^{CS1+R61K} BC	This study

^a For simplicity, this plasmid is named CS1. The actual mutations are: V20Y, Δ N21, S24V, R25G, P43G (**Figure 2.1**).

Table 2.2: Enzyme and Mo-bisPGD cofactor quantifications and enzyme activities determined by *in vitro* reduction assays and *in vivo* growth experiments

Enzym	[DmsABC] (nmol mg ⁻¹) ^a	Mo-bisPGD content ^b	Specific activity ^c		Growth ^d
			BV	LPCH ₂	
pBR322	0	0	11.8	0.44	No Growth
DmsABC	0.94	100	141	7.72	High
R61K	0.99	90	125	2.63	High
ΔN21	0.57	0	5.91	0.07	No Growth
CS1	0.62	13	5.22	0.14	No Growth
CS1+R61K	0.58	44	7.97	0.33	No Growth

^a The concentrations of wild-type and mutant DmsABC in each membrane sample were determined by HOQNO fluorescence quench titration. pBR322 is an empty vector, so no DmsABC could be detected.

^b The Mo-bisPGD cofactor content determined by the Form A fluorescence are qualitative and reported in terms of relative fluorescence intensities. The peak emission fluorescence for wild-type DmsABC was normalized to 100, and the relative fluorescence for the mutant enzymes were calculated using their peak emission fluorescence. The relative cofactor occupancies were then calculated using relative cofactor content and DmsABC concentrations, and shown in **Figure 2.5B**.

^c Specific enzyme activities of wild-type and mutant DmsABC were assayed by BV- or LPCH₂-dependent reductions of trimethylamine N-oxide. Assays were carried out in triplicate, and average enzyme specific activities are reported. The specific enzyme activities are given in μmoles BV or LPCH₂/min/mg of total protein. The turn-over rates (s⁻¹) were then calculated using the specific activities and DmsABC concentrations, and the relative rates with wild-type normalized to 100 are reported in **Figure 2.5B**.

^d DSS301 cells transformed with plasmid encoding wild-type DmsABC and its variants were grown anaerobically on glycerol/dimethyl sulfoxide minimum media.

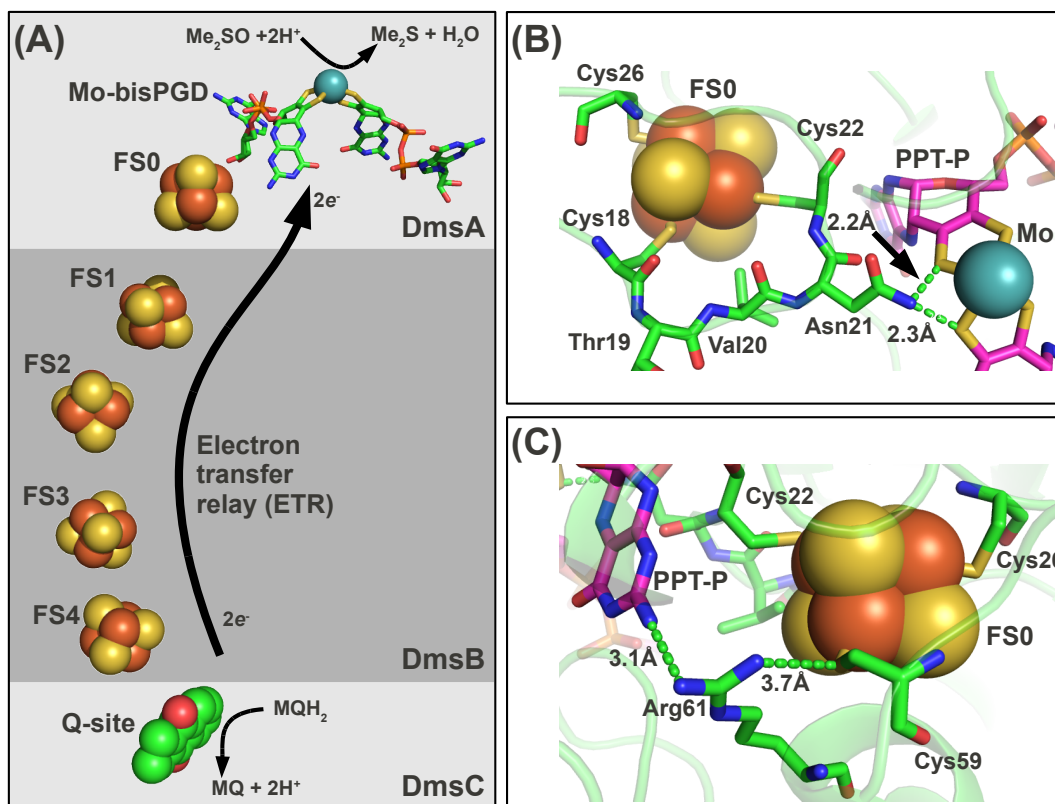


Figure 2.1 Electron transfer relay architecture and predicted DmsA structure around FS0. **A.** Predicted electron transfer relay in DmsABC connecting a menaquinol-binding site in the DmsC subunit with the Mo-bisPGD cofactor in the DmsA subunit. In this model, note that DmsC is predicted to be membrane-intrinsic and anchors to DmsA and DmsB to the periplasmic side of the *E. coli* cytoplasmic membrane (2). **B.** A structural model of DmsA was generated using the ESyPred3D server (29) with the structure of the NarG subunit of NarGHI as a template (Protein Data Bank code 1Q16) (40). The predicted position of the ¹⁸CTVNC²² loop is shown. The distances shown are arbitrary but indicate a possible H-bonding interaction between Asn-21 and one dithiolene sulfur from each pterin. **C.** The predicted position of Arg-61 between FS0 and the proximal pterin (PPT-P).

	18	22	26		59
	↓	↓	↓		↓
DmsA <i>E.coli</i>	C <u>T</u> V <u>N</u> C <u>G</u> S <u>R</u> C <u>P</u> L <u>R</u>	...	A <u>C</u> L <u>R</u> G		
R61K	C <u>T</u> V <u>N</u> C <u>G</u> S <u>R</u> C <u>P</u> L <u>R</u>	...	A <u>C</u> L <u>K</u> G		
ΔN21	C <u>T</u> V- <u>C</u> G <u>S</u> R <u>C</u> P <u>L</u> R	...	A <u>C</u> L <u>R</u> G		
CS1	C <u>T</u> <u>Y</u> - <u>C</u> G <u>V</u> G <u>C</u> G <u>L</u> R	...	A <u>C</u> L <u>R</u> G		
R61K+CS1	C <u>T</u> <u>Y</u> - <u>C</u> G <u>V</u> G <u>C</u> G <u>L</u> R	...	A <u>C</u> L <u>K</u> G		
FdnG <i>E.coli</i>	C <u>T</u> <u>Y</u> - <u>C</u> S <u>V</u> G <u>C</u> L <u>L</u> M	...	L <u>C</u> P <u>K</u> G		
NarG <i>E.coli</i>	H <u>G</u> V <u>N</u> C <u>T</u> G <u>S</u> C <u>S</u> W <u>K</u>	...	G <u>C</u> P <u>R</u> G		

Figure 2.2 Sequences of DmsA mutants in comparison with Cys group sequences of FdnG and NarG. Numbers mark the positions of four conserved Cys residues in the mature protein sequence. The amino acid residues that were mutated for this study are underlined. In the sequences of the mutants, the resultant residues of mutation are shown in boldface. Sequences of *E. coli* FdnG, a typical Type I enzyme and *E. coli* NarG, a typical Type II enzyme are also shown for comparison.

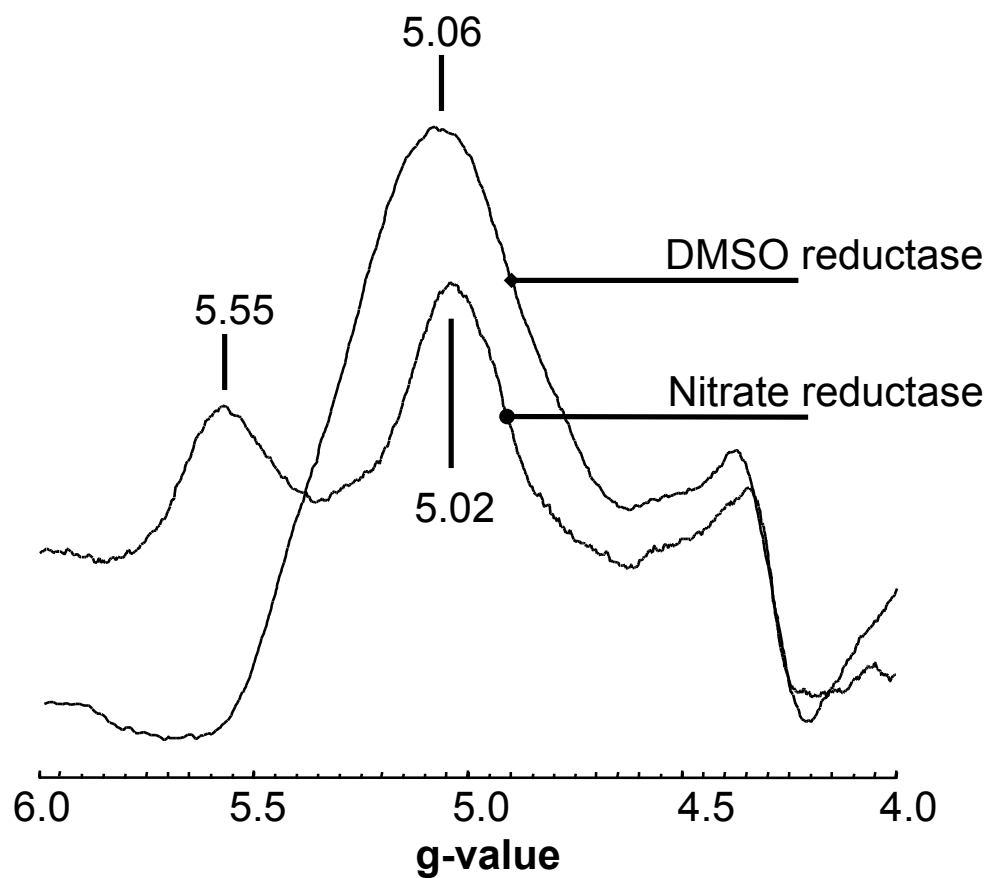


Figure 2.3 Low field EPR spectrum of purified DmsABC and NarGHI. Samples were reduced by anaerobic incubation with 6 mM sodium dithionite for 5 minutes. EPR conditions were as follows: temperature, 9 K; microwave power, 100 mW at 9.387 GHz; modulation amplitude, 20 G_{pp} at 100 KHz.

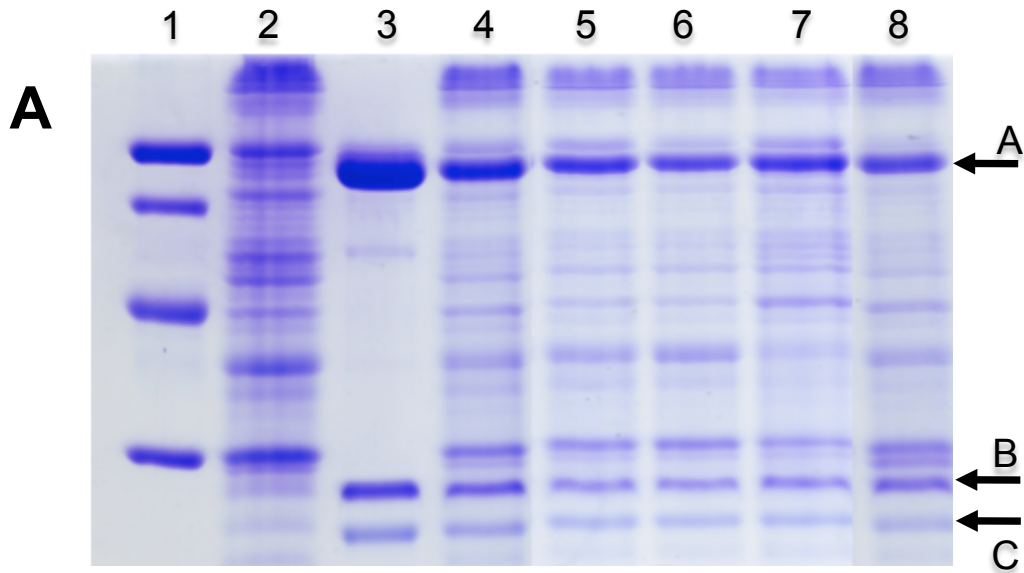


Figure 2.4 A. Sodium dodecyl sulfate-PAGE gel of DmsABC and its mutants. *Lane 1:* low molecular weight marker. *Lane 2:* membranes from the negative control TOPP2/pBR322. *Lane 3:* purified wild-type DmsABC. *Lane 4:* TOPP2 membranes containing over-expressed wild-type DmsABC. *Lane 5:* DmsA^{R61K}BC. *Lane 6:* DmsA^{CS1}BC. *Lane 7:* DmsA^{ΔN21}BC. *Lane 8:* DmsA^{CS1+R61K}BC. Position A marks DmsA (85.8 kDa), position B marks DmsB (22.7 kDa) and position C marks DmsC (30.8 kDa). 45 μg of total membrane protein were added per lane, except for lane 3 in which 30 μg of purified enzyme was used.

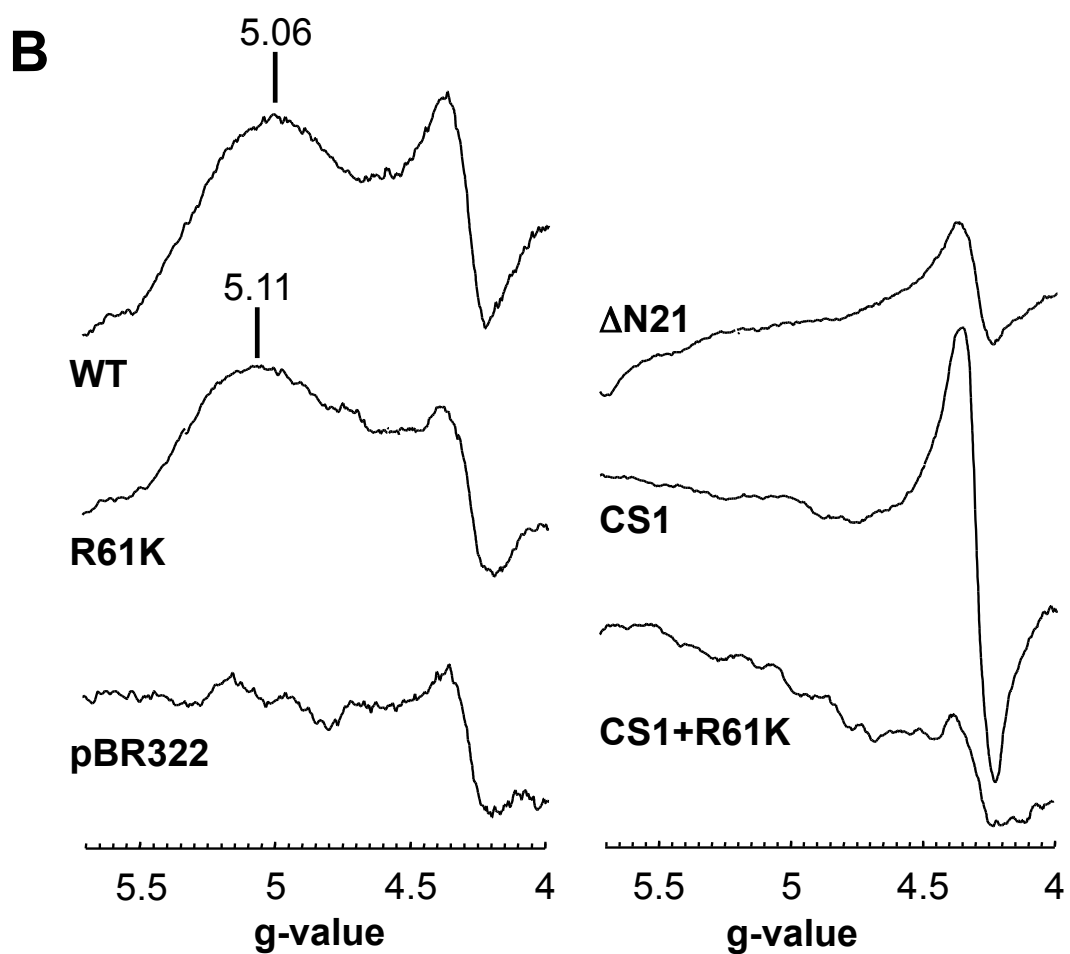


Figure 2.4 B. Effect of mutations of residues close to FS0 or the proximal pterin on the low field DmsABC EPR spectrum. EPR conditions were as for **Figure 2.3**, except that spectra are of membrane samples normalized to a protein concentration of 30 mg ml^{-1} .

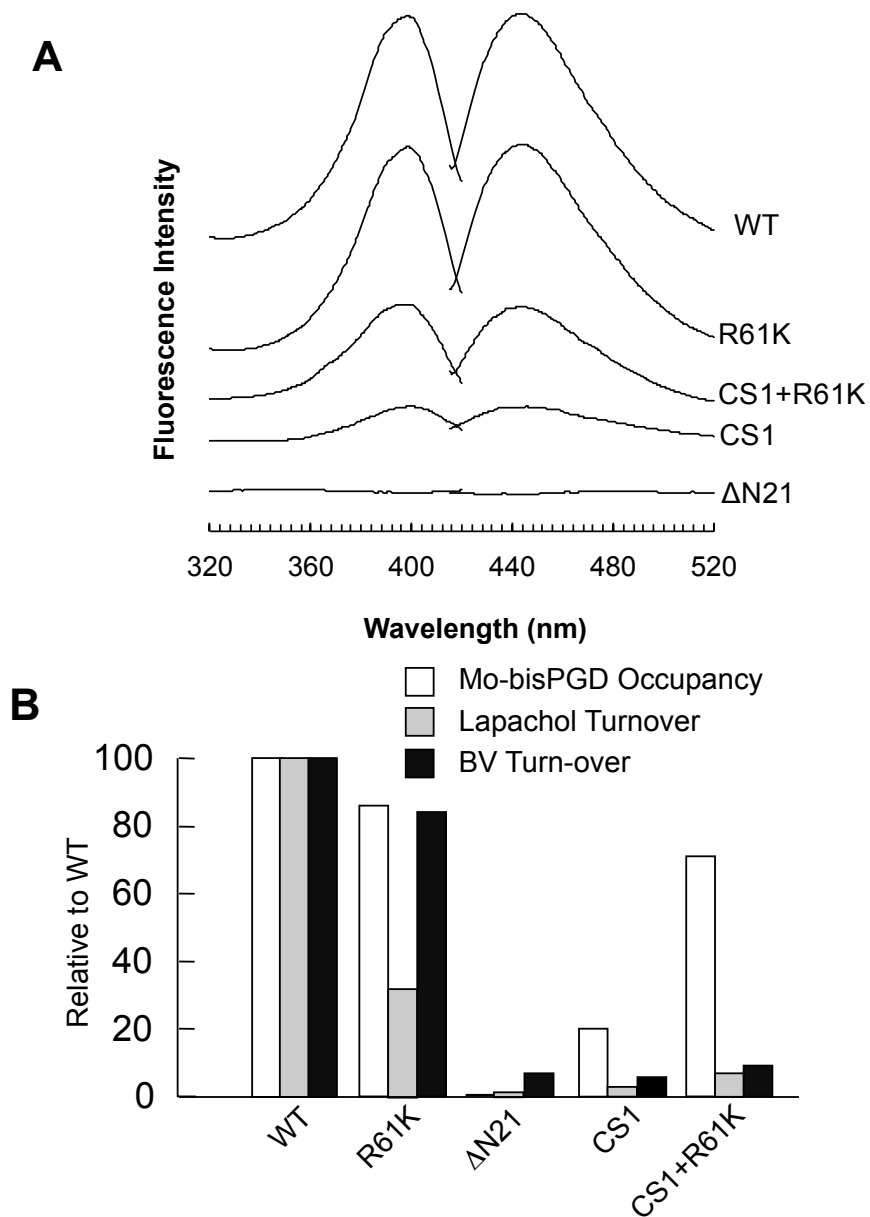


Figure 2.5 Mo-bisPGD cofactor occupancies and enzyme turn-over rates. **A.** Form A fluorescence spectra of extracts of membrane enriched in DmsABC wild-type or mutant variants. The fluorescence of the TOPP2/pBR322 membrane has been subtracted from each spectrum to eliminate the contribution from chromosomal DmsABC. **B.** *Relative cofactor occupancies and enzyme turn-over rates.* All values are normalized to wild-type being 100. Clear bars are relative Mo-bisPGD cofactor occupancies in DmsA mutant enzymes calculated using DmsABC concentrations and relative Form A fluorescence. Grey bars are relative enzyme turn-over rates calculated using enzyme specific activities when reduced lapachol (LPCH₂) is the substrate and DmsABC concentrations. Black bars are relative enzyme turn-over rates calculated using enzyme specific activities when reduced benzyl viologen (BV) is the substrate and DmsABC concentrations.

2.6 References

1. Weiner, J. H., Rothery, R. A., Sambasivarao, D., and Trieber, C. A. (1992) *Biochimica et Biophysica Acta (BBA) - Bioenergetics* **1102**, 1-18
2. Rothery, R. A., Workun, G. J., and Weiner, J. H. (2008) *Biochim. Biophys. Acta* **1778**, 1897-1929
3. Weiner, J. H., Bilous, P. T., Shaw, G. M., Lubitz, S. P., Frost, L., Thomas, G. H., Cole, J. A., and Turner, R. J. (1998) *Cell* **93**, 93-101
4. Plunkett, G., Burland, V., Daniels, D. L., and Blattner, F. R. (1993) *Nucleic Acids Res* **21**, 3391-3398
5. Berg, B. L., Baron, C., and Stewart, V. (1991) *J. Biol. Chem* **266**, 22386-22391
6. Blasco, F., Iobbi, C., Giordano, G., Chippaux, M., and Bonnefoy, V. (1989) *Mol. Gen. Genet* **218**, 249-256
7. Blasco, F., Iobbi, C., Ratouchniak, J., Bonnefoy, V., and Chippaux, M. (1990) *Mol. Gen. Genet* **222**, 104-111
8. Heinzinger, N. K., Fujimoto, S. Y., Clark, M. A., Moreno, M. S., and Barrett, E. L. (1995) *J. Bacteriol.* **177**, 2813-2820
9. Krafft, T., Bokranz, M., Klimmek, O., Schröder, I., Fahrenholz, F., Kojro, E., and Kröger, A. (1992) *Eur. J. Biochem* **206**, 503-510
10. Jormakka, M., Yokoyama, K., Yano, T., Tamakoshi, M., Akimoto, S., Shimamura, T., Curmi, P., and Iwata, S. (2008) *Nat. Struct. Mol. Biol* **15**, 730-737
11. Bogachev, A. V., Murtazina, R. A., and Skulachev, V. P. (1996) *J. Bacteriol.* **178**, 6233-6237
12. Sambasivarao, D., Scraba, D. G., Trieber, C., and Weiner, J. H. (1990) *J. Bacteriol.* **172**, 5938-5948
13. Trieber, C. A., Rothery, R. A., and Weiner, J. H. (1996) *Journal of Biological Chemistry* **271**, 4620 -4626
14. Trieber, C. A., Rothery, R. A., and Weiner, J. H. (1994) *J. Biol. Chem* **269**, 7103-7109
15. Rothery, R. A., Trieber, C. A., and Weiner, J. H. (1999) *Journal of Biological Chemistry* **274**, 13002 -13009
16. Rothery, R. A., Bertero, M. G., Cammack, R., Palak, M., Blasco, F., Strynadka, N. C. J., and Weiner, J. H. (2004) *Biochemistry* **43**, 5324-5333
17. Lanciano, P., Savoyant, A., Grimaldi, S., Magalon, A., Guigliarelli, B., and Bertrand, P. (2007) *The Journal of Physical Chemistry B* **111**, 13632-13637
18. Rothery, R. A., Bertero, M. G., Spreter, T., Bouromand, N., Strynadka, N. C. J., and Weiner, J. H. (2010) *Journal of Biological Chemistry* **285**, 8801 - 8807
19. Sambasivarao, D., Turner, R. J., Bilous, P. T., Rothery, R. A., Shaw, G., and Weiner, J. H. (2002) *Biochem. Cell Biol* **80**, 435-443
20. Sambasivarao, D., and Weiner, J. H. (1991) *J. Bacteriol.* **173**, 5935-5943
21. Sambasivarao, D., Turner, R. J., Simala-Grant, J. L., Shaw, G., Hu, J., and Weiner, J. H. (2000) *J. Biol. Chem* **275**, 22526-22531

22. Stanley, N. R., Sargent, F., Buchanan, G., Shi, J., Stewart, V., Palmer, T., and Berks, B. C. (2002) *Mol. Microbiol* **43**, 1005-1021
23. Rothery, R. A., Grant, J. L., Johnson, J. L., Rajagopalan, K. V., and Weiner, J. H. (1995) *J. Bacteriol.* **177**, 2057-2063
24. Blasco, F., Dos Santos, J. P., Magalon, A., Frixon, C., Guigliarelli, B., Santini, C. L., and Giordano, G. (1998) *Mol. Microbiol* **28**, 435-447
25. Lanciano, P., Vergnes, A., Grimaldi, S., Guigliarelli, B., and Magalon, A. (2007) *J. Biol. Chem* **282**, 17468-17474
26. Oresnik, I. J., Ladner, C. L., and Turner, R. J. (2001) *Mol. Microbiol* **40**, 323-331
27. Cheng, V. W. T., Rothery, R. A., Bertero, M. G., Strynadka, N. C. J., and Weiner, J. H. (2005) *Biochemistry* **44**, 8068-8077
28. Rothery, R. A., and Weiner, J. H. (1991) *Biochemistry* **30**, 8296-8305
29. Lambert, C., Léonard, N., De Bolle, X., and Depiereux, E. (2002) *Bioinformatics* **18**, 1250-1256
30. Sambrook, J., and Russell, D. W. (2001) *Molecular cloning: a laboratory manual*, CSHL Press
31. Bilous, P. T., and Weiner, J. H. (1985) *J. Bacteriol.* **162**, 1151-1155
32. Lowry, O. H., Rosebrough, N. J., Farr, A. L., and Randall, R. J. (1951) *J. Biol. Chem* **193**, 265-275
33. Markwell, M. A., Haas, S. M., Bieber, L. L., and Tolbert, N. E. (1978) *Anal. Biochem* **87**, 206-210
34. Cleveland, D. W., Fischer, S. G., Kirschner, M. W., and Laemmli, U. K. (1977) *J. Biol. Chem* **252**, 1102-1106
35. Zhao, Z., and Weiner, J. H. (1998) *Journal of Biological Chemistry* **273**, 20758 -20763
36. Van Ark, G., and Berden, J. A. (1977) *Biochim. Biophys. Acta* **459**, 119-127
37. Cammack, R., and Weiner, J. H. (1990) *Biochemistry* **29**, 8410-8416
38. Rothery, R. A., Chatterjee, I., Kiema, G., McDermott, M. T., and Weiner, J. H. (1998) *Biochem. J* **332 (Pt 1)**, 35-41
39. Johnson, J. L., Hainline, B. E., Rajagopalan, K. V., and Arison, B. H. (1984) *J. Biol. Chem* **259**, 5414-5422
40. Bertero, M. G., Rothery, R. A., Palak, M., Hou, C., Lim, D., Blasco, F., Weiner, J. H., and Strynadka, N. C. J. (2003) *Nat Struct Mol Biol* **10**, 681-687
41. Magalon, A., Asso, M., Guigliarelli, B., Rothery, R. A., Bertrand, P., Giordano, G., and Blasco, F. (1998) *Biochemistry* **37**, 7363-7370
42. Hettmann, T., Siddiqui, R. A., von Langen, J., Frey, C., Romão, M. J., and Diekmann, S. (2003) *Biochem. Biophys. Res. Commun* **310**, 40-47
43. Berg, B. L., and Stewart, V. (1990) *Genetics* **125**, 691-702
44. Jormakka, M., Törnroth, S., Byrne, B., and Iwata, S. (2002) *Science* **295**, 1863-1868
45. Rothery, R. A., and Weiner, J. H. (1996) *Biochemistry* **35**, 3247-3257
46. Gladyshev, V. N., Boyington, J. C., Khangulov, S. V., Grahame, D. A., Stadtman, T. C., and Sun, P. D. (1996) *J. Biol. Chem* **271**, 8095-8100
47. Breton, J., Berks, B. C., Reilly, A., Thomson, A. J., Ferguson, S. J., and Richardson, D. J. (1994) *FEBS Lett* **345**, 76-80

48. Duderstadt, R. E., Brereton, P. S., Adams, M. W., and Johnson, M. K. (1999) *FEBS Lett* **454**, 21-26
49. Kowal, A. T., Werth, M. T., Manodori, A., Cecchini, G., Schröder, I., Gunsalus, R. P., and Johnson, M. K. (1995) *Biochemistry* **34**, 12284-12293
50. Flint, D. H., Emptage, M. H., and Guest, J. R. (1992) *Biochemistry* **31**, 10331-10337
51. Müller, A., Schneider, K., Knüttel, K., and Hagen, W. R. (1992) *FEBS Lett* **303**, 36-40
52. George, S. J., Armstrong, F. A., Hatchikian, E. C., and Thomson, A. J. (1989) *Biochem. J* **264**, 275-284
53. Johnson, J. L., Indermaur, L. W., and Rajagopalan, K. V. (1991) *J. Biol. Chem* **266**, 12140-12145
54. Rothery, R. A., Seime, A. M., Spiers, A. C., Maklashina, E., Schröder, I., Gunsalus, R. P., Cecchini, G., and Weiner, J. H. (2005) *FEBS J* **272**, 313-326
55. Rothery, R. A., and Weiner, J. H. (1998) *Eur. J. Biochem* **254**, 588-595
56. Rothery, R. A., Blasco, F., Magalon, A., Asso, M., and Weiner, J. H. (1999) *Biochemistry* **38**, 12747-12757
57. Ray, N., Oates, J., Turner, R. J., and Robinson, C. (2003) *FEBS Letters* **534**, 156-160
58. Vergnes, A., Pommier, J., Toci, R., Blasco, F., Giordano, G., and Magalon, A. (2006) *J. Biol. Chem* **281**, 2170-2176
59. Li, H., and Turner, R. J. (2009) *Can. J. Microbiol* **55**, 179-188
60. Kirillova, O., Chruszcz, M., Shumilin, I. A., Skarina, T., Gorodichtchenskaia, E., Cymborowski, M., Savchenko, A., Edwards, A., and Minor, W. (2007) *Acta Crystallogr. D Biol. Crystallogr* **63**, 348-354
61. Stevens, C. M., Winstone, T. M. L., Turner, R. J., and Paetzl, M. (2009) *J. Mol. Biol* **389**, 124-133
62. Krissinel, E., and Henrick, K. (2004) *Acta Crystallogr. D Biol. Crystallogr* **60**, 2256-2268
63. Chan, C. S., Chang, L., Winstone, T. M., and Turner, R. J. (2010) *FEBS Letters* **584**, 4553-4558
64. Sambasivarao, D., Dawson, H. A., Zhang, G., Shaw, G., Hu, J., and Weiner, J. H. (2001) *J. Biol. Chem* **276**, 20167-20174

2.7 Appendix: Supplementary Figures

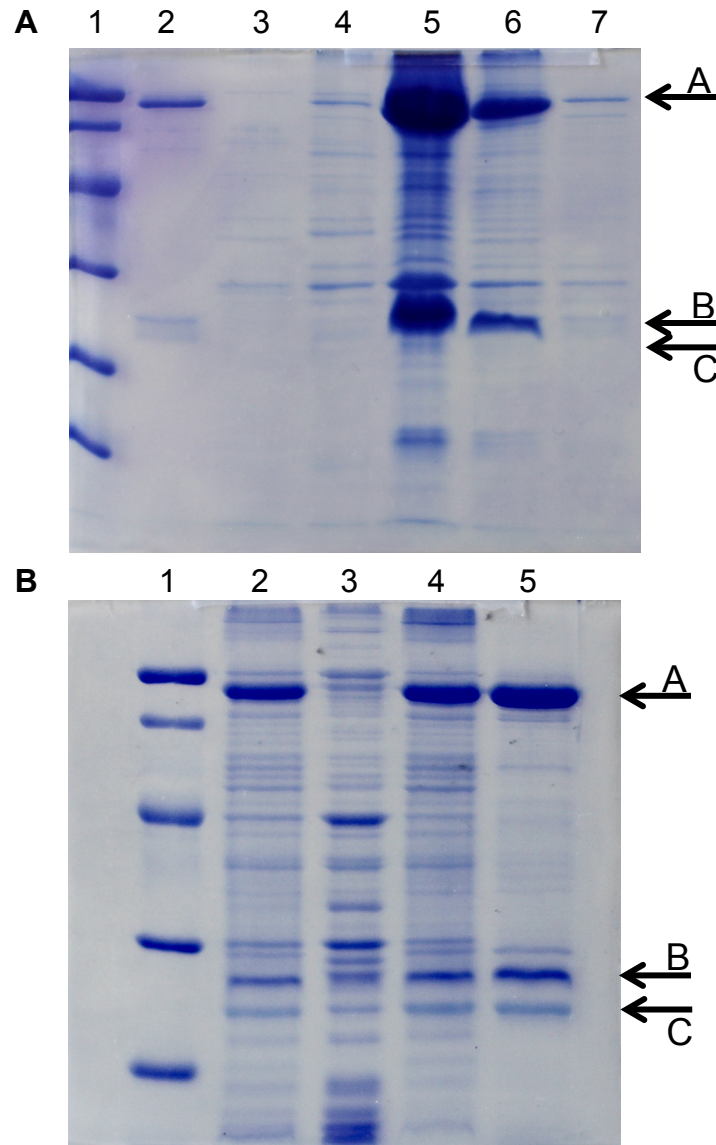


Figure 2.6 Purification of *E. coli* DmsABC. **Gel A:** Fractions collected from FPLC. Lanes were loaded as followed: 1, low molecular weight (LMW) standard; 2, DmsABC standard; 3-7, FPLC fractions 8-12, respectively. Fractions 10 and 11, which showed high concentration of DmsABC both in chromatogram and on gel, were collected and concentrated to final product. **Gel B:** Starting membrane sample and products at each purification step. The contents of the lanes are: 1, LMW standard; 2, membrane sample; 3, pellet after extraction with DDM; 4, supernatant (after extraction) that is to be purified via FPLC; 5, concentrated purified protein sample. 45 μ g of total protein was loaded for membrane sample. 30 μ g of total protein was loaded for each of other sample. Position A marks DmsA (85.8 kDa), position B marks DmsB (22.7 kDa) and position C marks DmsC (30.8 kDa).

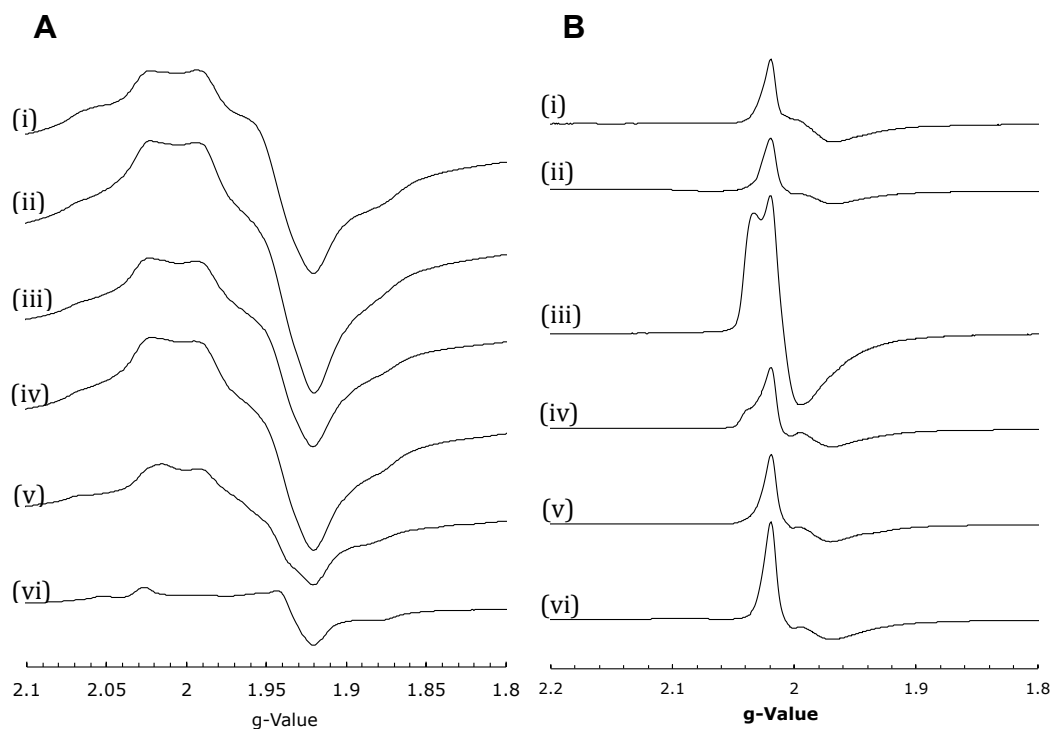


Figure 2.7 High field EPR spectrum of reduced (A) and oxidized (B) DmsABC wild-type and mutants enzymes. The membrane samples are wild-type (i), DmsA^{R61K}BC (ii), DmsA^{ΔN21}BC (iii), DmsA^{CS1}BC (iv), DmsA^{CS1+R61K}BC (v), and pBR322 (iv). Reduced samples were prepared by anaerobic incubation with 6 mM sodium dithionite for 5 minutes. Oxidized samples were prepared by mixing with air at room temperature. EPR conditions were as follows: temperature, 9 K; microwave power, 100 mW at 9.387 GHz; modulation amplitude, 20 G_{pp} at 100 KHz.

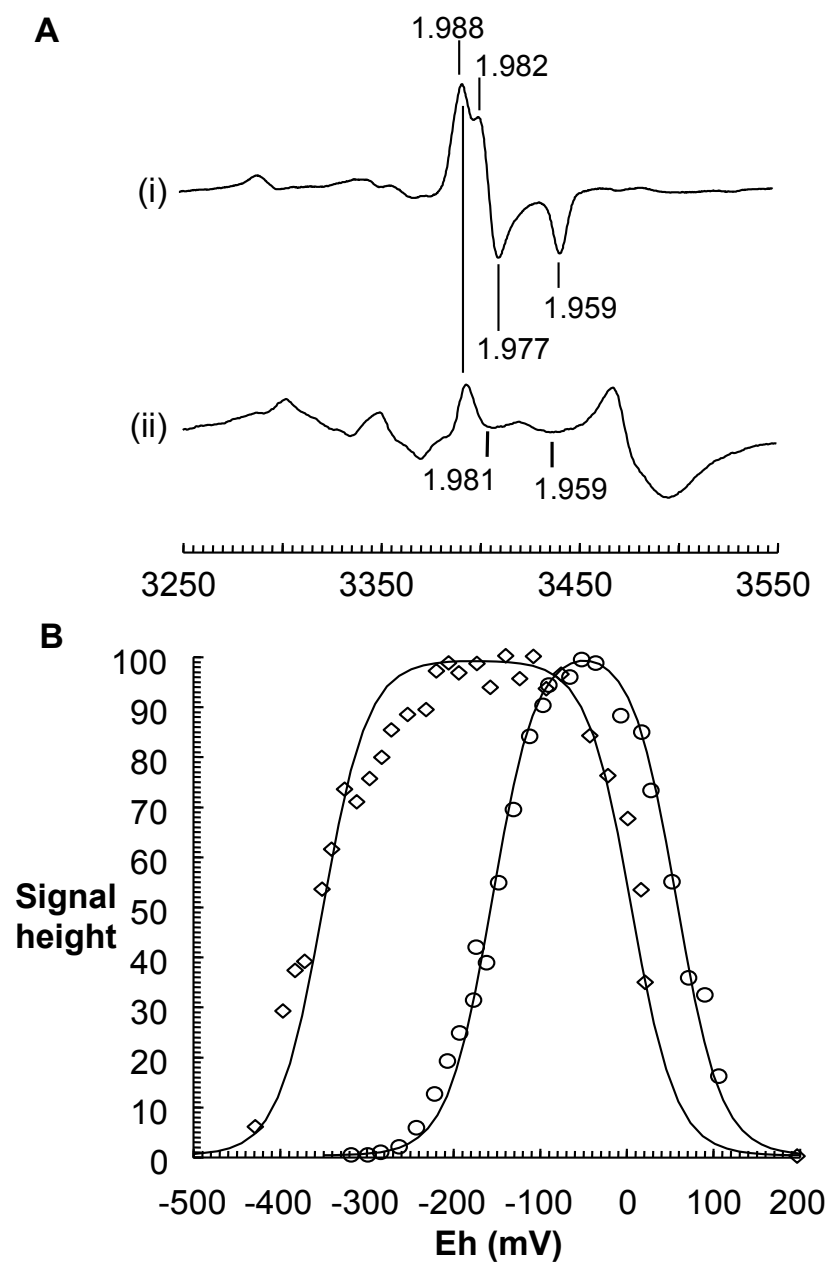


Figure 2.8 EPR characterization of Mo-bisPGD cofactor in DmsA^{CS1+R61K}BC. **A.** EPR spectra of Mo(V) signal from WT (i) and DmsA^{CS1+R61K}BC (ii). Spectra were recorded with the following EPR parameters: temperature, 150K; modulation amplitude, 3.8 G_{pp} at 100 KHz; microwave power, 2 mW. **B.** Redox titration of the g=1.98 peak-trough of the wild-type and DmsA^{CS1+R61K}BC Mo(V) signals. *Diamonds* - wild-type (Mo_(V/VI) E_{m,7} = 55 mV, Mo_(IV/V) E_{m,7} = -145 mV). *Circles* - DmsA^{CS1+R61K}BC mutant (Mo_(V/VI) E_{m,7} = 6 mV, Mo_(IV/V) E_{m,7} = -350 mV). Data were obtained from EPR spectra recorded as described for **A**.

Chapter 3

**A Mutant Conferring Cofactor-
Dependent Assembly of *Escherichia coli*
Dimethyl Sulfoxide Reductase***

*This work was a collaboration with Richard A. Rothery, James E. Voss, and Joel H. Weiner

3.1 Introduction

Members of the bacterial complex iron sulfur molybdoenzyme (CISM) family play critical roles in global geochemical cycles and bacterial metabolic diversity, contributing to the ability of prokaryotes to exploit the plethora of ecological niches on Earth [1,2]. Archetypal members comprise a catalytic subunit which contains a molybdo-bis(pyranopterin guanine dinucleotide) cofactor (Mo-bisPGD) and a single [4Fe-4S] cluster known as FS0, an electron-transfer subunit that typically contains four [Fe-S] clusters, and a membrane-anchor subunit that can contain zero or two *b*-type hemes. These enzymes support metabolic diversity by coupling redox reactions of soluble substrates at the Mo-bisPGD to the membrane-intrinsic quinone pool via a $\sim 100\text{\AA}$ multi-cofactor electron-transfer relay and a quinol binding site (Q-site) located in the membrane-anchor subunit. The diversity of soluble substrate specificity is derived from the utility of the Mo-bisPGD in catalyzing redox reactions ranging from the oxidation of formate to CO_2 ($E_{m,7} = -432\text{mV}$) to the reduction of nitrate to nitrite ($E_{m,7} = +420\text{mV}$) [3]. While delineation of the Mo-bisPGD biosynthetic pathway is largely complete [4], the final steps of its insertion into the respective enzymes remain poorly understood, but often involve a system-specific chaperone referred to as a redox enzyme maturation protein (REMP) [5].

Maturation of two *E. coli* CISM enzymes has been studied in detail: nitrate reductase A (NarGHI) and DMSO reductase (DmsABC) [2,5–7]. Importantly, one of these enzymes, NarGHI, is assembled to the inner surface

of the cytoplasmic membrane, whereas the other, DmsABC, is assembled to the outer surface, with its DmsAB subunits being translocated across the membrane by the *tat* translocon [8,9]. In both cases, a REMP, NarJ or DmsD, is required to facilitate both Mo-bisPGD binding and correct targeting of the enzyme to the cytoplasmic membrane. In the case of NarGHI, NarJ appears to hold the apomolybdoenzyme in a cofactor binding competent conformation during the final stages of maturation [10], and appears to do this by interacting with two sites on the NarG subunit: the approximately 50-amino acid pseudo-*tat* leader and a second site elsewhere on the subunit [11–13]. In the case of DmsABC, a *tat*-leader at the N-terminus of DmsA directs the fully folded cofactor-containing DmsAB catalytic dimer to the periplasmic compartment by binding DmsD and being directed to the *tat* translocon, where it associates with the membrane intrinsic DmsC subunit to form an active heterotrimer. Support for a role of DmsD in cofactor insertion comes from the observation that if the DmsA *tat* leader is replaced with that from the periplasmic TMAO reductase (TorA), DmsABC assembles to the membrane in its apomolybdo form [14], indicating a role for the cognate REMP in both targeting and cofactor insertion.

CISM maturation must coordinate subunit biosynthesis with cofactor insertion and membrane targeting. A working model involves biosynthesis of the apomolybdo catalytic subunit (DmsA/NarG) and the electron-transfer subunit (DmsB/NarH), followed by iron-sulfur cluster insertion via the cytosolic iron-sulfur cluster assembly (CIA) system [15,16]. In both cases,

cofactor insertion is mediated by the cognate REMP (DmsD/NarJ), but the precise sequence of FSO insertion and cofactor insertion is unknown. It is reasonable to assume, however, that the REMP binds to the *tat* or pseudo-*tat* leader soon after it is presented to the cytoplasmic aqueous milieu during DmsA/NarG biosynthesis. At some point, the electron-transfer (DmsB/NarH) subunit associates with the catalytic subunit to form the respective DmsAB/NarGH dimers that remain associated with DmsD/NarJ. It is known that the maturation process of both enzymes can bypass Mo-bisPGD insertion, leading to assembly of apomolybdo enzymes to the cytoplasmic membrane in heterotrimeric complexes with their cognate membrane-anchor subunits (DmsC/NarI) [2,14,17–19]. In NarGHI and the related monomeric DMSO reductase from *Rhodobacter sphaeroides*, the apomolybdo catalytic subunit binds GDP moieties at the positions occupied by the guanine nucleotides of the respective Mo-bisPGD containing enzymes [20–22]. As indicated above, in the case of DmsABC, the fully folded catalytic dimer must be translocated across the membrane by the *tat* system prior to attaching to the periplasmic side of the DmsC subunit to form the mature heterotrimer. In the case of NarGHI, the catalytic dimer attaches to the cytoplasmic side of the membrane anchor subunit (NarI), which is a diheme cytochrome *b* [1,23]. Critically, it has been proposed that association of NarGH with NarI is *tat*-dependent [24], even though the pseudo-*tat* leader is retained in the mature form of the enzyme [25]. NarI can assemble to the cytoplasmic membrane in the absence of NarGH [26,27]. Insertion of DmsC into the cytoplasmic

membrane in the absence of the DmsAB catalytic dimer results in a lethality phenotype due to dissipation of the transmembrane proton-electrochemical potential [28]. This effect is elicited by expression of DmsC in the absence of DmsA and DmsB [29], and by expression of all three subunits in strains deficient in the *tat* translocon [28]. Thus, in the case of DmsABC, but not in the case of NarGHI, the maturation pathway must be coordinated to avoid inadvertent insertion of the membrane-anchor subunit prior to availability of sufficient catalytic dimer to prevent membrane uncoupling.

An aspect of CISM maturation that has received little attention is the interplay between FS0 assembly and Mo-bisPGD insertion. Mutation of NarG-His50 to Ser results in assembly of an enzyme lacking both FS0 and Mo-bisPGD [22]. Mutants of the FS0-coordinating Cys motif in DmsA that eliminate its detection by EPR also eliminate insertion of Mo-bisPGD [30]. These observations indicate that insertion of FS0 is a pre-requisite for Mo-bisPGD insertion; specifically that correct folding of the FS0-binding domain of the CISM catalytic subunit is required prior to cofactor insertion. These observations prompted us to address the role of the pyranopterin itself in stabilizing protein structure during maturation. In this paper, we demonstrate that cofactor-protein contacts can stabilize the catalytic dimer (DmsAB) during enzyme maturation in a mutant with an unstable DmsA subunit.

3.2 Materials and Methods

Bacterial strains and plasmids — The *E. coli* strains and plasmids used in this study are listed in **Table 3.1**. *E. coli* strains HB101 and TOPP2 each have a wild-type chromosomal copy of the *dmsABC* operon, allowing accumulation of large quantities of both wild-type and mutant DmsABC [31,32]. In *E. coli* DSS301, the chromosomal copy of the *dmsABC* operon is replaced with a kanamycin resistance cartridge [33]. *E. coli* RK5209 is a *mod* mutant strain of *E. coli* defective in molybdenum uptake from the growth media [34,35]. *E. coli* F36 contains a point mutation in the *moeB* gene which prevents insertion of Mo-bisMGD into DmsABC [36]. Plasmid pDMS160 bears the wild-type *dmsABC* operon behind an FNR-dependent promoter [31]. pDMS160-C59S has a point mutation that changes Cys59 of DmsA to Ser [32]. As a control, the same plasmid lacking the *dmsABC* operon (pBR322) was used.

Growth of cells and preparation of membrane vesicles — Cells were grown anaerobically in 9L or 19L batch cultures at 37°C for 24 hours (TOPP2 and DSS301) or 48hrs (HB101 and F36) on a glycerol-fumarate minimal medium [37]. The growth medium was supplemented with either molybdate or tungstate (concentrations used are described in the table and figure legends). Where appropriate, ampicillin and kanamycin were added to a final concentration of 100 $\mu\text{g mL}^{-1}$ and 50 $\mu\text{g mL}^{-1}$, respectively. RK5209 cells were grown in 11 L batch cultures at room temperature (23.5°C) with either 0 or 100 μM molybdate in a minimal glycerol-fumarate media. These cells were

grown with 100 $\mu\text{g mL}^{-1}$ ampicillin and 100 $\mu\text{g mL}^{-1}$ streptomycin. Cells were harvested, and washed in 100mM MOPS and 5mM EDTA (pH7.0). Membranes were prepared by cell lysis using a French pressure cell or an Avestin microfluidizer, and differential centrifugation as previously described [31,38]. Respiratory growth on DMSO was evaluated using a Klett-Summerson spectrophotometer and 160mL side-arm Erlenmeyer flasks as previously described [18,31]. Cells were grown in the presence of 5 μM molybdate or 10 mM tungstate.

Purification of DmsABC — Membranes were detergent-solubilized with *n*-dodecyl- β -D-matoside and enzyme purification was performed as previously described [30].

Protein assays — Protein concentrations were determined by the Lowry method [39], modified by the inclusion of 1% (wt/vol) sodium dodecyl sulfate in the incubation mixture [40].

Immunoblot analysis of DmsABC content in cell membranes — Proteins from membrane vesicles were separated on a 10% SDS-PAGE gel and then blotted onto nitrocellulose. Antibodies to DmsA and DmsB were used for Western blot analysis. DmsA and DmsB were detected using the GE Healthcare chemiluminescence system and goat anti-rabbit IgG horseradish peroxidase conjugate [41].

Preparation of fluorescent pyranopterin derivatives — The presence of pyranopterin in membrane vesicles was assayed by acid denaturation followed by I_2 and KI oxidation to produce an extract that contained the Form

A fluorescent derivative of pyranopterin that will be referred herein to as a “Form A extract” [19,42]. 10 mg of membrane protein was used as starting material. Prior to recording fluorescence spectra using a Perkin-Elmer LS-50B luminescence spectrometer, 200 μ L of Form A extract were added to 3 mL of 1 M NH_4OH in a fluorescence cuvette. Excitation spectra were recorded from 240-420 nm (emission at 448 nm). Emission spectra were recorded from 410-520 nm (excitation at 397 nm).

Quantitation of quinol-binding DmsABC — Fluorescence quench titrations were used to quantitate membrane bound DmsABC by measuring the concentration of 2-*n*-heptyl-4-hydroxyquinoline-*N*-oxide (HOQNO) binding sites [30,43]. HOQNO is a menaquinol analog that binds to the quinol-binding site of DmsC with 1:1 stoichiometry and high affinity ($K_d \sim 7$ nM). It is fluorescent only when it's free in the solution. Quenching of HOQNO fluorescence was used to estimate the concentration of DmsC and thus DmsABC in the membrane samples [44,45]. HOQNO Fluorescence was recorded using a Perkin-Elmer LS-50B luminescence spectrophotometer using an excitation wavelength of 341 nm and an emission wavelength of 479 nm as aliquots of 0.1mM HOQNO were added to membrane samples with protein concentration of 1 mg mL^{-1} . The concentration of DmsABC is equal to the concentration of HOQNO added right before the fluorescence begins to rise [46].

Enzyme activity assay — Enzyme activity was determined as the rate of TMAO-dependent oxidation of dithionite reduced benzyl viologen (BVH•)

as previously described [47]. The extinction coefficient for BV is $7.4 \text{ mM}^{-1} \text{ cm}^{-1}$. The quinol-dependent enzyme activity was determined as the rate of TMAO-dependent oxidation of reduced lapachol (LPCH₂) as previously described [48]. The extinction coefficient of lapachol is $2.66 \text{ mM}^{-1} \text{ cm}^{-1}$.

Electron paramagnetic resonance (EPR) spectroscopy — Reduced samples were prepared by anaerobic incubation of purified DmsABC or membrane samples with 5 mM (final concentration) sodium dithionite for 5 minutes at room temperature. Oxidized samples have been oxidized by mixing with air. Redox titrations were carried out anaerobically at 25 °C under argon in presence of redox dyes as previously described [38,49,50]. The dyes added to a final concentration of 50 μM were quinhydrone, 2,6-dichloroindophenol, 1,2-naphthoquinone, toluylene blue, phenazine methosulfate, thionine, duroquinone, methylene blue, resorufin, indigo-trisulfonate, indigo-disulfonate, anthraquinone-2-sulfonic acid, phenosafranine, benzyl viologen, and methyl viologen. All samples were prepared in 3mm internal diameter quartz EPR tubes, and were rapidly frozen in liquid nitrogen-chilled ethanol and stored under liquid nitrogen until use. EPR spectra of [Fe-S] clusters were recorded using a Bruker Elexsys E500 spectrometer equipped with a Bruker SHQE cavity and an Oxford Instruments ESR-900 flowing helium cryostat. For EPR studies on the Mo-bisPGD cofactor, a Bruker ESP300E spectrometer equipped with a TE102 cavity and a Bruker liquid nitrogen evaporating cryostat was used (Bruker ER4111VT). Instrument conditions and temperatures used are described in

the figure legends. Microwave power saturation data were fitted to the equation:

$$S = K\sqrt{P}/(1 + P/P_{1/2})^{0.5b} \dots\dots\dots(\text{Equation 1})$$

where S is the signal height, K is a proportionality factor, P is the microwave power, $P_{1/2}$ is the microwave power for half-saturation, and b is the inhomogeneity parameter.

3.3 Results and Discussion

Position of DmsA-Cys59 within the DmsABC heterotrimer — **Figure 3.1A** shows a model for the electron-transfer relay that connects a menaquinol binding site within the DmsC subunit with the Mo-bisPGD cofactor of DmsA [30]. This relay comprises four [4Fe-4S] clusters located in the DmsB subunit and one [4Fe-4S] cluster known as FS0 that is close to the proximal pyranopterin of the Mo-bisPGD cofactor. **Figure 3.1B** shows the predicted protein structure surrounding the FS0 cluster and the role of the DmsA-Cys59 residue in providing one of the thiol ligands to FS0, and is based on a model generated by Tang *et al.* [30] The work presented herein addresses the effect of DmsA-Cys59Ser variant in rendering the assembly of the DmsABC complex (**Figure 3.1C**) sensitive to the availability of the Mo-bisPGD cofactor.

Assembly of DmsA^{C59S}BC is impaired by growth in the presence of tungstate — Crude membrane fractions from *E. coli* DSS301 cells (Δ dmsABC)

expressing either DmsABC or the DmsA-Cys59Ser variant in the presence of either molybdate or tungstate were subjected to immunoblot analysis (**Figure 3.2**). While tungstate has no demonstrable effect on assembly of the wild-type enzyme, it clearly diminishes assembly of the DmsA-Cys59Ser variant. The elimination of assembly of Cys59Ser mutant to the cytoplasmic membrane (**Figure 3.2A**) was not due to disrupted translocation leading to accumulation of DmsAB in the cytoplasm. **Figure 3.2B** clearly shows that there is no DmsA^{C59S} in the cytoplasm when grown in cultures supplemented with tungstate, probably as a result of rapid degradation of the unstable apoform of the mutant. Similar results were obtained when using the *E. coli* RK5209 that is deficient in molybdate uptake and *E. coli* F36 that is deficient in Mo-bisPGD cofactor insertion (data not shown).

The DmsA-Cys59Ser variant supports respiratory growth on DMSO —

We have previously demonstrated that the DmsA-Cys59Ser variant is able to support respiratory growth on DMSO [32], and have also shown that the wild-type strain HB101 assembles much higher levels of DmsABC to the cytoplasmic membrane than the $\Delta dmsABC$ deletion strain DSS301 [31,33,38,46]. In order to interpret experimental data derived from the HB101 strain, it is important to demonstrate consistent behaviour of the DmsA-Cys59Ser variant between the two strains. We did this by assessing anaerobic respiratory growth on DMSO in the presence and absence of tungstate. **Figure 3.3A** confirms that the DmsA-Cys59Ser variant supports respiratory growth on DMSO, and that, as expected, this growth is inhibited

by the molybdenum antagonist tungstate. Similar behavior is exhibited when the wild-type HB101 strain is used (**Figure 3.3B**), with the only significant difference being the slower overall growth rate exhibited by this strain. These results indicate that we can confidently interpret biochemical and biophysical data derived from the HB101 strain.

Tungstate inhibits maturation of the entire complex in the DmsA-Cys59Ser variant — **Figure 3.4A** shows the effect of tungstate on the relative amounts of fluorescent Form A pyranopterin derivative in membrane fractions. As expected (**Figure 3.4Ai, 3.4Aii**), a significant amount of cofactor is detected in membranes prepared from cells grown in the presence of molybdate [18,19]. The level of Form A derivative prepared from the DmsA-Cys59Ser derivative is comparable to that obtained from wild-type DmsABC (*cf.* **Figure 3.4Ai** and **Figure 3.4Aii**). As expected, growth in the presence of tungstate decreases the amount of cofactor released from membranes containing both wild-type (*not shown*) and DmsA-Cys59Ser enzyme. We have previously demonstrated that in both DmsABC and NarGHI, growth in the presence of tungstate has little or no effect on the total amount of wild-type apomolybdoenzyme assembled to the cytoplasmic membrane [18,19]. Overall, analyses of Form A extracts from membranes are consistent with the immunoblot analysis presented in **Figure 3.2**.

It is important to correlate cofactor detected by assaying Form A extracts with the overall assembly of the enzyme. Fluorescence quench titrations using the chromophore HOQNO allow the concentration of

DmsABC-associated quinol binding sites to be measured in membrane samples [43,46]. **Figure 3.4B** shows titrations performed with membranes containing wild-type, DmsA-Cys59Ser (molybdate) and DmsA-Cys59Ser (tungstate) enzymes, yielding HOQNO binding site concentrations of 0.74, 0.28, and 0.00 nmol/mg membrane protein, respectively. Growth in the presence of tungstate has no effect on the amount of HOQNO binding sites detected in membranes enriched with wild-type DmsABC as assayed by immunoblot (**Figure 3.2**) and fluorescence quench titration (data not shown). These results demonstrate that in the DmsA-Cys59Ser variant there is a correlation between a decreased level of DmsA and DmsB subunits detected by immunoblot (**Figure 3.2**) with decreased level of Form A derivative released from membrane samples (**Figure 3.4A**) and a decreased concentration of detectable HOQNO binding sites. Critically, this suggests a coordination of the maturation of the three subunits of the holoenzyme.

EPR characterization of the DmsA-Cys59Ser variant — **Figure 3.5** shows EPR spectra recorded at 12 K of dithionite-reduced membranes containing wild-type DmsABC and the DmsA-Cys59Ser variant grown in the presence and absence of tungstate. As expected, the spectrum of membrane containing wild-type DmsABC (**Figure 3.5a**) resembles those previously published [38,47]. This spectrum arises from the paramagnetic [4Fe-4S] clusters located in the DmsB subunit and has well-defined peaks at around $g=2.05$, 2.02 , and 1.99 ; and well-defined troughs at $g=1.92$ and 1.88 [38,47]. Because the membranes were derived from cells that were grown

anaerobically on fumarate, there is a minor contribution to the spectrum from the [Fe-S] clusters of fumarate reductase [31,32,38]. Specifically, fumarate reductase contributes to the peak at $g=2.02$ and to the trough at $g=1.92$. Spectra of membranes containing the DmsA-Cys59Ser variant (**Figure 3.5b**) broadly resemble those of membranes containing the wild-type enzyme, but have a more pronounced peak at $g=2.05$ (*indicated by position of the arrows in Figure 3.5*). Spectra of membranes containing the DmsA-Cys59Ser variant obtained from cells grown in the presence of tungstate (**Figure 3.5c**) are diminished in intensity and more closely resemble those observed for membranes containing fumarate reductase [43]. When the spectrum of membranes grown in the presence of tungstate are subtracted from the spectrum of membranes grown in the presence of molybdate, the result resembles that of purified enzyme [47] with the caveat that it has a more pronounced peak at $g=2.05$ (**Figure 3.5d**, see below).

Characterization of the FS0 cluster of the DmsA-Cys59Ser mutant.

Because of the proximity of the DmsA-Cys59 residue to the FS0 cluster and DmsA-Arg61 (**Figure 3.1B**) along with the effect of a DmsA-Cys59Ser mutant on enzyme assembly in the absence of Mo-bisPGD, it is important to evaluate any gross effects of the mutation on the electrochemistry of both the molybdenum center and the FS0 cluster. **Figure 3.6A** shows a comparison of redox poised EPR spectra recorded at 75K, demonstrating that the Mo(V) EPR spectra are essentially identical in both the wild-type (**Figure 3.6A(i)**) and DmsA-Cys59Ser variant enzyme (**Figure 3.6A(ii)**). **Figure 3.6B**

illustrates redox titrations for the two enzymes. The wild-type enzyme has reduction potentials ($E_{m,7}$ values) of approximately -5mV (Mo(VI/V)) and -140 mV (Mo(V/IV)), whereas the DmsA-Cys59Ser variant has reduction potentials of -10 mV (Mo(VI/V)) and -128 mV (Mo(V/IV)). Thus, there is modest 12mV increase in the Mo(V/IV) reduction potential in the DmsA-Cys59Ser variant. A final issue that can be addressed by studying the Mo(V) EPR spectrum is the paramagnetic interaction between it and the reduced form of the FS0 cluster [49]. **Figure 3.6C** shows the predicted change in spin relaxation of the Mo(V) center occurs as FS0 becomes reduced between ambient potentials of -29mV and -179mV [1,49]. Based on these observations, we predict that the E_m of FS0 in Cys59Ser lies slightly below -179mV as estimated by this indirect methodology, whereas the E_m of FS0 in wild-type DmsABC has been predicted to be around -140mV [49]. Unfortunately, FS0 has proven recalcitrant to efforts to directly measure the reduction potential of its high spin EPR spectrum [30] (see below).

To further investigate the line shape change observed in the low temperature (12K) EPR spectrum of reduced membranes containing the DmsA-Cys59Ser variant, we purified this enzyme from *E. coli* TOPP2 membranes [30]. **Figure 3.7** shows representative EPR spectra recorded at 9K at around $g=2.0$ (**Figure 3.7A**) and at around $g=5.0$ (**Figure 3.7B**). Reduced spectra at around $g=2.0$ confirm the difference between the wild-type and DmsA-Cys59Ser variant observed in HB101 membranes in **Figure 3.5**, with a more pronounced shoulder observed at $g=2.05$. Spectra of air

oxidized samples (**Figure 3.7A(i)** and **3.7A(iii)**) indicate that FS0 is not converted to a [3Fe-4S] cluster in the DmsA-Cys59Ser variant. The spectrum with features comprising a peak at $g=2.02$ with a broad trough upfield is the typical signal of a [3Fe-4S] cluster in fumarate reductase. The increased intensity of the signal from the mutant compared to that from the wild-type is likely due to a higher amount of contaminating fumarate reductase (cells were grown on fumarate). Inspection of the spectra of reduced purified samples at around $g=5$ reveals that the increased intensity of the $g=2.05$ shoulder is correlated with the almost complete elimination of a $g=5.07$ signal corresponding to a form of the FS0 cluster with a high spin $S = 3/2$ ground state [30]. Based on these observations, it is likely that the DmsA-Cys59Ser substitution changes the ground state of the reduced FS0 from $S = 3/2$ to $S = 1/2$.

Effect of the DmsA-Cys59Ser substitution on enzyme activity. In agreement with our previous work [32], the DmsA-Cys59Ser variant is able to support respiratory growth on DMSO. When corrected for enzyme concentration in membranes determined by fluorescence quench titration (e.g. **Figure 3.4B**), the data presented in **Table 3.2** demonstrate that the DmsA-Cys59Ser variant is as active as the wild-type, consistent with its ability to support respiratory growth on DMSO and the conclusion that its Mo center does not have a dramatically altered reduction potential in comparison with the wild-type enzyme (**Figure 3.6**).

Implications for the maturation pathway of DmsABC — In agreement

with our earlier observations on the assembly of both DmsABC and NarGHI [18,19], the effect of tungstate on the relative amounts of enzyme assembled to the cytoplasmic membrane clearly indicates that apomolybdoenzymes can bypass Mo-bisPGD insertion during maturation. In the case of DmsABC, this results in the accumulation of inactive membrane-bound enzymes assembled on the periplasmic side of the membrane, consistent with normal translocation of the apomolybdo-DmsAB dimer across the cytoplasmic membrane by the *tat* translocon followed by its association with DmsC. This parallels what is observed with NarGHI [50], but with the important difference that the NarGH catalytic dimer is assembled to the inside of the cytoplasmic membrane. The work presented herein confirms that apomolybdo-DmsAB can be translocated by the *tat* translocon. This has important implications for the proposed “proofreading” function of the NarJ/DmsD chaperones in that they do not appear to be able to discriminate between apomolybdo- and molybdo- forms of the enzyme. In the case of NarGHI, comparison of the structure of the apomolybdo- and molybdo- forms reveals no significant changes in externally-apparent protein structure that the cognate chaperone could use to distinguish between the two enzyme forms.

The work presented herein reinforces the relationship between FS0 assembly and cofactor insertion [22]. It extends this in a critical way by demonstrating for the first time that cofactor availability itself can overcome a destabilizing effect of the DmsA-Cys59Ser substitution. In a sense, this

imparts a chaperone function on the cofactor, presumably exploiting the hydrogen bonding contacts between the cofactor and its surrounding amino acids to stabilize the protein fold during maturation.

Previous work has demonstrated that plasmid constructs encoding DmsA and DmsB truncated at its C-terminus express DmsAB' able to reduce substrate using the artificial electron donor benzyl viologen. Critically, this DmsAB' dimer accumulates in the cytoplasmic fraction [33], revealing that an intact DmsAB dimer is necessary for effective targeting to the *tat* translocon [8]. Clearly, the *tat* translocon in combination with the DmsD REMP is able to distinguish between completely translated and folded DmsAB and a truncated derivative, with the latter not being targeted for translocation. Equally clearly, apomolybdo-DmsAB is recognized and translocated by the *tat* translocon.

In terms of delineating a generalized mechanism for CISM catalytic subunit maturation, our data clearly reinforce the interplay between FS0 and Mo-bisPGD assembly into the DmsA subunit. The simplest interpretation of the data is that these are assembled concurrently into the subunit, and in the case of the DmsA-Cys59Ser variant, failure at this step precipitates protein misfolding and subsequent degradation. In light of these observations, a model for DmsABC maturation can be proposed (**Figure 3.8**). This can be summarized as follows:

1. DmsD binds to the *tat*-leader of nascent DmsA, and holds the folding protein in a *Mo-bisPGD* and *FS0-binding competent conformation*.

2. Both Mo-bisPGD and FS0 bind to the DmsD complex. In the case of the DmsA-Cys59Ser variant, failure to bind Mo-bisPGD leads to protein instability and degradation.
3. DmsB associates with Mo-bisPGD and FS0-containing DmsA.
4. The DmsAB-DmsD complex is recognized by the *tat* translocon, and translocated across the cytoplasmic membrane, releasing DmsD into the cytoplasm.
5. Signal peptidase cleaves the *tat*-leader and the DmsAB dimer associates with the periplasmic side of DmsC, generating a quinol binding site detectable by fluorescence quench titration.

In the absence of cofactor, the wild-type DmsABC assembles FS0 (as has been observed in NarGHI [21,22]) (**step 2a**). This is followed by association of DmsB (**step 3a**), translocation and DmsD dissociation (**step 4a**), and *tat*-leader cleavage and assembly of apomolybdo-DmsABC (**step 5a**).

3.4 Conclusion

In this work, we have demonstrated the interplay between the FS0 cluster assembly and Mo-bisPGD cofactor insertion with the DmsA variant, Cys59Ser, which renders enzyme maturation cofactor-dependent. Correct assemblies of the FS0 cluster and the cofactor are important for correct folding and stability of the protein. The instability and subsequent degradation of the protein caused by different coordination of the FS0 cluster

can be rescued by the Mo-bisPGD insertion, suggesting a chaperone function of the cofactor.

3.5 Tables and Figures

Table 3.1: Bacterial Strains and Plasmids

Strains	Description	Source
HB101	<i>supE44 hsd20 (r_B⁻ m_B⁻) recA13 ara-14 proA2 lacY1 galK2 rpsL20 xyl-5 mtl-1</i>	Lab collection
DSS301	TG1, <i>kan^R ΔdmsABC</i>	Lab collection [33]
TOPP2	<i>rif^R F' proAB, lacI^qΔM15 Tn10 (tet^R)</i>	Stratagene
F36	HB101, <i>moeB</i>	[36]
RK5209	<i>ΔlacU169 araD139 rpsL gyrA non mod241:Mu cts</i>	[34,35]
Plasmids		
pDMS160-WT	pBR322 Amp ^R (<i>dmsABC</i>) ⁺	[31]
pDMS160-C59S	pBR322 Amp ^R (<i>dmsA^{C59S}BC</i>) ⁺	[32]

Table 3.2: Enzyme Activities determined by TMAO-dependent oxidation of reduced benzyl viologen or lapachol

Sample	Specific Activity ($\mu\text{moles (BV/LPCH}_2\text{) min}^{-1} \text{mg}^{-1}$)				Turn-over ^b (s^{-1})	
	BV		LPCH ₂		BV	LPCH ₂
	TOPP2	DSS301	TOPP2	DSS301	TOPP2	TOPP2
pBR322	11.8	0.12	0.00	0.00	n.d ^c	n.d.
WT (5 $\mu\text{M Mo}$)	146	80.8	6.44	2.05	3244	143
WT (10mM Mo)	--d	74.7	--d	1.82	--d	--d
WT (10mM W)	--d	7.19	--d	0.12	--d	--d
C59S (5 $\mu\text{M Mo}$)	54.4	20.3	2.40	0.29	3238	143
C59S (10mM Mo)	36.1	16.8	1.54	0.23	3008	128
C59S (10mM W)	9.01	5.16	0.00	0.07	n.d.	n.d.

a - Assays were carried out in triplicate and the average reported.

b - Turn-over numbers were based on enzyme concentrations calculated from fluorescence quench titrations.

c - Turn-over numbers were unable to be determined due to undetectable concentration of DmsABC by fluorescence quench titrations.

d - Sample not grown.

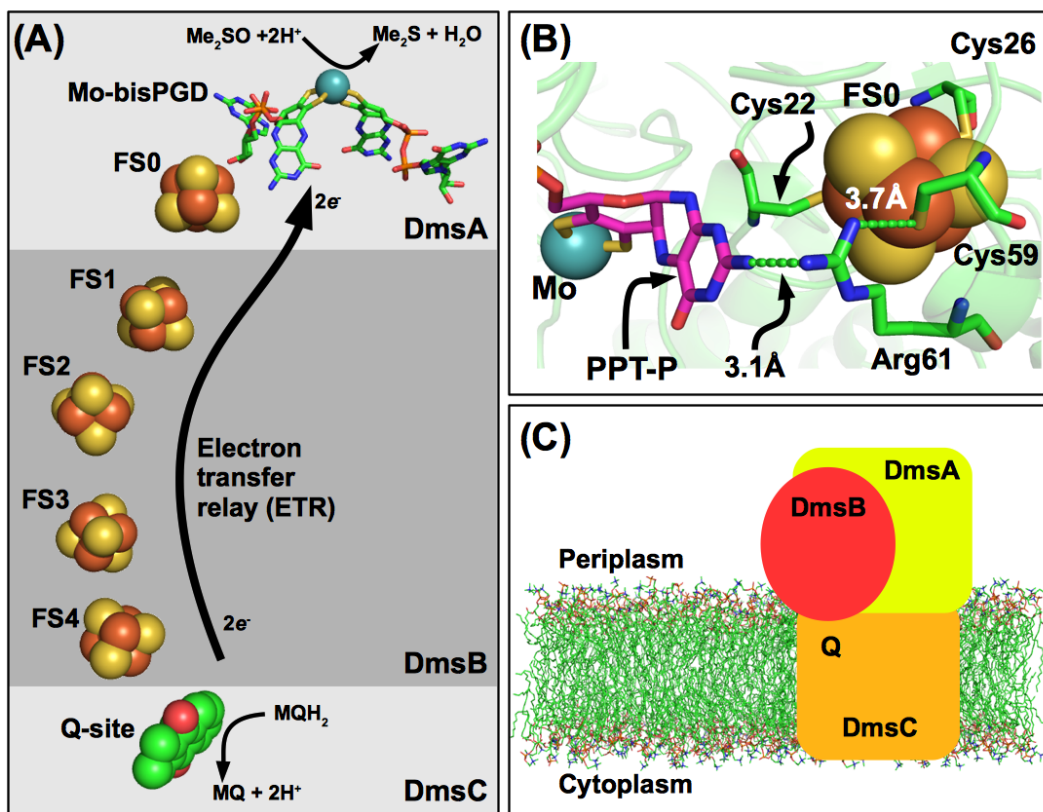


Figure 3.1 Electron-transfer relay architecture and predicted DmsA structure around FS0. (A) Predicted electron-transfer relay in DmsABC connecting a menaquinol-binding site in the DmsC subunit with the Mo-bisPGD cofactor in the DmsA subunit. In this model, note that DmsC is predicted to be membrane-intrinsic and anchors to DmsA and DmsB to the periplasmic side of the *E. coli* cytoplasmic membrane [1]. (B) Structural model of DmsA in the vicinity of FS0 was generated using the ESyPred3D server with the structure of NarG as the template (PDB code 1Q16) as previously described [30]. The predicted position of the DmsA-Cys59 is shown. The distances shown are arbitrary but indicate a possible H-bonding interaction between Arg61 and Cys59. (C) Overall topology of DmsABC in the cytoplasmic membrane with the DmsAB catalytic dimer attached to the periplasmic side of DmsC. The approximate position of the quinone-binding site is indicated as a “Q” in the panel.

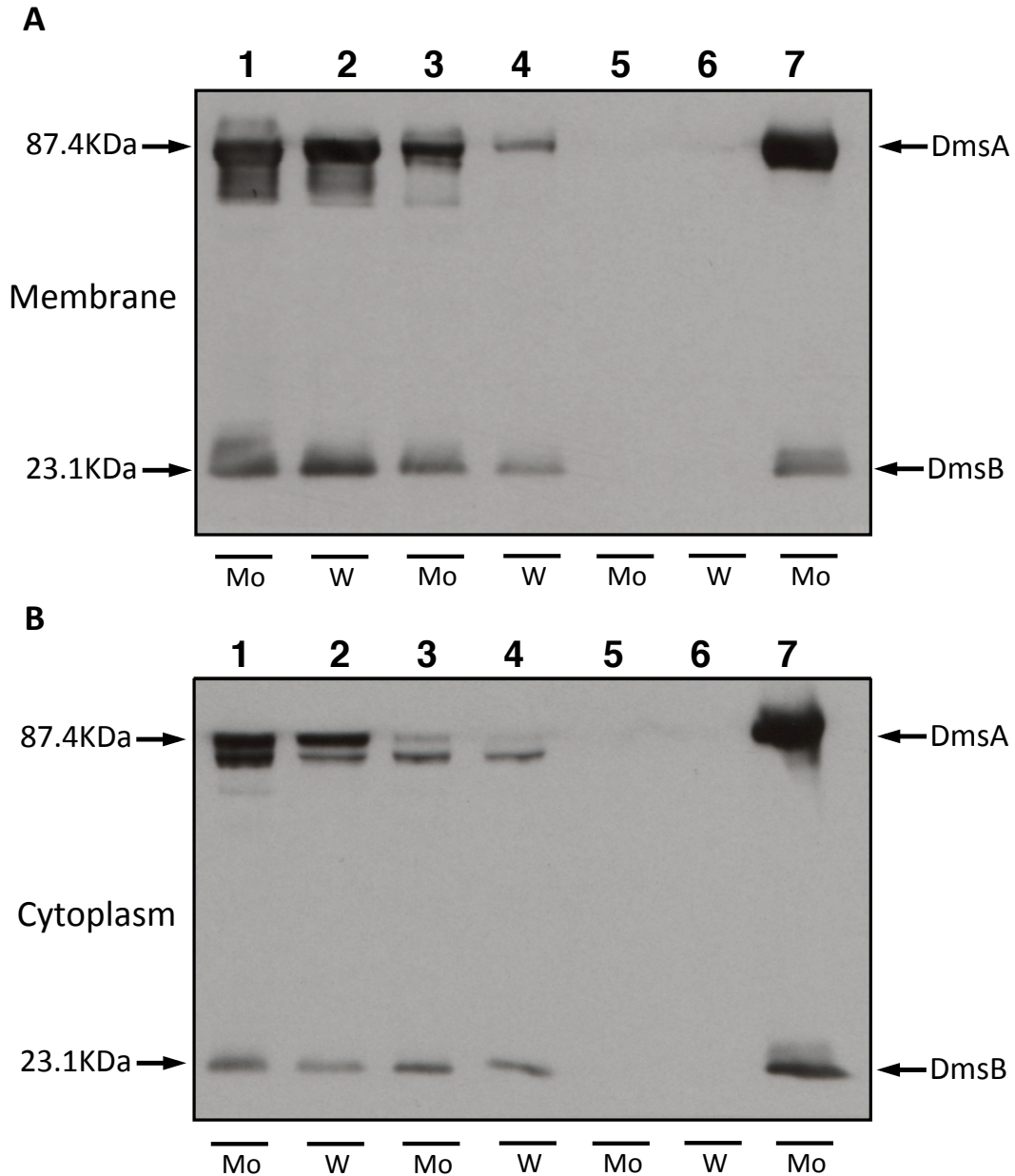


Figure 3.2* Tungstate decreases enzyme maturation in a DmsA-Cys59Ser mutant. Western blots* were performed on membrane (Top) and soluble (bottom) samples (from *E. coli* DSS301, $\Delta dmsABC$) run on a 10% SDS-polyacrylamide gel on which 45 μg of the following membrane samples or 30 μg of the following soluble samples had been run: lane 1 and 2: wild-type DmsABC; lane 3 and 4: DmsA^{C59S}BC; lane 5 and 6: background vector (pBR322); and lane 7: purified DmsABC standard. Lanes labeled Mo (lane 1, 3, 5 and 7) are samples grown from cultures supplied with molybdate. Lanes labeled W (lane 2, 4, and 6) are samples grown in cultures supplied with tungstate.

* The blots shown here were produced by James Voss. West blot for membrane samples was repeated by Huipo Tang (**Figure 3.9**) and same pattern was observed.

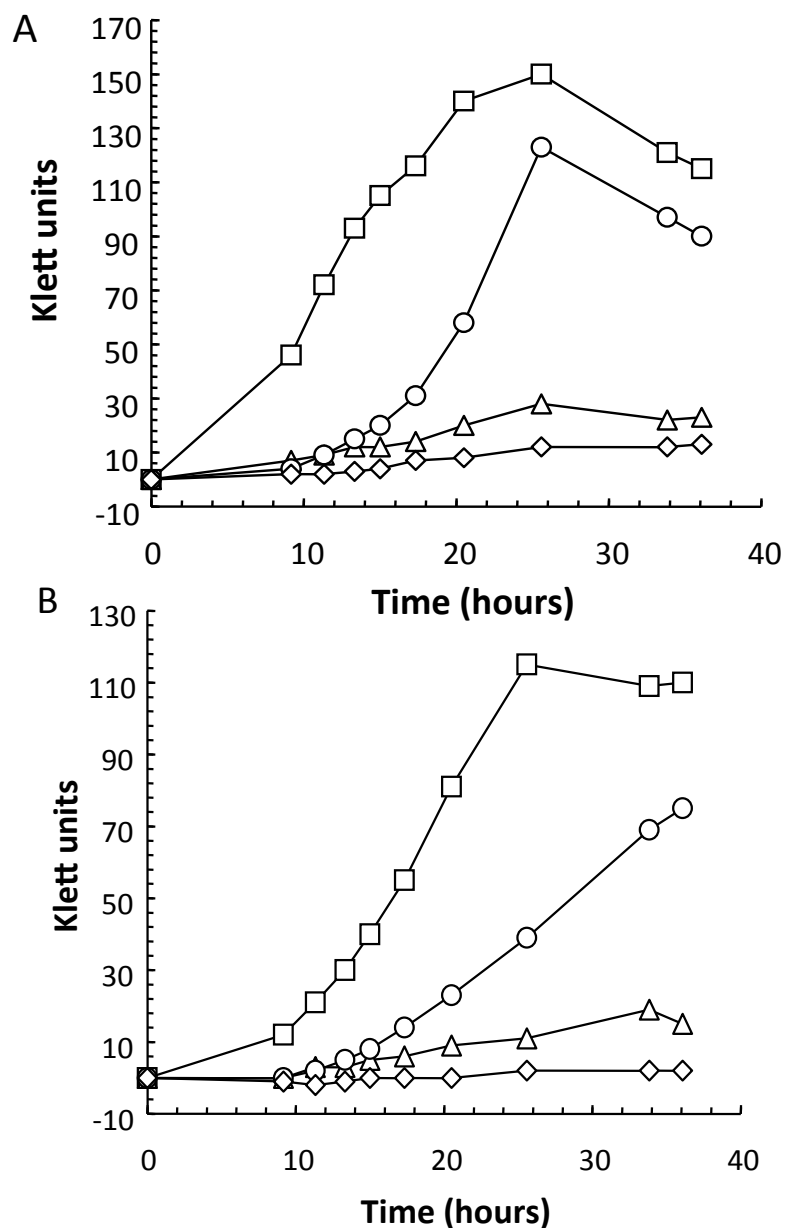


Figure 3.3* Effect of tungstate on respiratory growth on DMSO supported by DmsABC and DmsA^{C59S}BC. **(A)** Growth of *E. coli* DSS301 ($\Delta dmsABC$). **(B)** Growth of *E. coli* HB101. *Squares* - strains transformed with pDMS160 in the absence of tungstate. *Circles* - strains transformed with pDMS160-C59S in the absence of tungstate. *Triangles* - strains transformed with pDMS160 in the presence of 10mM tungstate. *Diamonds* - strains transformed with pDMS160-C59S in the presence of 10mM tungstate. Cell growth was measured with a Klett-Summerson spectrophotometer equipped with a number 66 filter.

* The growth shown here were produced by Richard A. Rothery. The growth experiment using DSS301 cells was repeated by Huipo Tang (**Figure 3.10**) and similar trends were observed.

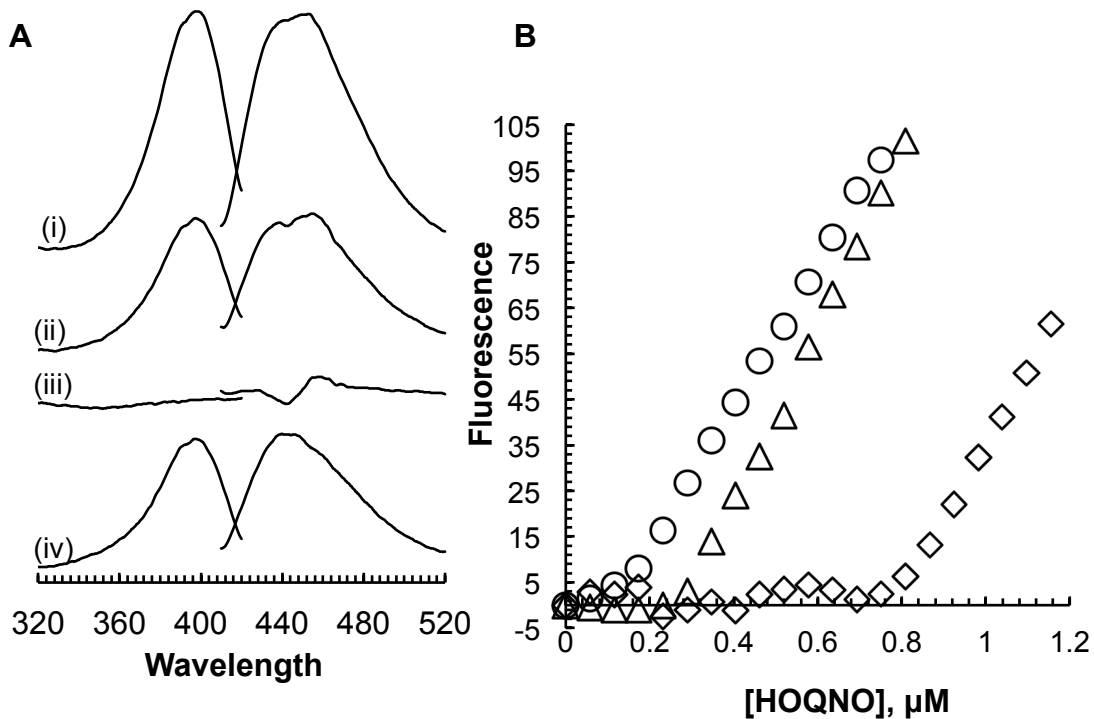


Figure 3.4 Loss of cofactor inhibits assembly of DmsA^{C59S}BC. (A) Fluorescence spectra of Form A extracts of membranes from cells grown the presence of molybdate and tungstate. (i) Wild-type DmsABC grown in the presence of 5 μM molybdate; (ii) DmsA^{C59S}BC grown in the presence of 5 μM molybdate; (iii) DmsA^{C59S}BC grown in the presence of 10mM tungstate; and (iv) difference spectra of (ii) minus (iii). 10mg of membrane protein were used as starting material. Spectra were recorded under the following conditions: excitation spectra (left of panel A), scanned from 240-420nm with an emission wavelength of 442nm; emission spectra (right of panel A), scanned from 410-520nm with an excitation wavelength of 395nm. (B) Quantitation by fluorescence quench titration of quinol binding sites in membranes containing wild-type and DmsA^{C59S} enzyme. Circles - wild-type DmsABC; triangles - DmsA^{C59S}BC in the presence of 5 μM molybdate; squares - DmsA^{C59S}BC in the presence of 10mM tungstate. Enzyme concentrations were estimated from the X-intercepts of the plots to be 0.74, 0.28, and 0.00 nmol (mg membrane protein)⁻¹ for the wild-type, DmsA^{C59S}BC (molybdate), and DmsA^{C59S}BC (tungstate) membranes, respectively. Titrations were carried out at a protein concentration of 1 mg mL⁻¹.

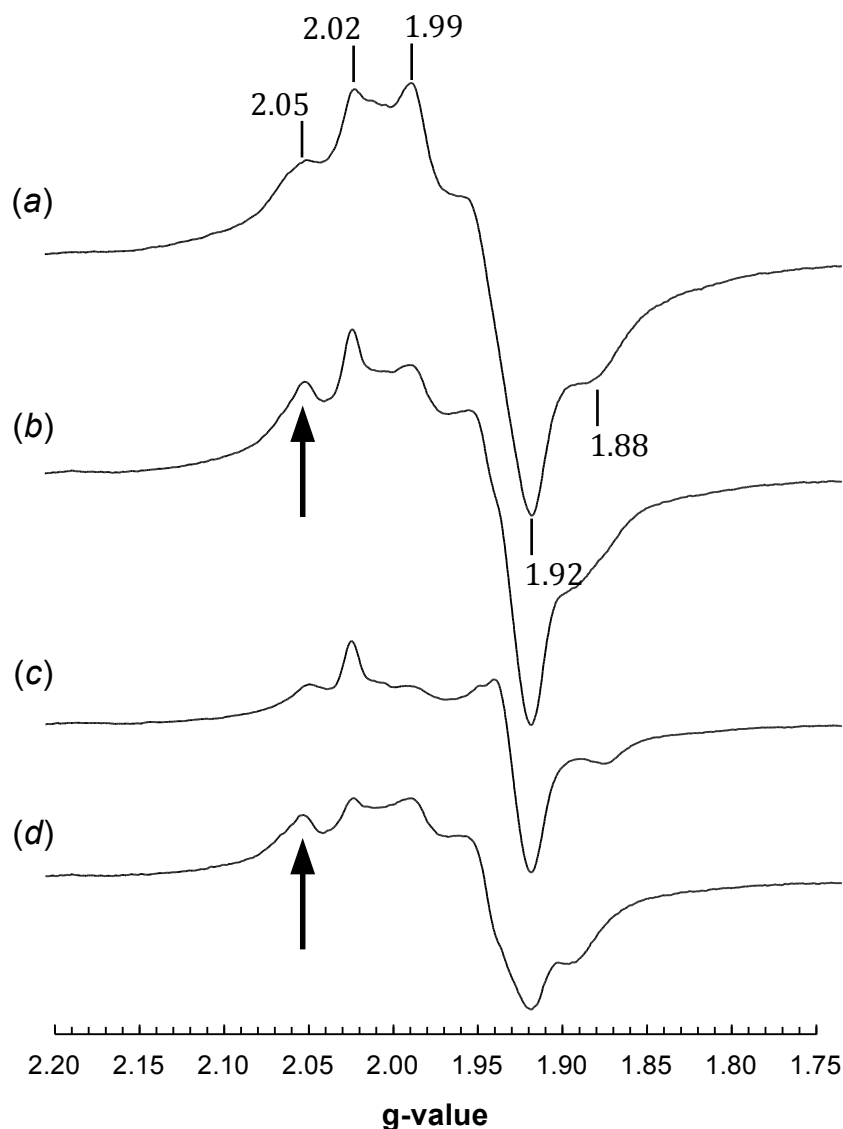


Figure 3.5* Effect of tungstate on DmsA^{C59S}BC assembly determined by EPR spectroscopy of the DmsABC [4Fe-4S] clusters. All spectra are of dithionite (5mM) reduced samples prepared as described in the *Materials and Methods*. **(a)** Spectrum of HB101/pDMS160 membranes from cells grown on molybdate-supplemented medium. **(b)** Spectrum of HB101/pDMS160-C59S membranes from cells grown on molybdate-supplemented medium. **(c)** Spectrum of HB101/pDMS160-C59S membranes grown on tungstate-supplemented medium (15 mM). **(d)** Difference spectrum of **(b)** minus 0.8X **(c)**. EPR spectra were recorded under the following instrument conditions: temperature, 12 K; microwave power, 20mW; microwave frequency, 9.47GHz; modulation amplitude, 10 G_{pp} at 100 KHz. Spectra were normalized to a protein concentration of 30mg mL⁻¹.

*EPR spectra shown here were produced by Richard A. Rothery.

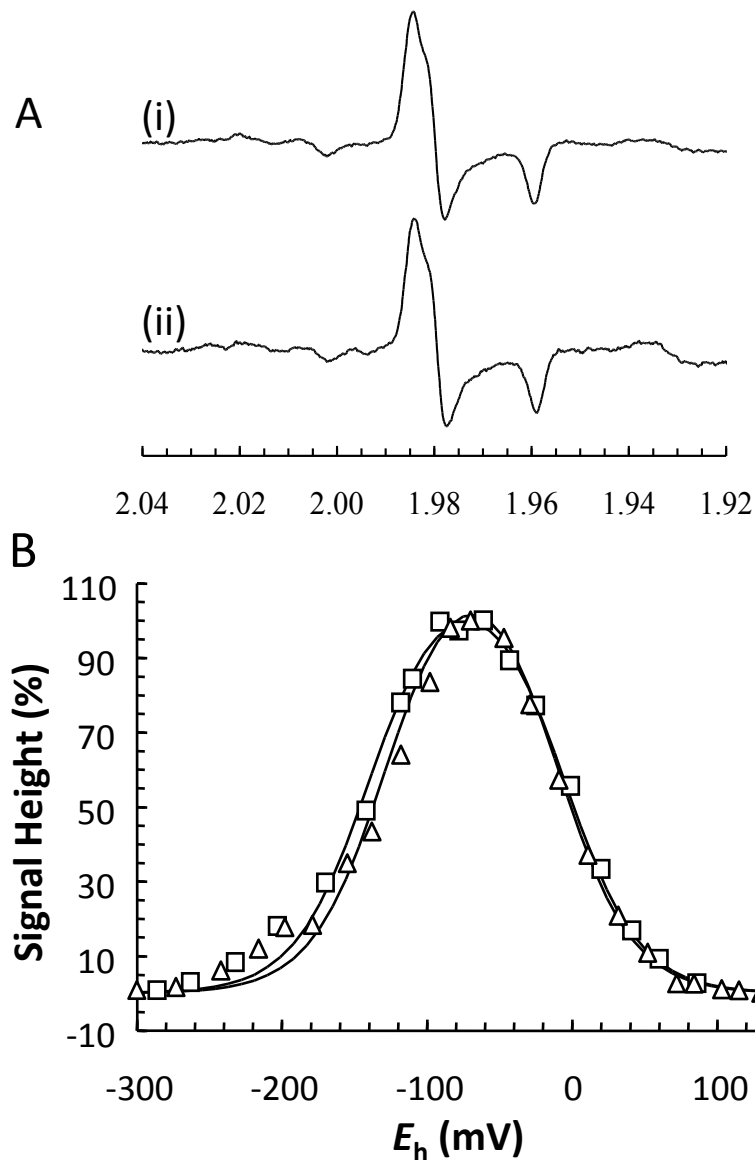


Figure 3.6* EPR characterization of Mo-bisPGD in the DmsA-C59S mutant. **A.** Mo(V) EPR spectra of membranes containing wild-type (**i**) and DmsA-C59S variant enzyme (**ii**). Samples were redox-poised as described in the *Materials and Methods* at -91 mV (**i**) and -98 mV (**ii**). Spectra were recorded with the following EPR parameters: temperature, 75K, modulation amplitude, 3.8 G_{pp} at 100 KHz; microwave power, 2 mW. **B.** Redox titration of the $g=1.98$ peak-trough of the wild-type and DmsA-C59S mutant Mo(V) signals. *Squares* - wild-type ($Mo_{(V/VI)}$ $E_{m,7} = -5$ mV, $Mo_{(IV/V)}$ $E_{m,7} = -140$ mV). *Triangles* - DmsA-C59S mutant ($Mo_{(V/VI)}$ $E_{m,7} = -10$ mV, $Mo_{(IV/V)}$ $E_{m,7} = -128$ mV). Data were obtained from EPR spectra recorded as described for **A**.

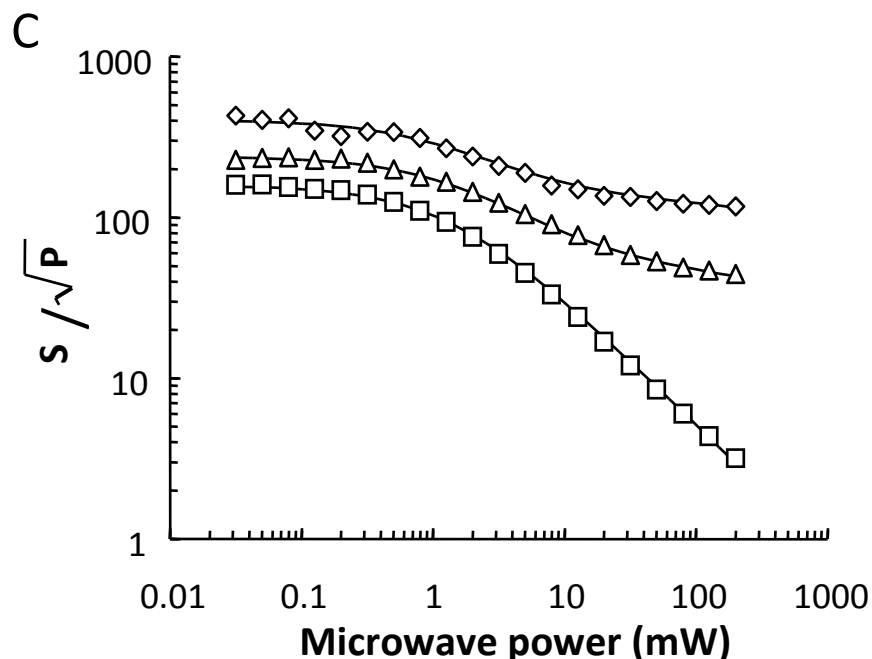


Figure 3.6* EPR characterization of Mo-bisPGD in the DmsA-C59S mutant. **C.** Microwave power saturation curves for the $g=1.98$ peak-trough of the DmsA-C59S Mo(V) spectrum of redox-poised samples. *Squares* - $E_h = -29\text{mV}$ ($P_{1/2} = 1.4\text{ mW}$, $b = 1.6$). *Triangles* - $E_h = -138\text{ mV}$ ($P_{1/2} = 1.5\text{ mW}$, $b = 1.6$, 82%). *Diamonds* - $E_h = -179\text{ mV}$ ($P_{1/2} = 1.1\text{ mW}$, $b = 1.6$, 70%). Percentages indicate the estimated amount of saturable versus non-saturable Mo(V). Where appropriate, a non-saturable component with nominal $P_{1/2}$ of 1000mW was included in the fits. EPR spectra were recorded as described for **A**, except that the temperature was 30 K and the modulation amplitude was $6G_{pp}$.

* EPR studies on Mo(V) in DmsA-C59S mutant (Figure 3.6) were done by Richard A. Rothery.

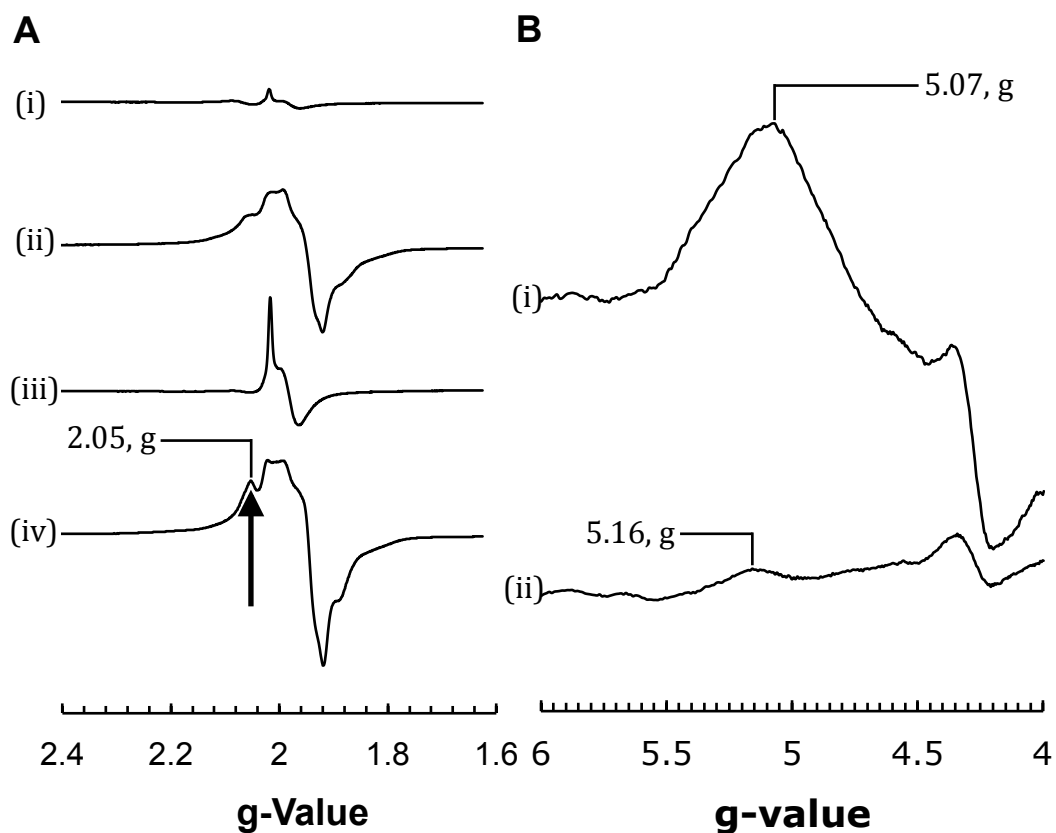


Figure 3.7 EPR spectra of the purified DmsA-Cys59Ser variant. Enzymes were purified from *E. coli* TOPP2 membranes as previously described [30]. **(A)** EPR spectra recorded in the $g=2.0$ region showing oxidized (*i*) and dithionite-reduced (*ii*) wild-type enzyme; and oxidized (*iii*) and reduced (*iv*) DmsA-Cys59Ser enzymes. **(B)** EPR spectra in the low field region showing the spectrum of reduced FSO with a high spin ground state ($S=3/2$) in the wild-type enzyme (*i*) and the lack of a similar spectrum exhibited by the purified DmsA-Cys59Ser variant (*ii*).

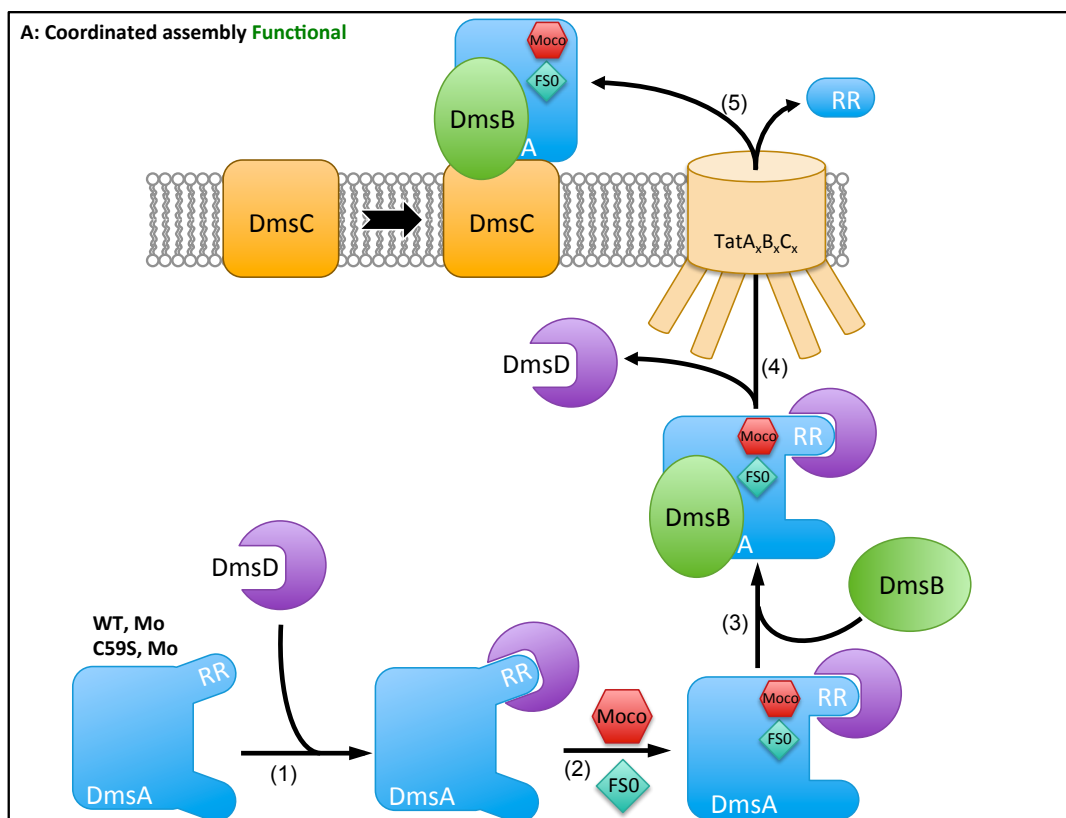


Figure 3.8 Model for DmsABC maturation. The maturation pathway of active DmsABC can be summarized as follows (A). (1) DmsD binds to the tat-leader of nascent DmsA, and holds the folding protein in a Mo-bisPGD (indicated as Moco in the figure) and FS0-binding competent conformation. (2) Both Mo-bisPGD and FS0 bind to the DmsD complex. In the case of the DmsA-Cys59Ser variant, failure to bind Mo-bisPGD leads to protein instability and degradation. (3) DmsB associates with Mo-bisPGD and FS0-containing DmsA. (4) The DmsAB-DmsD complex is recognized by the tat translocon, and translocated across the cytoplasmic membrane, releasing DmsD into the cytoplasm. (5) Leader peptidase cleaves the tat-leader and the DmsAB dimer associates with the periplasmic side of DmsC, generating a quinol binding site detectable by fluorescence quench titration.

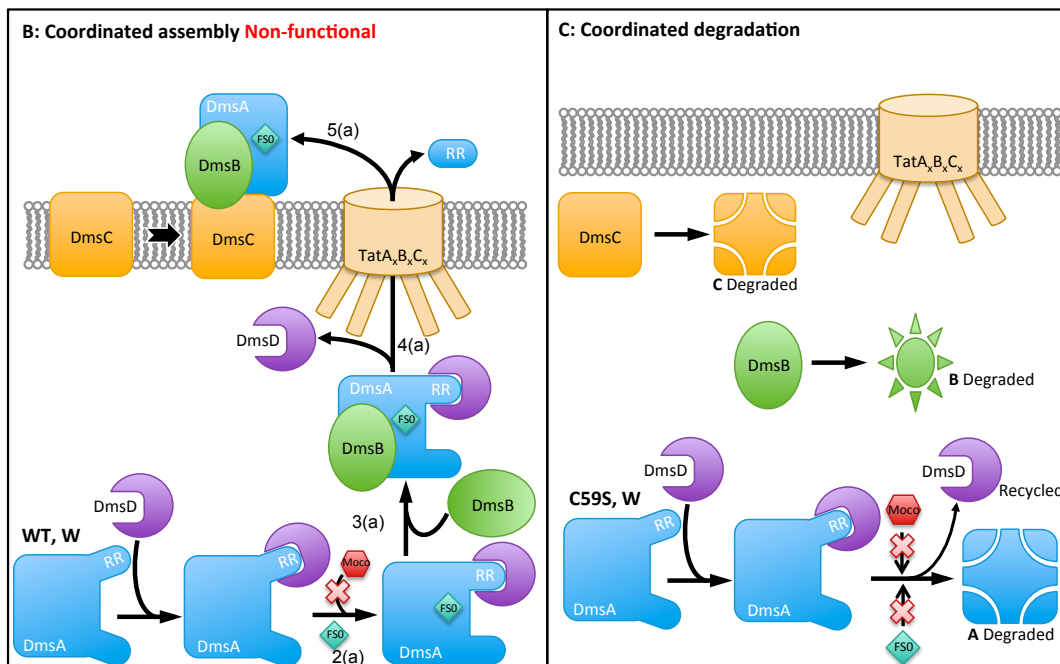


Figure 3.8 Model for DmsABC maturation (continued). In the absence of cofactor, the wild-type DmsABC (**B**) assembles FS0 (as has been observed in NarGHI [21,22]) (step 2a). This is followed by association of DmsB (step 3a), translocation and DmsD dissociation (step 4a), and tat-leader cleavage and assembly of apomolybdo-DmsABC (step 5a). The DmsA-Cys59Ser variant cannot assemble FS0 in absence of Moco (**C**). This leads to coordinated degradation of DmsA, DmsB and DmsC.

3.6 References

1. Rothery, R. A., Workun, G. J., and Weiner, J. H. (2008) The prokaryotic complex iron-sulfur molybdoenzyme family. *Biochim. Biophys. Acta* **1778**, 1897–1929
2. Magalon, A., Fedor, J. G., Walburger, A., and Weiner, J. H. (2011) Molybdenum enzymes in bacteria and their maturation. *Coord. Chem. Rev.* **255**, 1159–1178
3. Thauer, R. K., Jungermann, K., and Decker, K. (1977) Energy conservation in chemotrophic anaerobic bacteria. *Bacteriol. Rev.* **41**, 100–180
4. Leimkühler, S., Wuebbens, M. M., and Rajagopalan, K. V. (2011) The History of the Discovery of the Molybdenum Cofactor and Novel Aspects of its Biosynthesis in Bacteria. *Coord. Chem. Rev.* **255**, 1129–1144
5. Turner, R. J., Papish, A. L., and Sargent, F. (2004) Sequence analysis of bacterial redox enzyme maturation proteins (REMPs). *Can. J. Microbiol.* **50**, 225–238
6. Ramasamy, S. K., and Clemons, W. M. (2009) Structure of the twin-arginine signal-binding protein DmsD from *Escherichia coli*. *Acta Crystallogr. F Struct. Biol. Cryst. Commun.* **65**, 746–750
7. Oresnik, I. J., Ladner, C. L., and Turner, R. J. (2001) Identification of a twin-arginine leader-binding protein. *Mol. Microbiol.* **40**, 323–331
8. Stanley, N. R., Sargent, F., Buchanan, G., Shi, J., Stewart, V., Palmer, T., and Berks, B. C. (2002) Behaviour of topological marker proteins targeted to the Tat protein transport pathway. *Mol. Microbiol.* **43**, 1005–1021
9. Yen, M.-R., Tseng, Y.-H., Nguyen, E. H., Wu, L.-F., and Saier, M. H., Jr (2002) Sequence and phylogenetic analyses of the twin-arginine targeting (Tat) protein export system. *Arch. Microbiol.* **177**, 441–450
10. Blasco, F., Dos Santos, J. P., Magalon, A., Frixon, C., Guigliarelli, B., Santini, C. L., and Giordano, G. (1998) NarJ is a specific chaperone required for molybdenum cofactor assembly in nitrate reductase A of *Escherichia coli*. *Mol. Microbiol.* **28**, 435–447
11. Vergnes, A., Pommier, J., Toci, R., Blasco, F., Giordano, G., and Magalon, A. (2006) NarJ chaperone binds on two distinct sites of the aponitrate reductase of *Escherichia coli* to coordinate molybdenum cofactor insertion and assembly. *J. Biol. Chem.* **281**, 2170–2176
12. Li, H., and Turner, R. J. (2009) In vivo associations of *Escherichia coli* NarJ with a peptide of the first 50 residues of nitrate reductase catalytic subunit NarG. *Can. J. Microbiol.* **55**, 179–188
13. Zakian, S., Lafitte, D., Vergnes, A., Pimentel, C., Sebban-Kreuzer, C., Toci, R., Claude, J.-B., Guerlesquin, F., and Magalon, A. (2010) Basis of recognition between the NarJ chaperone and the N-terminus of the NarG subunit from *Escherichia coli* nitrate reductase. *FEBS J.* **277**, 1886–1895
14. Sambasivarao, D., Turner, R. J., Simala-Grant, J. L., Shaw, G., Hu, J., and Weiner, J. H. (2000) Multiple roles for the twin arginine leader sequence

- of dimethyl sulfoxide reductase of *Escherichia coli*. *J. Biol. Chem.* **275**, 22526–22531
15. Sharma, A. K., Pallesen, L. J., Spang, R. J., and Walden, W. E. (2010) Cytosolic iron-sulfur cluster assembly (CIA) system: factors, mechanism, and relevance to cellular iron regulation. *J. Biol. Chem.* **285**, 26745–26751
 16. Broderick, J. B. (2007) Assembling iron-sulfur clusters in the cytosol. *Nat Chem Biol.* **3**, 243–244
 17. Lanciano, P., Vergnes, A., Grimaldi, S., Guigliarelli, B., and Magalon, A. (2007) Biogenesis of a respiratory complex is orchestrated by a single accessory protein. *J. Biol. Chem.* **282**, 17468–17474
 18. Rothery, R. A., Grant, J. L., Johnson, J. L., Rajagopalan, K. V., and Weiner, J. H. (1995) Association of molybdopterin guanine dinucleotide with *Escherichia coli* dimethyl sulfoxide reductase: effect of tungstate and a mob mutation. *J. Bacteriol.* **177**, 2057–2063
 19. Rothery, R. A., Magalon, A., Giordano, G., Guigliarelli, B., Blasco, F., and Weiner, J. H. (1998) The molybdenum cofactor of *Escherichia coli* nitrate reductase A (NarGHI). Effect of a mobAB mutation and interactions with [Fe-S] clusters. *J. Biol. Chem.* **273**, 7462–7469
 20. Temple, C. A., and Rajagopalan, K. V. (2000) Mechanism of assembly of the Bis(Molybdopterin guanine dinucleotide)molybdenum cofactor in *Rhodobacter sphaeroides* dimethyl sulfoxide reductase. *J. Biol. Chem.* **275**, 40202–40210
 21. Rothery, R. A., Bertero, M. G., Cammack, R., Palak, M., Blasco, F., Strynadka, N. C. J., and Weiner, J. H. (2004) The catalytic subunit of *Escherichia coli* nitrate reductase A contains a novel [4Fe-4S] cluster with a high-spin ground state. *Biochemistry* **43**, 5324–5333
 22. Rothery, R. A., Bertero, M. G., Spreter, T., Bouromand, N., Strynadka, N. C. J., and Weiner, J. H. (2010) Protein crystallography reveals a role for the FS0 cluster of *Escherichia coli* nitrate reductase A (NarGHI) in enzyme maturation. *J. Biol. Chem.* **285**, 8801–8807
 23. Bertero, M. G., Rothery, R. A., Boroumand, N., Palak, M., Blasco, F., Ginet, N., Weiner, J. H., and Strynadka, N. C. J. (2005) Structural and biochemical characterization of a quinol binding site of *Escherichia coli* nitrate reductase A. *J. Biol. Chem.* **280**, 14836–14843
 24. Chan, C. S., Howell, J. M., Workentine, M. L., and Turner, R. J. (2006) Twin-arginine translocase may have a role in the chaperone function of NarJ from *Escherichia coli*. *Biochem. Biophys. Res. Commun* **343**, 244–251
 25. Bertero, M. G., Rothery, R. A., Palak, M., Hou, C., Lim, D., Blasco, F., Weiner, J. H., and Strynadka, N. C. J. (2003) Insights into the respiratory electron transfer pathway from the structure of nitrate reductase A. *Nat. Struct. Biol.* **10**, 681–687
 26. Magalon, A., Lemesle-Meunier, D., Rothery, R. A., Frixon, C., Weiner, J. H., and Blasco, F. (1997) Heme axial ligation by the highly conserved His residues in helix II of cytochrome b (NarI) of *Escherichia coli* nitrate reductase A. *J. Biol. Chem.* **272**, 25652–25658

27. Rothery, R. A., Blasco, F., Magalon, A., and Weiner, J. H. (2001) The diheme cytochrome b subunit (NarI) of *Escherichia coli* nitrate reductase A (NarGHI): structure, function, and interaction with quinols. *J. Mol. Microbiol. Biotechnol.* **3**, 273–283
28. Sambasivarao, D., Dawson, H. A., Zhang, G., Shaw, G., Hu, J., and Weiner, J. H. (2001) Investigation of *Escherichia coli* dimethyl sulfoxide reductase assembly and processing in strains defective for the sec-independent protein translocation system membrane targeting and translocation. *J. Biol. Chem.* **276**, 20167–20174
29. Turner, R. J., Busaan, J. L., Lee, J. H., Michalak, M., and Weiner, J. H. (1997) Expression and epitope tagging of the membrane anchor subunit (DmsC) of *Escherichia coli* dimethyl sulfoxide reductase. *Protein Eng.* **10**, 285–290
30. Tang, H., Rothery, R. A., Voss, J. E., and Weiner, J. H. (2011) Correct assembly of iron-sulfur cluster FS0 into *Escherichia coli* dimethyl sulfoxide reductase (DmsABC) is a prerequisite for molybdenum cofactor insertion. *J. Biol. Chem.* **286**, 15147–15154
31. Rothery, R. A., and Weiner, J. H. (1991) Alteration of the iron-sulfur cluster composition of *Escherichia coli* dimethyl sulfoxide reductase by site-directed mutagenesis. *Biochemistry* **30**, 8296–8305
32. Trieber, C. A., Rothery, R. A., and Weiner, J. H. (1994) Multiple pathways of electron transfer in dimethyl sulfoxide reductase of *Escherichia coli*. *J. Biol. Chem.* **269**, 7103–7109
33. Sambasivarao, D., and Weiner, J. H. (1991) Dimethyl sulfoxide reductase of *Escherichia coli*: an investigation of function and assembly by use of in vivo complementation. *J. Bacteriol.* **173**, 5935–5943
34. Santini, C. L., Ize, B., Chanal, A., Müller, M., Giordano, G., and Wu, L. F. (1998) A novel sec-independent periplasmic protein translocation pathway in *Escherichia coli*. *EMBO J.* **17**, 101–112
35. Stewart, V., and MacGregor, C. H. (1982) Nitrate reductase in *Escherichia coli* K-12: involvement of chlC, chlE, and chlG loci. *J. Bacteriol.* **151**, 788–799
36. Sambasivarao, D., Turner, R. J., Bilous, P. T., Rothery, R. A., Shaw, G., and Weiner, J. H. (2002) Differential effects of a molybdopterin synthase sulfurylase (moeB) mutation on *Escherichia coli* molybdoenzyme maturation. *Biochem. Cell Biol.* **80**, 435–443
37. Condon, C., and Weiner, J. H. (1988) Fumarate reductase of *Escherichia coli*: an investigation of function and assembly using in vivo complementation. *Mol. Microbiol.* **2**, 43–52
38. Rothery, R. A., and Weiner, J. H. (1996) Interaction of an engineered [3Fe-4S] cluster with a menaquinol binding site of *Escherichia coli* DMSO reductase. *Biochemistry* **35**, 3247–3257
39. Lowry, O. H., Rosebrough, N. J., Farr, A. L., and Randall, R. J. (1951) Protein measurement with the Folin phenol reagent. *J. Biol. Chem.* **193**, 265–275
40. Markwell, M. A., Haas, S. M., Bieber, L. L., and Tolbert, N. E. (1978) A

- modification of the Lowry procedure to simplify protein determination in membrane and lipoprotein samples. *Anal. Biochem.* **87**, 206–210
41. Sambasivarao, D., Scraba, D. G., Trieber, C., and Weiner, J. H. (1990) Organization of dimethyl sulfoxide reductase in the plasma membrane of *Escherichia coli*. *J. Bacteriol.* **172**, 5938–5948
 42. Johnson, J. L., Indermaur, L. W., and Rajagopalan, K. V. (1991) Molybdenum cofactor biosynthesis in *Escherichia coli*. Requirement of the chlB gene product for the formation of molybdopterin guanine dinucleotide. *J. Biol. Chem.* **266**, 12140–12145
 43. Rothery, R. A., Seime, A. M., Spiers, A.-M. C., Maklashina, E., Schröder, I., Gunsalus, R. P., Cecchini, G., and Weiner, J. H. (2005) Defining the Q-site of *Escherichia coli* fumarate reductase by site-directed mutagenesis, fluorescence quench titrations and EPR spectroscopy. *FEBS J.* **272**, 313–326
 44. Van Ark, G., and Berden, J. A. (1977) Binding of HQNO to beef-heart sub-mitochondrial particles. *Biochim. Biophys. Acta.* **459**, 119–127
 45. Okun, J. G., Lümmer, P., and Brandt, U. (1999) Three classes of inhibitors share a common binding domain in mitochondrial complex I (NADH:ubiquinone oxidoreductase). *J. Biol. Chem.* **274**, 2625–2630
 46. Zhao, Z., and Weiner, J. H. (1998) Interaction of 2-n-heptyl-4-hydroxyquinoline-N-oxide with dimethyl sulfoxide reductase of *Escherichia coli*. *J. Biol. Chem.* **273**, 20758–20763
 47. Cammack, R., and Weiner, J. H. (1990) Electron paramagnetic resonance spectroscopic characterization of dimethyl sulfoxide reductase of *Escherichia coli*. *Biochemistry* **29**, 8410–8416
 48. Rothery, R. A., Chatterjee, I., Kiema, G., McDermott, M. T., and Weiner, J. H. (1998) Hydroxylated naphthoquinones as substrates for *Escherichia coli* anaerobic reductases. *Biochem. J.* **332 (Pt 1)**, 35–41
 49. Rothery, R. A., Trieber, C. A., and Weiner, J. H. (1999) Interactions between the molybdenum cofactor and iron-sulfur clusters of *Escherichia coli* dimethylsulfoxide reductase. *J. Biol. Chem.* **274**, 13002–13009
 50. Magalon, A., Asso, M., Guigliarelli, B., Rothery, R. A., Bertrand, P., Giordano, G., and Blasco, F. (1998) Molybdenum cofactor properties and [Fe-S] cluster coordination in *Escherichia coli* nitrate reductase A: investigation by site-directed mutagenesis of the conserved His-50 residue in the NarG subunit. *Biochemistry* **37**, 7363–7370

3.7 Appendix: Supplementary Figures

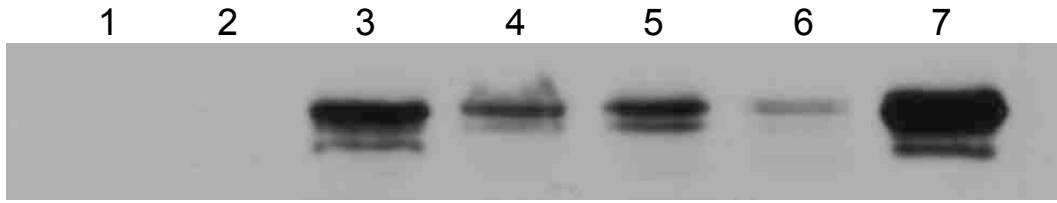


Figure 3.9 Tungstate prevent assembly of DmsA-Cys59Ser mutant to the membrane when Moco is not available. Western blot showing bands for DmsA assembled to the membrane of *E. coli* DSS301 ($\Delta dmsABC$). Lane 1: low molecular standard; lane 2: background vector (pBR322); lane 3: wild-type DmsABC; lane 4: DmsA^{C59S}BC grown in 5 μ M molybdate; lane 5: DmsA^{C59S}BC grown in 10mM molybdate; lane 6: DmsA^{C59S}BC grown in 10mM tungstate; lane 7: purified DmsABC standard.

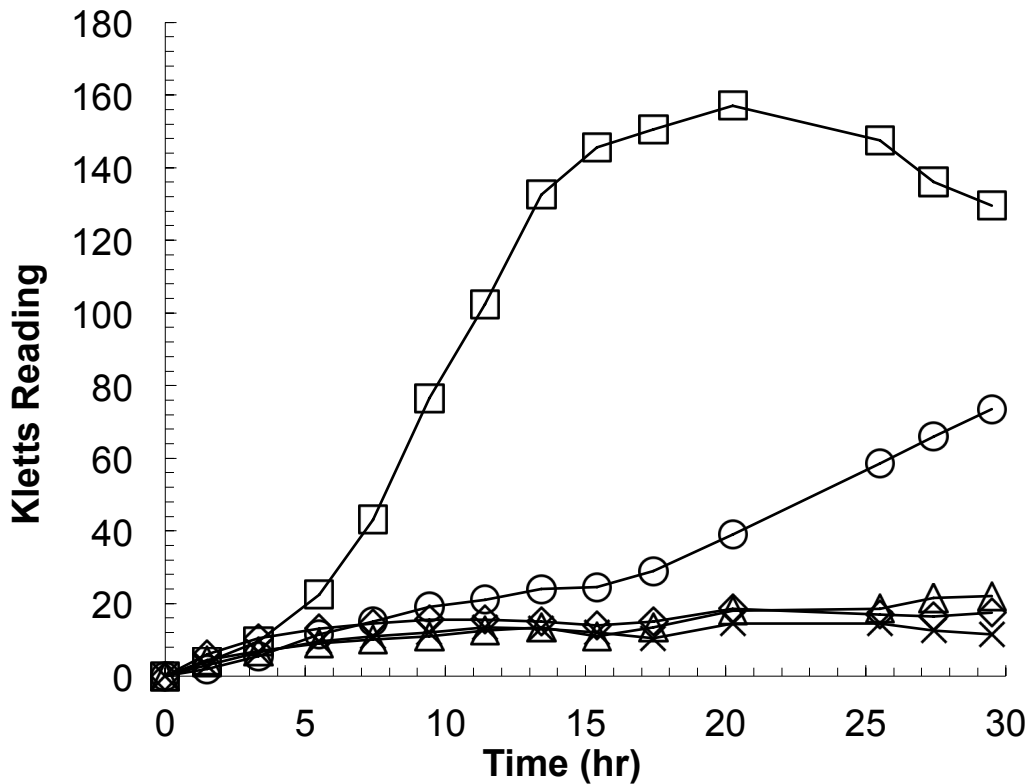


Figure 3.10 DmsABC and DmsA^{C59S}BC do not support respiratory growth of *E. coli* DSS301 ($\Delta dmsABC$) on DMSO when Moco is not available. Squares–pDMS160 in the presence of molybdate. Circles–pDMS160–C59S in the presence of molybdate. Triangles–pDMS160 in the presence of 10mM tungstate. Diamonds–pDMS160–C59S in the presence of 10mM tungstate. Cross–pBR322 in the presence of molybdate. Cell growth was measured with a Klett-Summerson spectrophotometer equipped with a number-66 filter.

Chapter 4

Conclusions and Future Directions

4.1 Conclusions and Summaries

In Chapter 2, direct spectroscopic evidence for the presence of the FS0 cluster in DmsA was presented. It has a high spin ground state ($S=3/2$) in its reduced form, which gives rise to a EPR spectrum with a peak at $g=5.06$. Mutagenesis studies showed that the FS0 has an important role in enzyme maturation in addition to its role in electron transfer between the ETR and cofactor. The N-terminal Cys group of DmsA coordinates FS0 and Mo-bisPGD assembly, making the correct assembly of FS0 cluster a prerequisite for cofactor insertion during enzyme maturation. A model structure of DmsA was generated using the X-ray crystal structure of NarG of *E. coli* NarGHI and predicted that the sequence $^{18}\text{CTVNC}^{22}$ is important in interactions with both FS0 and Mo-bisPGD. Our experiments indicate that the side chain of Asn-21 is critical for Mo-bisPGD insertion as deletion of this residue resulted in assembly of a [3Fe-4S] cluster in place of FS0 and complete abolition of cofactor insertion. A multi-mutation (CS1+R61K) changing the FS0 coordinating sequence $^{18}\text{CATVNCBGSRCCP}^{27}\dots\text{R}^{61}$ to $^{18}\text{CATYCBGVGCCG}^{26}\dots\text{K}^{61}$ (which resembles the N-terminal Cys group of FdnG) rescues cofactor insertion. However, this mutant does not have a detectable FS0 EPR signal or enzyme activity, indicating that its active site is defective. All of the mutants studied assembled to the membrane at a level comparable to wild-type, meaning that correct Moco insertion is not required for translocation or membrane targeting of the enzyme.

In Chapter 3, the mutation of an FS0-liganding Cys residue to Ser (C59S) renders the enzyme maturation Mo-bisPGD cofactor dependent. While the wild-type DmsABC can assemble apoenzyme to the membrane, the DmsA^{C59S}BC mutant cannot assemble any stable subunit (DmsA, B or C) of the enzyme in the absence of the cofactor. The cofactor availability alone could overcome the destabilizing effects of the mutant, leading to the assembly of fully functional mutant enzyme at the membrane that supports anaerobic growth on DMSO. This suggests a chaperone function of the cofactor in stabilizing the protein fold during maturation. Activity assays and EPR studies indicated that the mutation had drastic effects on the biophysical properties of FS0 but very mild effect on the Mo-bisPGD cofactor. The mutation changed the ground state of the reduced FS0 from $S=3/2$ to $S=1/2$. These observations reinforced the relationship between the FS0 assembly and enzyme maturation.

4.2 Future Directions

Although there have been extensive biochemical and biophysical studies to reveal information on *E. coli* DmsABC's maturation pathway and function, there is limited structural data due to lack of its crystal structure. The understanding of EcDmsABC in several aspects would benefit from the structural information. The proposed mechanism of DMSO reduction based on the structures of *Rhodobacter* DMSO reductase can be tested. The FS0

cluster, whose presence in *E. coli* DMSO reductase has been proven by EPR studies, can be better characterized in detail. Due to the limitations of conditions required for appearance of the EPR signal, one often cannot determine the presence of the FS0 cluster and changes in its coordinating environment in the mutants studied entirely based on the presence/absence or the characteristics of the EPR spectra. The structures of the mutant will be powerful and reliable evidence for studies on FS0's roles in maturation and catalytic function of DmsABC. Formation of the DmsAB complex before transportation by the *tat* translocation system and attachment of DmsAB to DmsC are also very important steps in maturation pathway. The inter-subunit interactions demonstrated by the crystal structure will reveal valuable information about these processes. Additionally, as the structure FdnGHI (1) had confirmed the periplasmic location of FdnGH (2, 3), the structure of DmsABC will greatly complement its proposed topology. The topology is not only important in understanding DmsABC but also important in understanding the function and mechanism of *tat* machinery.

The *tat* system and its associated system-specific chaperones have been of rising interest. DmsD belongs to the superfamily that includes well characterized TorD and NarJ. The differences between these chaperones make characterization of DmsD essential in building a thorough knowledge of the chaperones. For example, TorD interacts with TorA monomer while NarJ and DmsD interact with NarGH and DmsAB complexes, respectively. NarGH with a pseudo-*tat* leader is not transported by the *tat* system, while

TorD and DmsD also interact with the *tat* translocase. Both TorD and NarJ have been shown to interact with the apo form of their substrate protein at two distinct sites. However, although it has been suggested that DmsD likely has a second binding site on the mature protein domain of the DmsA precursor, there is only evidence for binding of DmsD to the *tat*-leader of DmsA. The structures of DmsD recently solved only shed more light on the interaction between DmsD and the twin arginine motif. Since the binding of DmsD is also dictated by the conformation of DmsA, studying effects on interaction between DmsD and the mutants defective in correct Mo-bisPGD cofactor insertion and/or sensitive to cofactor availability might help to better understand the mechanism of DmsD's chaperone activity.

Another intriguing question about the *tat* system is whether there is an intrinsic proofreading system in the *tat* system to recognize the folding states of substrate and remove misfolded proteins. So far only evidence for proofreading control performed by the system-specific chaperones and their mechanisms have been well studied. The ability of apoDmsABC to be translocated by the *tat* pathway and assembled to the membrane had made DmsABC and DmsD unique exceptions in their families of proteins. The DmsA-C59 to Ser mutation studied herein had made the apoform of the mutant incompatible for *tat* translocase. The mutant apoprotein components were also more efficiently degraded compared to wild-type. Whether the recognition and degradation of the misfolded protein is *tat* system dependent needs further investigation. The comparison of structures of the

wild-type and mutants will also provide more insights on how DmsABC wild-type enzyme was able to bypass the proof reading processes of the *tat* translocation pathway.

4.3 References

1. Jormakka, M., Törnroth, S., Byrne, B., and Iwata, S. (2002) Molecular basis of proton motive force generation: structure of formate dehydrogenase-N. *Science* **295**, 1863–1868
2. Stanley, N. R., Sargent, F., Buchanan, G., Shi, J., Stewart, V., Palmer, T., and Berks, B. C. (2002) Behaviour of topological marker proteins targeted to the Tat protein transport pathway. *Mol. Microbiol.* **43**, 1005–1021
3. Sargent, F., Berks, B., and Palmer, T. (2002) Assembly of membrane-bound respiratory complexes by the Tat protein-transport system. *Arch. Microbiol.* **178**, 77–84